Enhancing the sensitivity of NMR by Dynamic Nuclear Polarisation

by

Martin Graham Saunders

A thesis submitted to the

University of Birmingham

for the degree of

DOCTOR OF PHILOSOPHY

Supervisors: Ulrich Günther & Christian Ludwig

HWB-NMR

School of Cancer Sciences

College of Medical and Dental Sciences

The University of Birmingham

September 2010

Abstract

Dynamic Nuclear Polarisation (DNP) is a method used to increase the signal available for nuclear magnetic resonance (NMR) experiments. DNP is one of many hyperpolarisation methods and one implementation, so called *ex-situ* DNP, sees the sample polarised with a stable radical doping agent at low temperature and with microwave irradiation in a magnetic field before transfer to a second higher field NMR magnet to acquire a liquid state NMR spectrum. There have been some very strong polarisations reported using this method and it lends itself well to medical applications however, there are often unpredictable results with these experiments where some substances do not polarise effectively for no obvious reason. The primary goal of this project has been to gain an understanding of the underlying reasons for unpredictable *ex-situ* DNP polarisation failures and to develop methods to overcome these limitations. In the course of the work an additional polarisation mechanism arising from hindered methyl rotors was discovered. The work in this thesis can be divided into two sections. Firstly, the preparation of DNP samples and the way in which DNP-NMR experiments are performed have been optimised. The concept of a co-polarisation agent has been introduced and methods employing a Nuclear Overhauser Effect have been implemented. The second part has been focused on the identification and characterisation of a quantum tunnelling effect that is a variant of the commonly known Haupt effect but has not previously been described in the context of experiments at temperatures < 3.8K, such as with *ex-situ* DNP. This effect can interfere with DNP, either constructively or destructively and can lead to a relatively strong polarisation enhancement as an independent effect. Finally these methods have been combined in a number of situations to give results that would have otherwise been unobtainable.

Acknowledgements

Abbreviations

ADC - Analogue to digital converter

ALTADENA - Adiabatic Longitudinal Transport and Dissociation Engenders Net Alignment

CIDNP - Chemically induced dynamic nuclear polarisation

DC - Direct current

DMF - N,N'-Dimethylformamide

DMSO - Dimethylsulphoxide

DNP - Dynamic nuclear polarisation

EDTA - Ethylenediaminetetraacetic acid

ESR - Electron spin resonance

FID - Free induction decay

FT - Fourier transform

HDPE - High density polyethylene

HMQC -Heteronuclear multi quantum correlation spectroscopy

HPLC - High pressure liquid chromatography

HSQC - Heteronuclear single quantum correlation spectroscopy

LDH - Lactate dehydrogenase

LFE - Low frequency excitation

MAS - Magic angle spinning

MEOP - metastable-exchange optical pumping

MRI - Magnetic resonance imaging

MRS - Magnetic resonance spectroscopy

NAD - Nicotinamide adenine dinucleotide

NMR - Nuclear magnetic resonance

NOE - Nuclear Overhauser effect

NOESY - Nuclear Overhauser effect spectroscopy

NSAID - Non-steroidal anti-inflammatory drug

OE - Overhauser effect

OIMBL - Oxford Instruments Molecular Biotools Limited

PASADENA - Parahydrogen and synthesis allow dramatically enhanced nuclear alignment

PFE - Perfluoroethylene

PHIP - Parahydrogen induced polarisation

QR - Quantum rotor

RF - Radio frequency

SABRE - Signal Amplification By Reversible Exchange

SEOP - spin-exchange optical pumping

SSD - Spin-symmetry diffusion

TEMPO - (2,2,6,6-Tetramethylpiperidin-1-yl)oxyl

TOCSY - Total correlation spectroscopy

Contents

II   Experimental   56

Chapter 3   Materials and methods   57

Chapter 4   Using a Nuclear Overhauser Effect to polarise secondary nuclei within a molecule after DNP and transfer   69

List of Figures

x

xiv

List of Tables

Part I

Introductions

Chapter 1

Introduction

1.1 Introduction

It is of prime importance to medical science to understand the underlying mechanisms that cause disease states. In 1924 Otto Warburg hypothesised that cancer cells have an altered metabolism[12]. This difference can be understood in terms of allowing cancer cells to grow un-hindered but it is still unclear whether these alterations to metabolism are a cause or an effect. The ability to detect and analyse small molecule metabolites and measure their flux is highly desirable as is the study of potential chemotherapeutic agents that may counter such diseases. Nuclear magnetic resonance (NMR) offers a method that has the potential to allow these kinds of studies and is a powerful, non-destructive spectroscopic technique. However, NMR suffers greatly from its low sensitivity. In standard NMR experimental conditions the nuclear spin populations are only slightly polarised and this has a direct link to the amount of magnetisation available for detection in an NMR experiment. The nuclear spin polarisation can be increased by a number of hyperpolarisation techniques but recent promise has been shown by an *ex-situ* implementation of DNP commercially packaged as the HyperSense™ dynamic nuclear polarisation DNP polariser. The HyperSense™ instrument has the potential to deliver extraordinarily strong hyperpolarisation[13] but inexplicable inefficiencies in the polarisation mechanisms prevent a general applicability. A more powerful and consistent methodology lends itself well to a diverse range of applications such as

medical research, spectroscopy, pharmaceutical chemistry and engineering and has the potential to facilitate advances in these areas.

1.2   Aims

The aims of this project are to provide an increase in both absolute enhancement values as well as reliability in *ex-situ* dynamic nuclear polarisation (DNP) experiments through investigation of the mechanisms by which substances become polarised.

Chapter 2

Theoretical

2.1 Nuclear magnetic resonance

2.1.1 Spin

All matter possesses a property called spin, which is a fundamental property along with magnetism, electric charge and mass. Spin is so called because it has very similar behaviour to classically spinning systems with properties such as angular momentum and a frequency. Mass has an important role in many physical properties of substances and mainly resides in atomic nuclei. Electric charge is a vitally important property that gives rise to electrostatic bonds between atoms and allows molecules to form. Electronic charge has a primary role in the chemistry of substances. Magnetism has a less obvious impact on the physical properties of matter but the magnetism of ferrous material arises from the electronic magnetism. In ferromagnetic materials the magnetic moments of unpaired electrons spontaneously align in so-called domains. This alignment leads to the magnetic interaction. In a bulk material, such as a block of iron, the domains are normally randomly aligned, consequently no overall magnetisation is seen. When placed in an external magnetic field the domains will align to give a durable bulk magnetic moment.

The spin is much less evident on the macroscopic scale but is fundamentally important for the properties of sub-atomic entities such as atomic nuclei. The nuclear magnetism can be used to gain an insight into the inner workings of atomic nuclei and their local environment by their interaction

with external magnetic fields and the impact of the spin property. The concept of spin is very abstract and is hard to visualise as there is no real classical analogue, at least not for nuclear spins. It can be understood mathematically or by analogy to other physical processes with similar behaviour. Spin is a form of angular momentum but for the total angular momentum here the quantum number S is used instead of the angular momentum quantum number J to make a distinction between spin angular momentum and rotational angular momentum. S can take half integer values such as $1/2$, 1, $3/2$ etc [14]. Particles with integer spin are termed Bosons and are responsible for forces. Particles with half-integer spin are termed Fermions and generally have mass, thus forming matter. There is no easy way to visualise a half integer spin. A spin value of $1/2$ effectively means that the body must rotate twice before returning to the same state. Spin is not an inherited property as with rotational angular momentum. Rather, spin is an intrinsic property of the particle that is a description of its nature.

For a particle of spin $I = 1/2$, such as a proton, the magnetic moment is,

$$\hat{\mu} = \gamma \hat{I} = \hbar \gamma \sqrt{I(I + 1)} \tag{2.1}$$

where γ is the gyromagnetic ratio of the spin, $\hbar$ is Planck's constant over 2π. When an external magnetic field, B, is applied to the spin a Hamiltonian,

$$\hat{H} = -\mu \bullet B \tag{2.2}$$

results. If the external magnetic field is then assumed to run along the z axis the Zeeman Hamiltonian,

$$\hat{H} = -\hbar \gamma B_0 \hat{I}_z \tag{2.3}$$

can be obtained where the angular momentum operator, I, is defined by,

$$\hat{I} \rightarrow \hbar I \tag{2.4}$$

The spin quantum number, m_I can take values $m_I = I, I - 1... - I$. As the eigenvalues of the Zeeman Hamiltonian are proportional to the eigenvalues of I the possible energies of the spin in the magnetic field are,
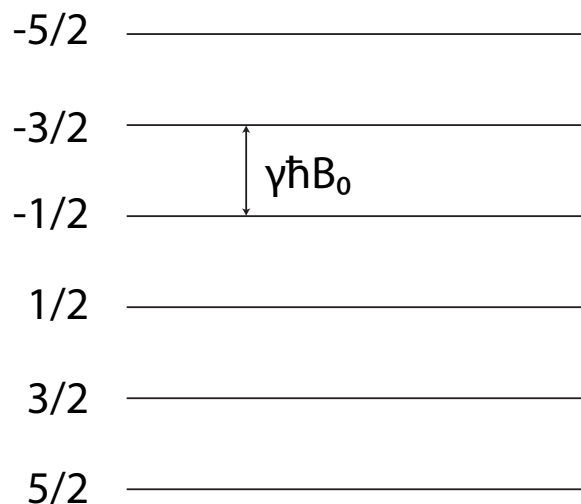
Figure 2.1: Cartoon illustrating the Zeeman energy level splitting for a spin with $m_I = \frac{5}{2}$.

$$E_m = -\gamma \hbar B_0 m_I \tag{2.5}$$

These energy levels are separated by,

$$\Delta = \gamma \hbar B_0 \tag{2.6}$$

which is otherwise known as the Zeeman splitting. See Figure 2.1 for an illustration of these levels in a $m_I = \frac{5}{2}$ spin.

2.1.2 Polarisation

For a spin $\frac{1}{2}$ nucleus in an oriented magnetic field there are two possible energy states, α and β, corresponding to an m_I of $+\frac{1}{2}$ and $-\frac{1}{2}$ respectively. The α state has lower energy than the β state so is always slightly more populated, owing to the finite amount of energy available in a system. Where spins can exist in two non-degenerate energy levels a distribution (the Boltzmann distribution) will establish itself depending on the available thermal energy. At absolute zero there is not enough energy for any spins to exist in the high energy state. At infinitely high temperature there is enough energy to allow each spin to exist in either state with equal probability so the

populations of each state will be equal. Individual spins in the ensemble can alternate between states but the population as a whole is described by a Boltzmann distribution,

$$P = \frac{N_\alpha - N_\beta}{N_\alpha + N_\beta} = tanh\left(\frac{\gamma\hbar B_0}{2k_B T}\right) \tag{2.7}$$

where γ is the gyromagnetic ratio of the nucleus, $\hbar$ is Planck's constant divided by 2π, B_0 is the static magnetic field strength, k_B is the Boltzmann constant and T is the temperature in Kelvin. N_α and N_β are the populations of the α and β states respectively. From equation 2.7 it is clear that the difference in populations, the polarisation, varies with both the external magnetic field and temperature. Figure 2.2 shows how the polarisation, P, varies with temperature at a fixed magnetic field strength of 3.35T. The polarisation also depends on the gyromagnetic ratio so spins with a greater value for γ will have an inherently higher spin polarisation.

2.1.3   Precession around the external magnetic field

Although the phenomenon of spin does not follow classical physics the movement of a magnetic moment of a spin ensemble in an external magnetic field, the force of which is its torque, can be treated as:

$$\frac{d\mu}{dt} = \gamma\mu \times B \tag{2.8}$$

Assuming that the external magnetic field is aligned with the z axis the motion can be described in each coordinate as

$$\frac{d\mu_x}{dt} = \gamma\mu_y B_z$$

$$\frac{d\mu_y}{dt} = -\gamma\mu_x B_z \tag{2.9}$$

$$\frac{d\mu_z}{dt} = 0$$
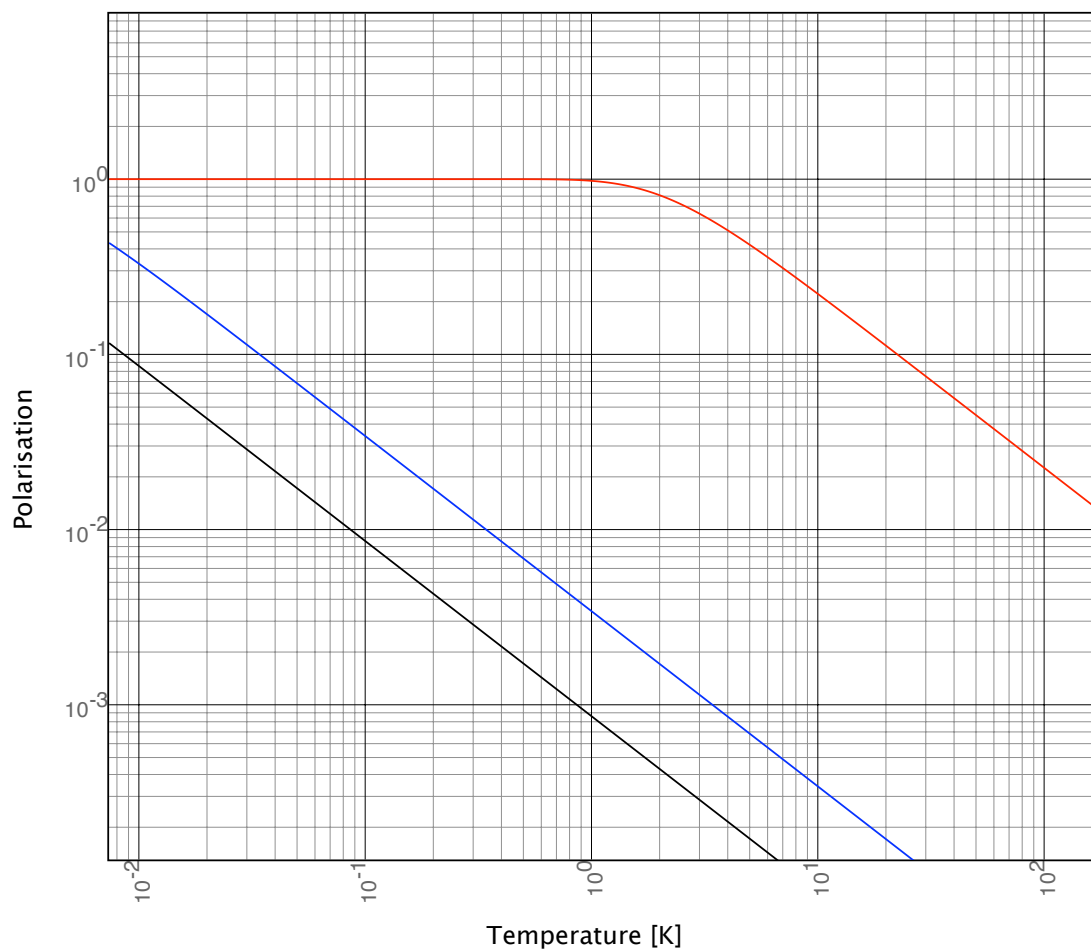
Figure 2.2: Zeeman Boltzmann polarisation for electrons (red), protons (blue) and carbon (black) nuclei vs. temperature in a magnetic field strength of 3.35T according to equation 2.7 on a logarithmic scale.
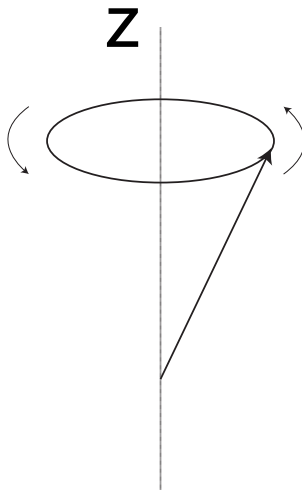
Figure 2.3: The cone of precession for a spin around the z-axis.

These give a path of motion for the magnetic moment that traces a cone around the z axis in a so-called precession pattern, see Figure 2.3.

2.1.4   The Bloch equations and relaxation

If the vectors of all of the magnetic moments in a spin ensemble are averaged a vector, M, that describes the bulk magnetisation is derived. Because we are dealing with an average of a large ensemble rather than a single spin, this vector can be treated classically. The motion of the bulk magnetisation vector in an applied field is described by,

$$\frac{dM}{dt} = \gamma M \times B \tag{2.10}$$

This gives a bulk magnetisation vector that is aligned with the external magnetic field at thermal equilibrium (Figure 2.4a). Upon application of a resonant RF pulse of a specific power and length the populations become equalised and a transverse phase coherence is induced rotating M to be perpendicular to the external magnetic field (Figure2.4b). The vector, M, would continue to precess in the transverse plane indefinitely, however small fluctuations in the magnetic micro-environment, such as those that result from molecular motions, as well as resonant frequencies
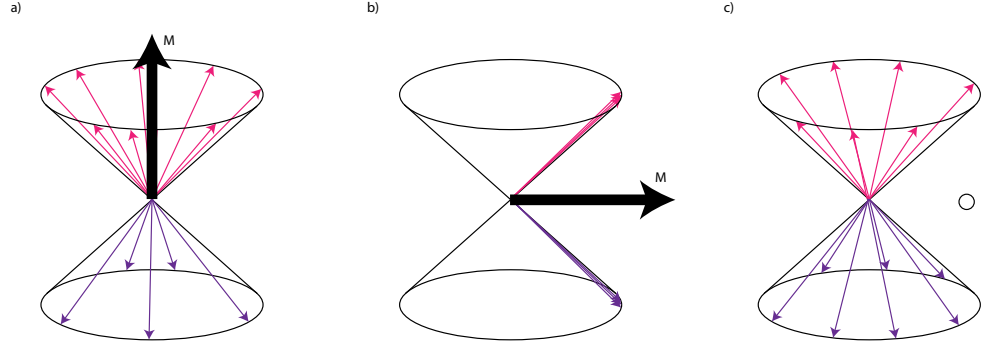
Figure 2.4: Cartoon illustrating the Bloch relaxation model. In a) the spins are at equilibrium with slightly more spins in the low energy, α, state than the high energy β state. The bulk magnetisation vector M is depicted by an arrow. in b) a resonant RF pulse causes the populations in the two states to equalise and a phase transverse phase coherence occurs. The bulk magnetisation vector M is depicted by an arrow. In c) the phase coherence breaks down with T_2 tending towards no bulk magnetisation vector and the populations relax back to equilibrium (state a) with T_1.

allow the system to return to thermal equilibrium. From here there are two separate relaxation pathways that can be followed. The faster route depends on the time constant T_2 and sees the phase coherence break down and the size of M decrease[15]. This kind of relaxation occurs because the speed of precession, the Larmor frequency entirely depends on the total experienced field for a spin. As magnets are not perfect the exact field may differ through a sample causing inhomogeneity in the field. Also, molecular motions can cause other spins to move relative to one another and the influence of the spins magnetic fields on each other and variations in dipole moments also cause minute variations in the experienced field for a given spin population. The second relaxation pathway causes the populations of the α state and β state to return to their equilibrium value with the time constant T_1. This type of relaxation is due to spins experiencing resonant frequencies from other nearby spins, and flipping randomly to return M to the equilibrium value. Longitudinal relaxation rates vary greatly from less than a second to many minutes in some solids. The time constant T_2 can only be smaller or equal to T_1[14]. Both relaxation routes generally follow an exponential decay. However, as can be seen from the Bloch equations the two rates are independent as they act on different axes.

This process of relaxation can be described mathematically by altering equation 2.10 to include

relaxation terms.

$$\frac{dM_x}{dt} = \gamma M_y B_z - \frac{M_x}{T_2}$$

$$\frac{dM_y}{dt} = -\gamma M_x B_z - \frac{M_y}{T_2} \tag{2.11}$$

$$\frac{dM_z}{dt} = 0 - \frac{M_z - M_0}{T_1}$$

These equations are collectively known as the Bloch equations[16]. Felix Bloch was awarded the 1952 Nobel prize for deriving these equations. The second part on the right hand side of each equation describes the relaxation in each respective axis and T_1 and T_2 are constants that define the rate of relaxation.

2.1.5   The NMR experiment

In high field NMR the external magnetic field is usually generated by supercooled, superconducting magnets with field strengths in the range of 5-20 Tesla. Superconducting magnets have the advantage that they do not require a permanent external power supply to induce a field in the magnet coils once the coils are charged. The magnetic field is generated perpendicular to the electric field in the magnet coils. In a non-superconducting magnet, resistance in the wire of the coils leads to heating and dissipation of energy from the coils. In a superconducting magnet this does not occur so, provided the superconductivity remains the electrical current will remain in the coils even when the main supply is removed, therefore the magnetic field also remains. Superconducting magnets can produce highly homogeneous magnetic fields because they do not require an external power source so do not inherit any physical vibrations or fluctuations in the supplied electric current. The one limiting requirement that these magnets do have is that their magnetic coils are maintained at liquid helium temperatures, of around 4.2K, in order to retain superconductivity. This practical consideration results in physically large magnets. For many NMR experiments the magnetic fields needs to be highly homogeneous. If a strong but inhomogeneous field is applied broad lines are seen in the resulting NMR spectra because the resonances Larmor frequency (ω) depends on B_0 ($\omega = \gamma B_0$) which will be different for spins in different parts of the sample.

Once a sample is placed within the applied field of an NMR spectrometer the spins' bulk magnetisation vector will begin to relax with T_1 towards a new equilibrium with polarisation following a Boltzmann distribution according to the temperature and field. All NMR experiments consist of at least two components. Firstly, one or more radio frequency pulses are applied to the sample. Secondly, the spectrometer's receiver is opened and a signal is acquired. An NMR experiment may involve arrangements of multiple pulses to manipulate spin states, including delays and repetitions of the pulse sequence. A radio frequency pulse is applied as an oscillating field by a radio frequency coil of a probe inside the magnet. This oscillating field induces spin precession if its frequency matches the precession frequency of the spins (γB_0). Although the induced field strength is very small when compared to the applied static field (B_0), it has the effect of causing nutation of the spin ensemble. This causes a rotation around the induced field as well as the applied field giving a spiral path of motion.

In the same way as an applied RF pulse causes a rotation of the bulk magnetisation vector in a spin population, the precession of the spin ensemble induces an oscillating current in the receiver coils of the NMR spectrometer's probe. In the spectrometer this oscillating current is amplified, digitised and recorded. NMR signals are very weak owing to the small population difference between α and β states leaving only an excess of 7.2×10^{-5} proton spins in α vs β at room temperature and 21.1 T (900MHz Larmor frequency for protons). However, NMR spectra are highly reproducible allowing averaging of multiple identical scans of an experiment. Because the noise signal is random, it will average with the square root of the number of scans while the actual signals will add linearly. The resulting increase in the signal to noise ratio is given by the square-root of the number of scans averaged. The data recorded is often referred to as a "FID" or a free-induction-decay because the signals are recorded by induction of a signal without any active trigger and they decay with the transverse relaxation time of the spins.

Modern NMR spectroscopy typically uses quadrature detection to obtain complex data. This can in principle be achieved with the receiver coils placed at an angle of 90°. In practise the complex signal is generated by subtracting reference signals with alternating phase. The NMR spectrometer includes an analogue-to-digital converter (ADC) to generate digital data from the analogue signal acquired by the receiver. Many spectrometers also use fast ADC converters which digitise complex

data with massive oversampling using digital filters to further improve signal quality.

2.1.6 The Fourier transform

In a raw format the FID data from an NMR experiment it is very difficult to identify individual component waveforms. In order to visualise the data in the form of a spectrum it needs to be converted into the frequency domain by Fourier Transformation (FT). A Fourier Transform is essentially a mathematical procedure that converts oscillatory data from a time domain into a frequency domain.[14] Richard R Ernst was awarded a Nobel prize in 1991 for his work on FT-NMR[17].

For a signal containing just one resonance the complex detected signal can be described as:

$$s\left(t\right) \sim e^{(i\Omega_0 - \lambda)t} \tag{2.12}$$

For multiple signals this becomes

$$s\left(t\right) = \sum_l s_{l(t)} \tag{2.13}$$

or,

$$s(t) = e^{i\Omega_L t}e^{-t/T_2} \tag{2.14}$$

Where $\lambda = T_2^{-1}$ and Ω_L is the Larmor frequency. The Fourier Transformation integrates the signal according to:

$$S\left(\Omega\right) = \int_0^\infty s\left(t\right)e^{-\Omega t}dt = \int_0^\infty e^{-i(\Omega_L - \Omega)t}e^{-t/T_2}dt \tag{2.15}$$

Both the time domain signal, $s\left(t\right)$, and the frequency domain spectrum, $S\left(\Omega\right)$, are complex functions. Both the real and imaginary parts of the signal are required to produce both parts of the spectrum. The real and imaginary parts of the spectrum are described by:

$$Re[S(\Omega)] = \frac{\lambda}{(\Omega - \Omega_L)^2 + \lambda^2} \tag{2.16}$$

$$Im[S(\Omega)] = -\frac{\Omega - \Omega_L}{(\Omega - \Omega_L)^2 + \lambda^2} \tag{2.17}$$

.

2.1.7 Chemical shift

The Larmor frequency of a given spin is primarily determined by the strength of the magnetic field it experiences ($\omega_0 = \gamma B_0$). For protons in a 11.75T magnet this frequency is approximately 500MHz. However, in typical NMR spectra of molecules with multiple protons, several resonances with slightly different frequencies are usually seen. These small variations in frequency arise from the local magnetic environment of different nuclei. This variance in local magnetic environment arises from the electronic environment surrounding the spins which can shield or de-shield the magnetic field ($\Omega_L = \gamma(B_0 - \sigma)$). The Larmor frequency is exhibited in an NMR spectrum as 'Chemical Shift'. This is a representation of the Larmor frequency that is consistent independent of the applied field so allows a fair comparison for a given sample on different NMR instrumentation. In an NMR experiment a reference sample is normally used to calibrate the measurements. The chemical shift is determined by dividing the difference in frequency from the reference sample by the operating frequency of the magnet for the isotope in question (i.e. 500MHz for an 11.7T magnet observing protons).

A higher electron density near the nucleus will cause a spin to be more shielded leading to an increased chemical shift ('down-field shift'). In the vicinity of more electronegative groups de-shielding is observed leading to a smaller chemical shift. This is exemplified by the effect of aromatic ring currents on the chemical shifts of protons either inside or outside of the aromatic ring. If an aromatic ring is perpendicular to the external field a current is induced in the π electrons as a result of Ampère's law which says that a magnetic field is proportional to the electric current that provides its source and vice-versa. The aromatic ring current in turn induces a magnetic field around the ring structure. Because of this field any protons on the outside of the ring are de-shielded, giving a greater chemical shift, because the ring induced field acts in the same direction to the external field. Conversely, protons on the inside of an aromatic ring are shielded and show a lesser chemical shift. The application of NMR in analytical chemistry depends largely on the chemical shift phenomenon. This is because the chemical shift information can allow assignment of each nucleus to its unique position in a chemical structure (see Figure 2.5).[14]
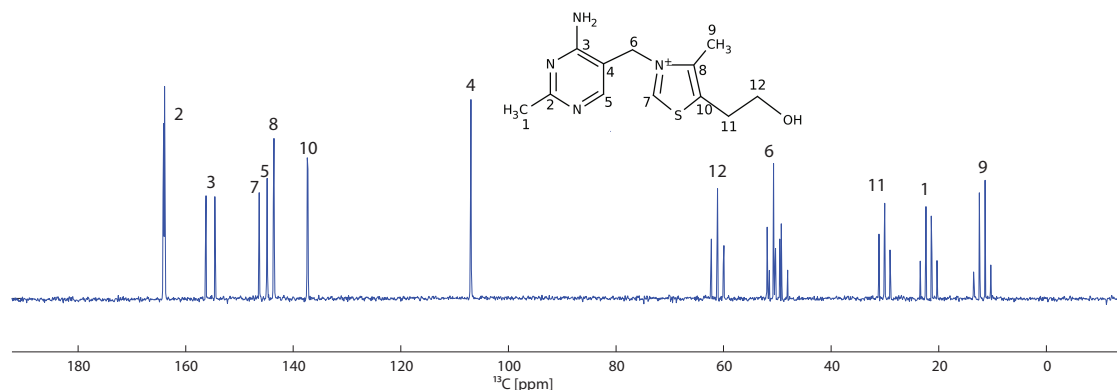
Figure 2.5: A ^{13}C-NMR spectrum of thiamine with assignments of resonances indicated on the structure. The spectrum also shows line multiplets arising from ^{13}C-^{1}H scalar couplings as it has been recorded without decoupling.

2.1.8   Scalar couplings

Another feature of NMR spectra is highlighted in figure 2.5. Scalar couplings between nuclei facilitated by the chemical bonds between atoms cause the splitting of lines into multiplets. This is because the chemical shift of an individual spin depends on the state of coupled spins. For spin $^{1}/_{2}$ nuclei there are two possible states, (α and β) which affect the resonance frequency of other spins through scalar couplings. For example for a ^{13}C atom bound to one single proton the resonance in the ^{13}C-NMR spectrum will be split into a doublet of signals with approximately equal intensity and vice-versa for the proton resonance. The intensity of the individual multiplets depends on the frequency of a given bonded state. This therefore gives a measure of polarisation for the attached spin. The size of the splitting, as described by the scalar coupling constant J , depends on the strength of the coupling between nuclei. The distribution of the peak heights for a split line is determined by the polarisation of the coupled spin. If more than one spin $1/2$ atom is chemically bound further splittings are observed, resulting in a 1:2:1 triplet for two other spins, a 1:3:3:1 quartet for 3 other spins. In more generalised terms a binomial distribution of signals is obtained that follows Pascal's Triangle. The relative intensity of one line of a multiplet follows $^{n}C_{r}$. That is for the r'th line in the multiplet multiplet for a nucleus split by n other scalar coupled nuclei the intensity is,

$$^{n}C_{r} = \frac{n!}{(n-r)!r!}!$$
(2.18)

The scalar coupling (with coupling constant J) is a result of an indirect coupling between nuclei via the bonding electrons. The coupling is indirect because it is mediated by the electrons in a chemical bond. The electrons in a bond can be considered a superposition of an up-down and down-up state. A bonding nucleus can interact with the electron through a hyperfine interaction and has the effect of causing the electron closest to the nucleus to adopt the same polarisation as the nucleus. For a second nucleus, if the nuclear spin is antiparallel to the first nucleus, a fairly low energy state results because the electronic spins are also antiparallel. If the nuclei have the same polarisation state, they are parallel, then the electrons are forced to adopt a higher energy configuration. It is the energy of this coupling that is the J coupling value and as only discrete energies are possible this is exhibited as a multiplet in an NMR spectrum.

The size of the J coupling constant depends on molecular orientation and the isotopic identity of the coupled nuclei; whether there is a homonuclear or heteronuclear coupling. A good example of a situation where the orientation dependence of J coupling values is used comes from protein structure determination. The ^3J coupling between an amide proton and a C_α proton has a variable "Torsional Angle" and as this angle changes so does the respective ^3J coupling value. As the torsional increases the ^3J coupling value follows a sinusoidal pattern and this "Karplus relationship" can be used to estimate bond angles and hence assist in the process of protein structure determination[18].

2.1.9 Dipolar couplings

Dipolar couplings arise from interactions between nuclei through space without any need of a chemical bond. Dipolar couplings are large in solids but average out in solution, at least for molecules with sufficiently fast rotational tumbling. Dipolar couplings are used in solid-state NMR to transfer polarisation between nuclei. Dipolar couplings are also used in liquid state NMR to determine inter-nuclear distances.[14]. Dipolar interactions can be the cause of relaxation effects. For example, the nuclear Overhauser effect (NOE) arises from dipolar couplings between spins which perform pairwise spin flips. For a dipolar-coupled system comprising two nuclei there are four possible states as depicted in the Solomon diagram in Figure 2.6. Also shown are the possible transitions and their probabilities. The transitions W_1 and $W_{1'}$ show the likelihood of individual transitions. The transitions W_0 and W_2 correspond to coupled transitions where both nuclei make a

simultaneous spin-flip. If the system is irradiated with a frequency of ν_e (the electronic Larmor frequency) the transitions 4→2 and 3→1 occur leading to an imbalance in the coupled populations. Here, states 1 and 2 are overpopulated and states 3 and 4 are underpopulated. This shift in equilibrium is counteracted by an increase in relaxation. As the nuclei are coupled the transitions W_0 and W_2 occur. The probability per unit time of these transitions are:

$$W_0 = \frac{1}{10}b_{IS}^2\mathcal{J}(\omega_I^0 - \omega_S^0) \tag{2.19}$$

$$W_2 = \frac{3}{5}b_{IS}^2\mathcal{J}(\omega_I^0 + \omega_S^0) \tag{2.20}$$

where $\mathcal{J}$ is the spectral density function describing the distribution of power with frequency and the dipole-dipole coupling constant b_{IS} is:

$$b_{IS} = -\frac{\mu_0}{4\pi}\frac{\gamma_I\gamma_S\hbar}{r^3} \tag{2.21}$$

It is through this route that an induced spin-flip and a coupled transitions can cause the coupled spin population density to be affected. For the nuclei the transitions 2→3 and 1→4 lead to nuclear polarisation enhancement as depicted in Figure 2.6. Initially the states 3 & 4 are more populated that 1 & 2. On irradiation with a frequency resonant to the S spin the populations of 1 & 3 and 2 & 4 become equalised. Now the system will seek to reestablish an equilibrium but paired spin-flips, so-called "Flip-Flop" and "Flip-Flip" transitions, are more likely than single spin flips. This leads to the transitions 1→4 and 2→3 having probabilities per unit time of W_0 and W_2 respectively. The net result is an increase in polarisation at 3 or 4. The NOE is important to transfer polarisation between nuclei for structural elucidation and the more general Overhauser Effect is also the basis for dynamic nuclear polarisation (DNP).

2.1.10 Multidimensional NMR

Despite ^{13}C signals being well dispersed across a range of chemical shift values they often overlap. In order to separate these overlapping signals a second or higher dimension is introduced to
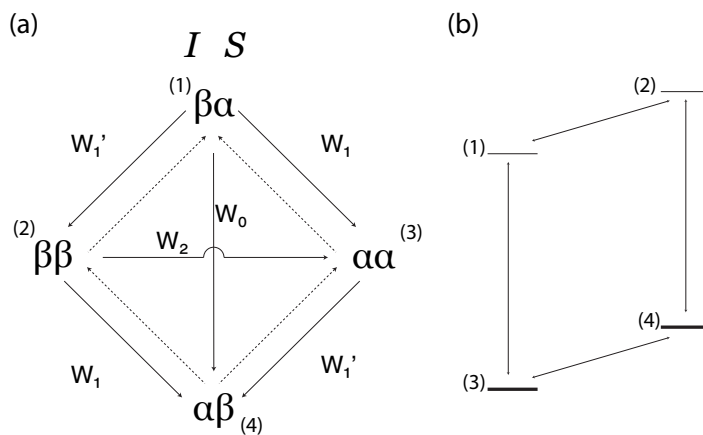
Figure 2.6: (a) Solomon diagram showing the possible transitions in a dipolar coupled system. (b) The transitions irradiated in a Nuclear Overhauser Enhancement and the resulting populations depicted by the strength of the lines.

the experiment by incrementing one parameter, such as a chemical shift or coupling, evolution between two nuclei. If such spectra yield a sinusoidal evolution of a parameter with successive increments[19,17] a Fourier transformation can be performed in this second dimension to transform both dimensions into the frequency domain. This can also be extended to multiple dimensions with several parameters being varied. In many 2D spectra the second dimension evolves a chemical shift of another nucleus which is either in a scalar or dipolar coupling to the directly observed nuclei. In this way 2D spectra provide information about scalar networks ("Total Correlation Spectroscopy" - TOCSY), through space interactions ("Nuclear Overhauser Effect Spectroscopy" - NOESY) or heteronuclear chemical shifts ("Heteronuclear Single Quantum Coherence" - HSQC, "Heteronuclear Multiple Quantum Coherence" - HMQC). Three-dimensional spectra which form the basis for NMR protein structure determination work in the same manner by spanning a third independent dimension.[14,19,17,20]

Most multi-dimensional NMR experiments record a series of independent spectra but a special class of multidimensional spectra use alternative secondary dimension encoding methods such that only a single scan is required. This may, for example, be achieved by encoding frequency in spacial dimensions using a CHIRP pulse to allow a single chain of echoes in the FID to decode the multidimensional spectral information. Alternatively an RF pulse that corresponds to a small flip

angle may be used with a pulse sequence that allows only a small amount of the total magnetisation to be used in successive scans. This way these successive scans can be rapidly acquired consecutively without a relaxation delay between each.

2.2 Hyperpolarised NMR

2.2.1 Introduction

The greatest limitation of NMR has always been its lack of sensitivity. Historically the most successful measures to increase the sensitivity of NMR have been the introduction of FT-NMR vs CW-NMR[17], the steady increase of magnet and spectrometer technology giving higher fields, along with higher sensitivity receivers etc. and more recently the introduction of cryogenically cooled probes[21,22,23] as well as the use of stable isotopic enrichment. In CW-NMR it is important not to saturate the sample so only a small proportion of the polarisation can be used. In FT-NMR short high-power pulses are used that act on the entire population giving a much greater available signal. High magnetic fields increase the polarisation of the nuclear spins increasing the available signal in the NMR experiment. Cryogenically cooled probes reduce instrument noise and subsequently cause the signal-to-noise ratio to be increased without increasing the actual signal. For ^{13}C NMR the natural abundance is only $\sim 1\%$ with the remainder the NMR-inactive ^{12}C isotope. If a substrate is synthesised to incorporate a higher proportion of ^{13}C there will be proportionally more spins active in the experiment and hence more signal.

While some of these methods, such as higher magnetic field strengths, increase the signal intensity it is the hyperpolarisation methods that yield the most dramatic and significant enhancements of up to four orders of magnitude[13]. Hyperpolarisation methods can also be combined with other signal enhancement methods to obtain the best possible signal-to-noise ratios.

Abragam and Goldman[24] start their 1982 article on DNP with the following statement:

> Legend has it that when Kammerling Onnes liquefied helium, he predicted that henceforth every experiment in physics could be repeated by adding the condition "at low temperature". The same had been said of Bridgman with "At high pressure". For experiments where atomic nuclei play a part, a similar addition could be "with polarised

nuclei"...

In practise there are a number of issues that can complicate hyperpolarisation experiments. A number of different hyperpolarisation methods exist and their use can open new avenues of investigation that would otherwise not be available, such as the measurement of intermediate states in a chemical reaction or the flux of a metabolite. Even without increasing the amount of information that we have about the underlying mechanisms in a given system, the increased signal intensity can allow experiments to be performed much more rapidly than otherwise because of a reduction in the number of repetitions required to gain a sufficient signal to noise ratio.

The low sensitivity of NMR arises from the small energy difference between the α and β state and the consequently small difference in the two populations at normal operating temperatures. From equation 2.7 it is apparent that polarisation increases with the static magnetic field strength and decreases as temperature increases with temperature. Figure 2.2 shows the nuclear polarisation of electrons, protons and carbon nuclei according to equation 2.7 in a fixed magnetic field (3.35T) depending on the temperature. For protons at 3.35T decreasing the temperature from 300K to 1K results in an increase in polarisation of 300 fold. However, this still only amounts to 1ppm whereas for electrons the polarisation is approaching unity.

Hyperpolarisation methods increase the nuclear polarisation level and therefore the signal intensity. These methods can also be combined with other methods to obtain the best possible signal-to-noise ratios.

2.2.2 Cooling

One relatively simple route to achieve hyperpolarisation, as briefly mentioned above, is to cool the sample to extremely low temperatures, for example to within the millikelvin range. At these temperatures the Boltzmann distribution results in a very large polarisation. For protons in a magnetic field of 11.7T (500MHz proton frequency) the polarisation reaches 83.2% at 10mK. This method is very simple but there are some practical considerations in the cooling of samples to these exceptionally low temperatures that make this approach difficult to implement for nuclei; in particular the performance of high resolution NMR on ultra-cooled samples. Also, as biological samples will freeze below 273K this method is poorly suited to liquid state NMR of biological

samples.

2.2.3   Dynamic Nuclear Polarisation (DNP)

The first true hyperpolarisation method to be reported was dynamic nuclear polarisation (DNP). The concept of DNP was originated by Albert Overhauser in 1953 and essentially provides a mechanism whereby polarisation can be exchanged between two coupled spins by irradiation with a specific frequency[25,26,13]. In the case where one partner is a proton and the other is an electron (typically from a stable radical) there is a significant difference in the polarisation state of the populations. When exchange is induced the lesser polarised nuclear population gains the greater polarisation of the electrons. The earliest form of DNP required that the radical and polarisation target be in solution with irradiation at the electronic frequency[25]. This has been extended into so-called 'Flow DNP' where a sample is pumped through an irradiation chamber[27]. DNP has also been performed in the solid state using a variety of radicals. TEMPO and its derivatives have been widely used to polarise protons with MAS by Griffin et al. and this group has refined the method to use a specific effect to maximise polarisation with a TEMPO biradical[28]. Colder still, at $\approx$ 1K ^{13}C resonances have been polarised with trityl radicals before dissolution with a hot pressurised solvent and transfer to a high field liquid state NMR magnet in '*ex-situ*' DNP[13]. DNP can give very high polarisation enhancements and methodology is fairly well established with commercial polarisers available. The range of substances that can be polarised is broad but the sample has to be able to survive the rigours of the experiment. This can include being rapidly cooled, irradiated with microwaves, rapidly heated and a turbulent liquid state transfer process. In addition it is necessary to dope each sample with a stable radical (most often but not necessarily a trityl or TEMPO derivative) and this will change the composition of the sample Also, the sample must be presented in a matrix that forms a glass on cooling if ex-situ DNP is used. This is to prevent segregation of the sample and the radical on cooling due to crystal formation. Again, the practical consideration is that the experimental conditions can be altered artificially by this step and it is not always possible to find a suitable glassing solvent system. DNP is arguably the most successful hyperpolarisation method developed to date and is described in much greater detail in the next chapter[13,28,3,1,29].

2.2.4 Optical pumping

Another approach used to achieve nuclear hyperpolarisation is optical pumping[30,31,32]. This is commonly used to hyperpolarise ^{3}He or ^{129}Xe for medical imaging applications. Optical pumping hyperpolarisation can be achieved by two methods: spin-exchange optical pumping (SEOP)[33] and metastable-exchange optical pumping (MEOP)[34]. In SEOP circularly polarised laser light at a frequency tuned to the frequency of a valence electron of a vaporised alkali metal is used to induce the polarisation. The alkali metal rubidium, with a wavelength of 794.8nm, is commonly used because it readily forms a gas, has only one valence electron and is high abundance (72% ^{85}Rb, 28% ^{87}Rb; both active). The circularly polarised laser polarises the valence electrons of the alkali metal and it is this polarisation that is transferred to the nuclear spins of the noble gas on collision with the alkali metal[35]. In MEOP the alkali metal intermediate is not required as the noble gas is polarised directly via a metastable $1s2s^3S_1$ noble gas state. SEOP is by far the most frequently used method to achieve hyperpolarised gases by optical pumping, with MEOP hardly used at all due to it's low efficiency. The most common application of optical pumping is to use the hyperpolarised gas to image cavities[36]. ^{129}Xe has the advantages that it is soluble in blood and the longitudinal relaxation rates are extremely slow at low temperatures allowing pre-polarisation and storage of solid hyperpolarised ^{129}Xe[37]. In a medical context this is very convenient for lung imaging and can show the location of tumours. Owing to xenon's solubility in blood it is also possible to introduce hyperpolarised xenon into the circulatory system to image the vasculature and organs such as the brain.

2.2.5 Chemically induced dynamic nuclear polarisation (CIDNP)

An alternative route to hyperpolarisation is known as "Chemically Induced Dynamic Nuclear Polarisation" (CIDNP). This method follows the same mechanism as biological photosynthetic centres. The DNP part of the name is a historical relic from the mechanism originally thought to lead to the effect[38]. CIDNP is an important tool in the study of radical and photo-chemistry and is exemplified by the photosynthetic flavin system.

The original work that lead to the discovery of CIDNP was the thermal decomposition of dibenzoyl peroxide in cyclohexanone[39,40,41,42]. When dibenzoylperoxide is heated it decomposes to
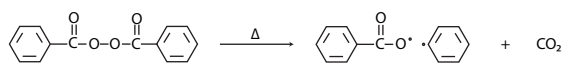
Figure 2.7: Dibenzoyl peroxide decomposes to form a benzoyloxy radical, a phenyl radical and release CO_2 on heating.

form two radicals, which remain temporarily coupled, in the form shown in Figure 2.7. As a result the NMR spectrum shows an enhanced emission signal for the benzyl radical.

There are two effects that can lead to the type of enhancement seen. The "Net Effect" is an enthalpic process that results in enhanced absorption or emission signals. The "Multiplet Effect" sees enhancements of anti-phase multiplets. Because the radicals have formed from the breaking of a chemical bond the coupled state is a singlet, with the two electrons 180° out of phase. In this form the radicals are able to recombine, reforming the original bond, but as the Larmor frequencies of the two radical electrons are slightly different they precess at slightly different frequencies until such a time as they are in phase to form a triplet state (see Figure 2.8). When an attached proton is considered there are two possible variants. Either the experienced field for the electron is increased by an β proton spin, or decreased by a proton α spin. Radicals attached to a proton β spin precess slightly more rapidly than with a α spin so a triplet state is reached earlier where the attached proton is in the β state. As the radical with the α form of the proton remains as a singlet for a greater time it is more likely to recombine to the original molecule. The net result is that the the benzene radical product has a higher population of β protons than α leading to the enhanced signal seen.

The observable magnetisation of a radical pair CIDNP reaction is given by:

$$(bI_{1y} + cI_{2y})sin\alpha + d(I_{1z}I_{2y} + I_{1y}I_{2z})sin2\alpha \tag{2.22}$$

where the b and c contribute to the Net Effect and d, the Multiplet effect[43]. CIDNP can be a very powerful technique but is limited in terms of the molecules that it can be used to study making it quite a specialised method.

Figure 2.8: (a) Radical electron pairs are initially in a singlet state after the chemical bond is broken. (b) As the two radical electrons precess at different frequencies due to the Zeeman splitting of the attached proton a triplet state can result.

2.2.6 Parahydrogen induced polarisation (PHIP)

Yet another route to achieve an enhancement in the nuclear spin polarisation utilises the properties of molecular hydrogen; "Parahydrogen Induced Polarisation" (PHIP)[44,45,46,47,48,49]. Diatomic hydrogen can exist in two possible states; ortho and para. In orthohydrogen the nuclear spins are parallel forming a triplet state. Conversely, the nuclear spins in parahydrogen are anti-parallel forming a singlet state. The lifetimes of singlet states have been shown repeatedly[50] to be greater than the nuclear longitudinal relaxation times. A singlet state can be created artificially and used to store polarisation in a number of contexts so offers a useful tool in hyperpolarised NMR experimentation. By offering a convenient store of polarisation, however achieved, a singlet enables a species to be hyperpolarised and then stored or manipulated prior to the actual NMR experiment. Parahydrogen can be prepared in a number of ways but the most commonly used method is simply to cool molecular hydrogen where at ~4K there is 99.9% parahydrogen. Once prepared, parahydrogen can be stable at room temperature for months. Parahydrogen is inactive in NMR unless the symmetry of the molecular group is broken in some way. If a molecule, for example a barbiturate[51], is substituted with parahydrogen using a catalyst such as Wilkinson's catalyst[52] a product is formed in which the singlet state still exists. However, assuming that the product breaks the symmetry of the singlet, there will be a significantly enhanced signal available for NMR experiments. There are two common methods utilised to achieve this, both developed by Daniel Weitekamp; PASADENA[44] and ALTADENA[53]. The essential difference is that in PASADENA the reaction occurs inside the NMR magnet whereas in ALTADENA the reaction is carried out at low

field and the product is transferred adiabatically into the NMR magnet. Both methods have been shown to deliver high degrees of nuclear hyperpolarisation.

As with CIDNP, PHIP has limitations in the substances that can be successfully polarised. In certain circumstances it is possible to gain an enhancement via parahydrogen with only reversible exchange. In the NMR-SABRE method proposed by Ducket et al.[54], exchange with parahydrogen occurs via a metal complex at low field and has been shown to give strong enhancements of up to 800-fold for e.g. pyridine with an iridium complex. The iridium complex $[Ir(H)_2(PCy_3)(substrate)_3][BF_4]$ is formed on reaction of $[Ir(COD)(PCy_3)(MeCN)_3][BF_4]$ with parahydrogen and an excess of the desired substrate. The spin polarisation is passed from parahydrogen to the substrate enabling a hyperpolarised NMR to be performed. It is likely that a long lived singlet state is formed on the substrate enabling the polarisation to be stored for later use.

2.3 Dynamic nuclear polarisation

2.3.1 Introduction

The principle of dynamic nuclear polarisation (DNP) has been widely exploited to overcome the poor sensitivity inherent to NMR[55,26]. In DNP the high spin polarisation of an unpaired electron is transferred to an atomic nucleus by irradiation with a resonant electromagnetic wave. The unpaired electron may exist as a stable radical, as a free electron in a conductor or as a result of an irregular crystal lattice. The electronic spin polarisation is higher than the nuclear spin polarisation at any given temperature and magnetic field (see Figure 2.2). This is because the polarisation is dependent on the gyromagnetic ratio of the spins in question, which for electrons is approximately three orders of magnitude higher than that of nuclei. DNP was first theorised by Albert Overhauser in 1953 in his PhD thesis[25]. Several notable scientists of the time described the effect as "thermodynamically improbable" but proof that Overhauser was correct was gained by Carver and Slichter in the same year[56]. The process described was a time-dependent cross relaxation effect, now generally known as an Overhauser effect; although this effect is better known in the context of the "Nuclear Overhauser Effect", (NOE). For the Overhauser effect to occur paramagnetic centres must be present and must be capable of motion on a suitable timescale. Where the Overhauser effect is active the enhancement

maximum occurs where the irradiation frequency equals the electronic Larmor frequency.

Where paramagnetic centres are incapable of motion the Overhauser effect cannot occur but additional time-independent mechanisms have been described that operate through different pathways. In these non-Overhauser effect DNP mechanisms it is the energy of a coupling between two or more spins that is irradiated rather than one spin directly. Where these processes occur there are generally two irradiation frequency enhancement maxima, one either side of the electronic Larmor frequency.

DNP has been shown to be a very powerful technique with enhancements on the order of tens of thousand fold achieved[13]. It has been applied to the creation of spin frozen targets (where a highly polarised state is prepared and stored such that the polarisation is retained for an extended period) for neutron scattering[57], in the study of diamonds[58] and coal[26], in the investigation of amyloid fibril structure[2] and to create contrast agents for imaging of cancer metastases[59]. Although there are clearly a very wide range of applications of DNP a thorough understanding of the physics involved is essential to the design of experiments that can successfully utilise the full potential of DNP.

2.3.2   Theory

2.3.2.1   Coupled electron-nuclear systems

A general Hamiltonian for an interacting electron-nuclear system is given by:

$$H = -\omega_e S_z - \omega_n I_z + H_{nn} + H_{en} + H_{ee} \tag{2.23}$$

The first two terms describe the interaction of the electronic and nuclear Zeeman systems with the external magnetic field. The last three terms describe the spin-spin interactions. DNP is concerned with the electron-nuclear spin-spin interaction described by H_{en}. This term can be further divided into an isotropic part and an anisotropic part. The isotropic part, H_{en}^{iso}, corresponds to electrons in spherical s orbitals whereas the anisotropic part, H_{en}^{aniso}, corresponds to electrons in non-spherical p, d & f orbitals according to spherical harmonics. These parts are given by[26]:

$$H_{en}^{iso} = \sum_{i,j} a_{ij} I_i \cdot S_j = \sum_{i,j} \frac{1}{2} a_{i,j} (I_i^+ S_j^- + I_i^- S_j^+) + I_z^i S_z^j \tag{2.24}$$

$$H_{en}^{aniso} = \sum_{i,j} \frac{\gamma_e \gamma_n \hbar}{r_{i,j}^3} (A_{ij} + B_{ij} + C_{ij} + D_{ij} + E_{ij} + F_{ij}) \tag{2.25}$$

$$A_{ij} = (1 - 3cos^2\theta_{ij})I_z^i S_z^j \tag{2.26}$$

$$B_{ij} = -\frac{1}{4}(1 - 3cos^2\theta_{ij})(I_i^+ S_j^- + I_i^- S_j^+) \tag{2.27}$$

$$C_{ij} = -\frac{3}{2}sin\theta_{ij}cos\theta_{ij}e^{-i\phi_{ij}}(I_z^i S_j^+ + I_i^+ S_z^j) \tag{2.28}$$

$$D_{ij} = -\frac{3}{2}sin\theta_{ij}cos\theta_{ij}e^{i\phi_{ij}}(I_z^i S_j^- + I_i^- S_z^j) \tag{2.29}$$

$$E_{ij} = -\frac{3}{4}sin^2\theta_{ij}e^{-2i\phi_{ij}}I_i^+ S_j^+ \tag{2.30}$$

$$F_{ij} = -\frac{3}{4}sin^2\theta_{ij}e^{2i\phi_{ij}}I_i^- S_j^- \tag{2.31}$$

Where r_{ij}, θ_{ij} and ϕ_{ij} are the polar coordinates of the vector between the position of the nucleus, i, and the position of the electron, j, averaged over it's orbital. This equation is valid if the anisotropic component of the electron-nuclear interaction is symmetrical perpendicular to the vector of the electron-nuclear dipole. When irradiation around the electronic Larmor frequency is performed, a coupled electronic and nuclear transition can occur leading to enhancement of the nuclear population,Wind et al.[26]. The exact frequency maximum and nature of the enhancement depends on the electron-nuclear coupling and the time dependence on the interaction. As the electronic relaxation is very fast[60] compared to the nuclear relaxation there is a generally constant pool of cold electrons to drive the polarisation of the nuclei.

2.3.2.2 The Overhauser effect

For a coupled electron-nuclear system, represented by H_{en} in equation 2.2, there are four possible states as depicted in the Solomon diagram in Figure 2.9a. As with the Nuclear Overhauser Effect described above the transitions W_1 and $W_{1'}$ represent the probability of individual electronic

or nuclear transitions. The transitions W_0 and W_2 correspond to coupled transitions where both the electron and nucleus make a simultaneous spin-flip. On irradiation with a frequency of ν_e the transitions 4→2 and 3→1 occur leading to an imbalance in the coupled populations. In this instance, states 1 and 2 are overpopulated and states 3 and 4 are underpopulated. This shift in equilibrium is counteracted by an increase in relaxation. As the electron and nucleus are coupled the transitions W_0 and W_2 occur. The probability of these transitions are:

$$W_0 = \frac{1}{10} b_{IS}^2 \mathcal{J}(\omega_I^0 - \omega_S^0) \tag{2.32}$$

$$W_2 = \frac{3}{5} b_{IS}^2 \mathcal{J}(\omega_I^0 + \omega_S^0) \tag{2.33}$$

Where the dipole-dipole coupling constant b_{IS} is given in equation 2.21 and the $\mathcal{J}$ functions sample the spectral density giving the power available for the given frequency. The spectral density is derived from the correlation function. That is the function that describes the correlation between the motional separation of the two spins. If the correlation of spin orientations decays with an exponential function then the spectral density will be the Fourier transform of the decay function; a Lorentzian. It is through this route that an induced spin-flip and a coupled transition can cause the coupled spin population density to be affected. The transitions 1→4 and 2→3 lead to nuclear hyperpolarisation as described in section 2.1.9 and depicted in Figure 2.9b.

The same process can occur in a coupled nuclear-nuclear system. In this context the effect is known as the "Nuclear Overhauser Effect" and is far more well known than the electron-nuclear case. "Nuclear Overhauser Enhancements" or NOE's are used in liquid state NMR to indicate distance as the strength of an Overhauser enhancement decreases with the inter-spin distance r^{-6} due to the b_{IS}^2 terms of equations 2.32 and 2.33 and the r^3 term of equation 2.21. For DNP utilising the Overhauser effect the implication of this is that the radical and polarisation target molecule must be in close proximity for the enhancement to be significant.

In the DNP case, as these transitions require an exchange of quanta, they are only active where H_{en} is time dependent on a timescale comparable to ν_e. This is usually as a result of motion in the
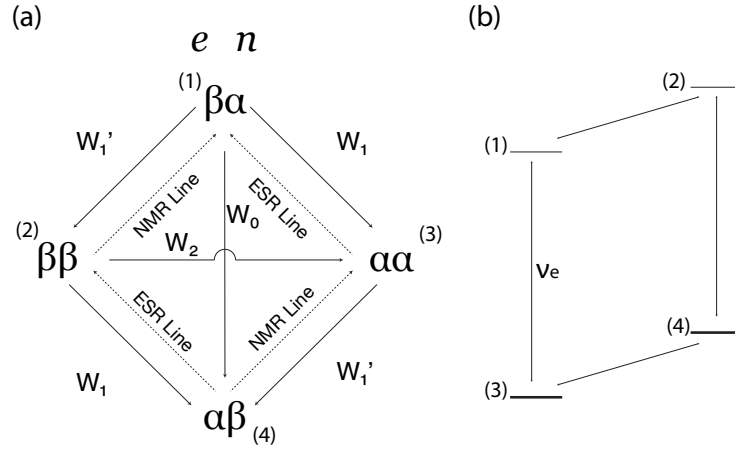
Figure 2.9: (a) Solomon diagram showing the possible transitions in a coupled electron-nuclear system. (b) The transitions irradiated in an Overhauser enhancement (W_1 in (a)) and the resulting populations depicted by the strength of the lines.

system but can also arise from relaxation effects in the electronic system. Consequently, where there are mobile paramagnetic centres the Overhauser effect can occur with a polarisation maximum at an irradiation frequency equal to ν_e [61].

The electronic and nuclear systems can be coupled by dipolar or scalar couplings although in practise, owing to the motional dependence, the dipolar couplings are the primary coupling means. The signal enhancement factor, ϵ, for a nuclear spin, i, with radical electrons, j, is given by [62]:

$$\epsilon = \frac{<I_Z>}{<I_0>} = 1 - \rho f_S \frac{|\gamma_j|}{\gamma_i} \tag{2.34}$$

where $<I_0>$ is the equilibrium polarisation, the coupling factor, ρ, is the ratio of the electron-nuclear spin cross relaxation rate ($W_2 - W_0$ - from equations 2.33 and 2.32 respectively) and the nuclear spin relaxation rate due to the presence of unpaired electrons ($W_2 + 2W_1 + W_0$). This expresses the strength of the coupling between the electronic and nuclear spins.

$$\rho = \frac{W_2 - W_0}{W_2 + 2W_1 + W_0} \tag{2.35}$$

The leakage factor, f,

$$f = \frac{W_2 + 2W_1 + W_0}{W_2 + 2W_1 + W_0 + W^0} = 1 - \frac{T_1^*}{T_1} = \frac{kCT_1}{1 + kCT_1} \tag{2.36}$$

can be expressed in terms of the T_1 in the absence of the radical or T_1^* in the presence of the radical. Additionally the leakage factor can be written as a function of the concentration of the radical where C is the concentration of dissolved radical and k is the relaxivity constant[27]. The term W^0 describes the rate of depolarisation due to extrinsic factors such as those arising from the presence of radical.[61].

The saturation factor, s:

$$s = \frac{1}{n}\frac{\alpha P}{1 + \alpha P} \tag{2.37}$$

is a function of the irradiation power, P, that excites the electron spins, s. In this equation the term $\frac{1}{n}$ adjusts for the number of hyperfine ESR lines present for the radical. As only one hyperfine ESR line is usually excited this reduces the possible saturation accordingly. The α term describes the relaxation properties of the electrons.

2.3.2.3 The solid effect

If H_{en} is independent of time on a time-scale equivalent to ν_e, several different related effects can occur. The simplest such effect is termed the solid effect and occurs where the electronic spins do not interact significantly. If there is little inter-electron interaction in a given system H_{ee} is small and the ESR line is narrow. When irradiated with an appropriate frequency, this can lead to a well resolved solid effect. In the solid effect a paired spin-flip occurs between an electron and a nuclear spin, when the energy of the nuclear spin is approximately equal to the mismatch between the irradiation frequency and the electron frequency. Therefore, a maximal effect is seen with an irradiation frequency of $\omega_e \pm \omega_n$.

Paired spin-flips occur as a function of entropy. The Hamiltonian for a population of N spins I, all spin $^1/_2$, is given by:

$$\hat{H} = \hbar\omega_{0I}\sum_{i=1}^{N}I_z^i \tag{2.38}$$

where ω_{0I} is the nuclear Larmor frequency of I where there are eigenstates $|m_1>$ to $|m_N>$, where $m_i = \pm^1/_2$. Here the polarisation can be expressed as:

$$P = \frac{N_+ - N_-}{N} \tag{2.39}$$

Owing to significant degeneracy the number of eigenstates is given by:

$$\binom{N}{N_+} = \frac{N!}{N_-!N_+!} \tag{2.40}$$

where the left-hand term is a binomial coefficient. Using the Stirling approximation the entropy of a polarised spin population is given by[63]:

$$\frac{S}{NK_B} = \frac{1}{N} \ln\left(\frac{N!}{N_+!N_-!}\right) \approx \ln(2) - \frac{1}{2}\{(1+P_I)\ln(1+P_I) + (1-P_I)\ln(1-P_I)\} \tag{2.41}$$

where P_I is the nuclear polarisation and S is the entropy of the system. This shows that in effect a highly polarised population can be treated as having low entropy. This leads to paired spin-flips acting to minimise entropy and thus becoming energetically favourable.

Where H_{en}^{iso} and H_{en}^{aniso} are time independent the electron-nuclear system cannot be described purely by product states but by mixtures of other states. This is a result of the terms $I_i^+ S_z^j$ and $I_i^- S_z^j$ of equations 2.24-2.31. For a nucleus i in the state $|+>_i$ and a coupled electron j in the state $|->_j$, $(|+>_i |->_j)$, to mix proportional to $I_i^+ S_z^j$ a contribution of $q_{ij}|->_i |->_j$ is made where:

$$q_{ij} = -\frac{3}{4}\frac{\gamma_e \gamma_n \hbar}{\omega_n} \cdot \frac{1}{r_{ij}^3} \cdot sin\theta_{ij} cos\theta_{ij} e^{-\phi_{ij}} \tag{2.42}$$

.

Mixtures for $|->_i |+>_j$, $|+>_i |+>_j$ and $|->_i |->_j$ also exist so irradiation at a frequency $\omega = \omega_e \pm \omega_n$ induces a paired transition of a nucleus and an electron with a probability $W^\pm$. This is a forbidden transition with:

$$W^\pm = 2|q_{ij}|^2 \pi \gamma_e^2 B_1^2 g(\omega_e - \omega \pm \omega_n) \tag{2.43}$$

Additionally, the double quantum forbidden transition W_n^e equals:
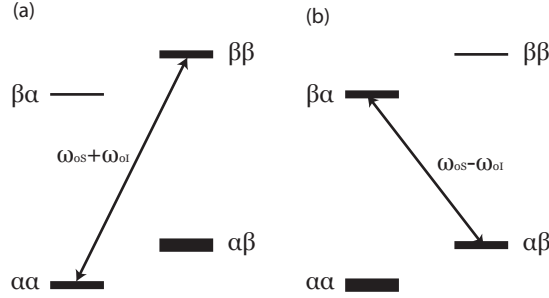
Figure 2.10: Cartoon showing the transitions irradiated and population enhancements in the solid effect.

$$W_n^e = 4|q_{ij}|^2 \frac{\omega_n^2 T_{1e}}{1 + \omega_n^2 T_{1e}^2} \tag{2.44}$$

where B_1 is the induced field due to RF irradiation and g is the lineshape function for a given frequency giving the probability of a transition for a specific frequency[64].

Both of these terms are proportional to $|q_{ij}|^2$ as they both depend on the same perturbation term so both frequencies can give rise to equally strong polarisations with opposite signs. A representation of these two cases with the transitions irradiated and the resulting polarisations is given in Figure 2.10.

When the ESR line is narrow the polarisation at high and low frequency occurs in two discrete regions with what is known as the "Well resolved Solid Effect". If the ESR line is broad a differential solid effect is seen[65,66,63]. This is, in effect, a summation of well resolved solid effects for each narrow band in the ESR spectrum. As each of the two DNP polarisation regions overlap they interfere destructively to give an overall polarisation profile as depicted in Figure 2.11b. The maximum enhancement here has a lower amplitude and does not necessarily occur with an irradiation frequency of $\omega_e \pm \omega_n$.

2.3.2.4 Thermal mixing

Where there is significant interaction between electrons in an electron-nuclear system, H_{ee} is large. In a radical the g-tensor is a measure of the distribution of a radical electron population in space. A greater deviation from a spherical distribution gives a greater g anisotropy. If the g anisotropy of the electronic system is small, only homogeneous broadening can occur in the ESR
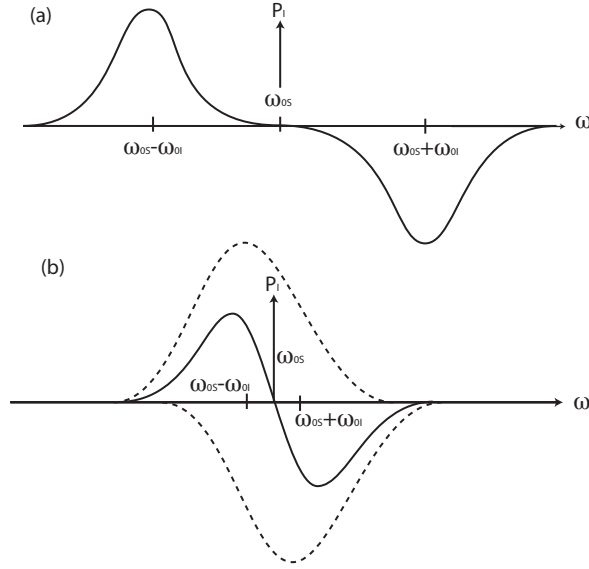
Figure 2.11: A representation of the polarisation enhancement with irradiation frequency for (a) the well resolved solid effect with two discrete polarisation regions, and (b) the differential solid effect where the dashed lines give the separate enhancement components and the solid line gives the resultant polarisation profile.

spectrum and thermal mixing can occur on irradiation with an off-resonance frequency. Unlike with the solid effect these transitions are allowed. As the ESR line-width broadens with the applied magnetic field the thermal mixing effect scales with B_0^{-1}. Thermal mixing occurs when multiple electrons are coupled implying that the effect is most efficient where a high concentration of electronic spins is present. This can be counteracted by unwanted paramagnetic relaxation effects at high radical concentrations.

Thermal mixing is often described by the thermal bath model as described by Provotorov[67]. This is possible because where multiple electrons are coupled they act as a pool rather than individually. In this treatment it is the electron bath that is in contact with the nuclear Zeeman system rather than individual electrons. Irradiation around the electronic Larmor frequency, ω_e, cools the electronic broadening system which is in thermal contact with the nuclear Zeeman system. There is also coupled relaxation as with the solid effect in this situation making the enhancement maximum more complex in shape. With this approach a few assumptions are made. Firstly, the ESR line is assumed to be homogeneously broadened. This assumption allows the electrons in the local field to be characterised by a single temperature, T_{ss}. Electrons in the external field are

described by the temperature T_z and, at equilibrium both T_z and T_{ss} are equal to the lattice temperature, T_L. These temperatures can be changed by irradiation with a given frequency, ω, where a proportion, $\hbar\omega_e$, is absorbed by the electronic Zeeman system and the remainder, $\hbar(\omega - \omega_e)$, is either absorbed or emitted by the electronic broadening system.

Unlike the case of the solid effect the transitions here are allowed. The treatment of this also deals with the electronic broadening system rather than the nuclear Zeeman system. This treatment was first made by Provotorov where the time dependence of polarisation within the electronic Zeeman system is given by:

$$\dot{p}_e = -W\left(p_e - \frac{1}{2}\beta\Delta\right) - W_e\left(p_e p_e^0\right)$$

and the broadening system by

$$\dot{\beta} = W\frac{2\Delta}{\omega_L^2}\left(p_e - \frac{1}{2}\beta\Delta\right) - W_D\left(\beta - \beta^0\right)$$

Where $W = \pi\gamma_e^2 B_1^2 g(\Delta)$, $\Delta = \omega - \omega_e$ and $\beta = \hbar/kT_{ss}$. From the static solutions obtained by Goldman[68,24] irradiation acts to enhance β, the inverse of the broadening system temperature. This is because where pure states are affected by a dipolar interaction:

$$\gamma_I\gamma_S\hbar^2 r^{-3}[I.S - 3(I.n)(S.n)] \tag{2.45}$$

mixed states form. For these mixed states only the flip-flop and flip-flip transitions can be affected by irradiation analogous to W_0 and W_2 transitions of the Overhauser effect.

A positive enhancement is attained where $\omega < \omega_e$ and a negative enhancement where $\omega > \omega_e$. As the electronic and nuclear systems are coupled in this situation energy conservation processes exist. Where the electronic flop-flop transitions yield quanta $\hbar\omega_n$, this energy can be conferred via the electron-nuclear interaction H_{en} leading to a polarisation of the nuclear Zeeman system.

The thermal mixing effect is not completely understood and is not as strong as the solid effect. However, it has been possible to polarise biological samples such as glycine and even acquire a DNP enhanced two-dimensional ^{13}C-^{13}C correlation spectrum of U-^{13}C,[^{15}N]proline through this effect[69].

2.3.2.5   The cross effect

The cross effect follows a similar principle to the thermal mixing effect. However, rather than irradiating a bath of electrons in a network, in the cross effect one specific electron pair is targeted. When the Larmor frequencies of the electron pair are separated by the nuclear frequency a three centred mechanism allows a coupled nuclear spin-flip that can ultimately result in polarisation enhancement of the nuclear spin population. This mechanism is dependent on inhomogeneous broadening in the electron system due to g anisotropy. A requirement for the cross effect to occur is that the difference in the electronic Larmor frequencies, $\delta > \omega_n$.

A stable bi-radical can be designed such that the g anisotropy leads to a separation in the electronic Larmor frequencies, $\Delta\omega_e$, exactly equal to a target nucleus. If the flip-flop transition is now irradiated a strong nuclear enhancement is seen with the effect maximum lying between the two electronic frequencies. Griffin et al. have performed these experiments with a bi-radical they have named "TOTAPOL"[28,70]. Unlike the case of the Thermal Mixing effect there is no dependence on a wide network of dipolar coupled electrons. Consequently a lower radical concentration can be employed and this means that the cross effect is not as susceptible to paramagnetic relaxation effects as thermal mixing. The cross effect does however scale as B_0^{-1} to the applied magnetic field in the same way as in thermal mixing.

2.3.2.6   Summary

In summary, the mechanism under which polarisation is generated by DNP depends on the experimental parameters:

2.3.3   Existing applications

2.3.3.1   Flow DNP

The mechanisms that can lead to DNP can be divided into two sub-categories depending on the mobility of the paramagnetic centres. If the paramagnetic centres are mobile compared to the nuclei on the timescale of ν_e then the Overhauser effect can be exploited. The group of H Dorn, of Virginia Tech, used a system as depicted in Figure 2.12a where an HPLC pump is used to pump a sample through a microwave cavity and past an immobilised TEMPO radical. The sample then passes into

Mechanism	Conditions	Irradiation frequency	Pros	Cons
Overhauser effect	H_{ee} time dependent on scale of ω_e^{-1}.	ω_e	Can be used with liquid samples.	Only one ESR line irradiated so where there are three lines only 1/3 of the total possible polarisation is achieved. Poor performance with broad ESR lines.
Solid effect	$< H_{en}^{iso} >$ is non-zero.	$\omega_e \pm \omega_n$	A simple, well defined effect.	Sensitive to high radical concentrations. A forbidden transition so needs high power.
Thermal Mixing	$< H_{en}^{iso} >$ is non-zero, large number of electrons with homogeneous ESR broadening.	$> \omega_e - \omega_n,$ $< \omega_e + \omega_n,$	Strong enhancements.	Required high radical concentration. Effect decreases as field increases with B_0^{-1}.
Cross effect	$< H_{en}^{iso} >$ is non-zero, $\Delta\omega_e \geq \omega_n$.	$\omega_e \pm \frac{\omega_n}{2}$	Strong enhancements with less power needed than thermal mixing.	Protons only. Availability of biradicals. Effect decreases as field increases with B_0^{-1}.

Table 2.1: Table summarising the different DNP effects with their irradiation frequencies and the pros & cons of each effect.
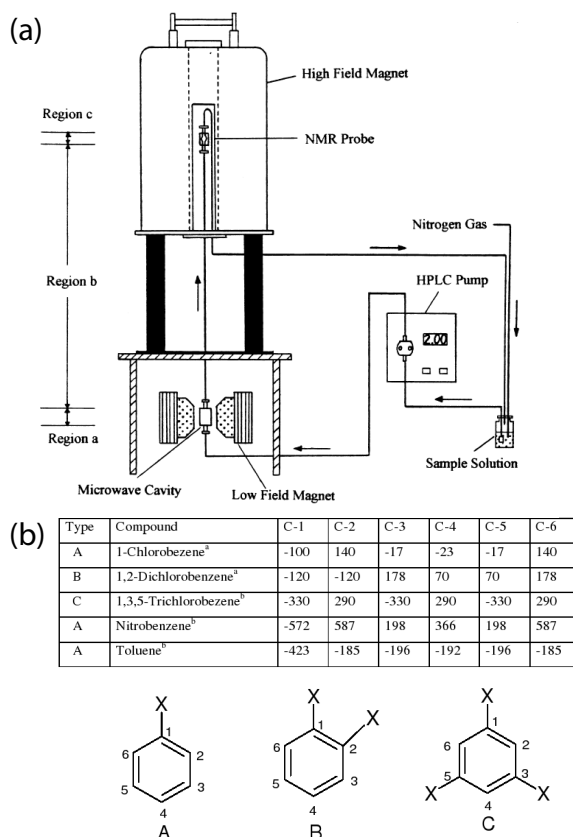
Figure 2.12: (a) The flow DNP apparatus of Dorn et al. (b) Examples of the enhancement values achieved for a number of substances. Adapted with permission from [1].

a high-field magnet for acquisition of a DNP polarised NMR spectrum [1]. An example of the results attained with this instrument are shown in Figure 2.12b where differential poly-substitution of benzene leads to varying polarisation at the ring protons.

More recently the group of S Han at the University of California in Santa Barbara have used a number of similar approaches to use polarised bulk water as a probe in varying contexts. They have reported that rather than the one-third of the total possible polarisation that would be expected, as only one in three ESR lines is irradiated, they see the full polarisation due to Heisenberg spin exchange between radical electrons. They have also attempted to use a tethered radical approach and have applied their polarised bulk water scheme to the study of micelle hydration amongst other things.

Figure 2.13: (a/b) EM image of amyloid fibril crystals. (c) 2D DNP spectrum attained. Adapted with permission from[2].

2.3.3.2   High field solid state DNP

A pioneer of DNP, Professor RG Griffin works with solid state sample cooled to around 100K and spun at the magic angle[71,72]. This temperature does not give the greatest Boltzmann polarisations of all DNP methods but it does allow magic angle spinning (MAS) probes to be used giving the ability to directly observe the polarised samples with relatively narrow line-widths[73,74]. Another advantage of this system is that a relatively high field magnet and high power microwave source, such as a gyrotron, can be used[69,75]. This gives a higher resolution spectrum and in combination with the use of their "TOTAPOL" TEMPO bi-radical, to utilise the Cross effect, strong DNP enhancements can be achieved[28]. An example of the application of this methodology is shown in Figure 2.13 where high resolution 2D DNP spectra were obtained in the study of amyloid fibrils.

Another approach taken by the Griffin group was to use the additional benefit of the Boltzmann polarisation by repeatedly cooling, polarising and melting the sample with a laser prior to spectrum acquisition[3]. This method is summarised schematically in Figure 2.14 and an example of the polarisation buildup seen with ^{13}C urea is shown. Other methodologies have also been employed such as polarisation in the nuclear rotating frame[76].

Figure 2.14: (a) A flow chart illustrating the experimental steps in the laser temperature-jump experiment. (c) The pulse sequence used in the laser temperature-jump experiment. (c) The buildup seen for ^{13}C urea with the laser temperature-jump method. Adapted with permission from[3].

2.3.3.3   *Ex-situ* DNP

In order to maximise the polarisation of the electrons participating in DNP many implementations of DNP are carried out at very low temperatures of around 1K[77,78,13]. At this temperature the electron polarisation approaches 100% so the greatest possible nuclear polarisation is possible through DNP. In order to apply DNP to biological systems the polarised samples must be heated to biologically compatible temperatures in a time frame that is much shorter than the nuclear longitudinal relaxation time (T_1) before acquisition as a normal liquid state NMR experiment. Such an implementation of DNP has been reported[13] where the sample is dissolved in a glassing agent[79,80] in the presence of a stable radical doping agent. The doping agent is usually a trityl radical which allows a strong solid effect due to their narrow ESR lines and the glassing agent ensures contact between the radical and the substrate. The sample is then cooled to ~1.1K in a 3.35T magnet and irradiated with microwaves at ~94GHz, tuned by sweeping the irradiation frequency through a range of values to determine the enhancement maximum. This frequency is approximately equal to the electronic Larmor frequency plus or minus the nuclear Larmor frequency. After irradiation for the desired time, usually one or more hours, the polarised sample is then

dissolved by the release of hot pressurised solvent from a pressure vessel to the sample to be delivered to a conventional liquid state NMR spectrometer for acquisition of an NMR spectrum. In addition to the DNP effect, extra polarisation enhancements arise from the jumps in temperature and magnetic field . These factors alone give an enhancement factor of ~65 in our system.

The highest enhancement factor reported with this DNP method to date is 44000 for urea where high resolution imaging of the rat cardiovascular system was performed[13]. The system has also been commercialised by Oxford Instruments Molecular Biotools Ltd.[29] (OIMBL), Tubney Wood, Oxon. as a product termed HyperSense™. This polariser is based on the work of Golman et al and is licensed from GE Healthcare for *ex-vivo* research. It is this instrument on which the work in this thesis has been carried out. Using this system pyruvic acid has so far been the most applied substance as it shows strong polarisations, has an exceptionally long longitudinal relaxation time constant and directly enters into cellular metabolism. A demonstration of the use of hyperpolarised pyruvic acid to monitor cellular metabolic flux was performed by Golman, Zandt and Thaning[78]. Here hyperpolarised pyruvic acid was injected into both rat and pig and the pyruvate, lactate and alanine signal intensities were monitored by magnetic resonance spectroscopy (MRS). This has been extended to the study of cancer metabolism where the pyruvate to lactate conversion process acts as a probe for tumour tissue due to the altered metabolism of cancer tissue first reported by Warburg[12]. This application uses the rapid conversion of pyruvate to lactate by lactate dehydrogenase (LDH) in cancer tissue. In healthy tissue this process only occurs rapidly in muscle tissue during exercise. Once injected the lactate signal rises where the LDH mediated process occurs indicating the site of tumour tissue. The exact results depend on the tissue and cancer type as metabolic rates vary but the location of metastases can be conferred to a surgical procedure.

In a further advancement of this methodology the flux of pyruvate to lactate has been used as a measure for chemotherapeutic agent efficacy[59]. Mice with artificially created lymphoma tumours were injected with hyperpolarised pyruvic acid and the pyruvate and lactate signals were monitored by MRS. The ratio of pyruvate and lactate was then determined at equilibrium. These mice were then treated with a chemotherapeutic agent; etoposide and, after a twenty-four hour delay, injected with hyperpolarised pyruvic acid. The pyruvate to lactate ratio was again determined. There was a significant drop in this ratio where the drug was effective in inducing apoptosis. This effect was

identified as being due to a loss of the co-enzyme NAD(H) in the apoptotic process.

Another application of this technology has been the combination of *ex-situ* DNP with an existing ultrafast 2D method[81]. This method lends itself to DNP experiments as the whole experiment is acquired in a single scan it is not susceptible to problems arising from the relaxing nuclear polarisation. The ultrafast 2D method itself uses a spatial frequency encoding for the indirect dimension similar to the method used in echo-planar imaging. Therefore each part of the sample contributes only to a particular frequency in the indirect dimension reducing the overall signal intensity. This makes the method relatively insensitive so the very large polarisation enhancements provided by DNP allow many more substances to be analysed. An example of this method applied to pyridine is illustrated by L Frydman and D Blazina[82].

2.4   Hindered quantum rotor effects

2.4.1   Introduction

While the rotation of bodies on a macroscopic scale can be described effectively by classical physics, the rotation of molecular groups has long been understood to exhibit quantum tunnelling behaviour. This is that, rather than following a continuous path, the constituents of a group 'hop' from one possible position to another by a series of quantum exchanges. Quantum tunnelling stems from the particle-wave nature of quantum entities such as electrons, photons or protons. This duality means that in some circumstances particle-like behaviour is seen while in others a more wave-like nature is exhibited. A consequence of this is that there is a probability or a particle-wave being positioned beyond a barrier that decreases with the size of the barrier. In the case of a molecular group where one substituent can occupy one of several discrete positions the wave-like behaviour of the molecular group allows an apparent hop from one position to another. The most studied case, and the subject of interest in this thesis, for a hindered molecular rotor is that of a methyl group. As a methyl group rotates it passes through increasing and decreasing energy positions. As the symmetry of the methyl group is three-fold a sinusoidal energy surface emerges with three potential energy maxima and three potential energy minima. In a classical interpretation, if the methyl group does not possess the required energy to surmount the potential energy maximum

then the methyl group will not rotate. However, because molecular groups are quantum entities it is quantum physics rather than classical physics that applies allowing the methyl group to tunnel through the barrier allowing a non-classical analogue of rotation. The rate of this tunnelling rotation is known as the tunnelling frequency.

Symmetry conversion within the rotational tunnelling system can lead to an exchange of energy that is well studied. The temperature jump dynamic nuclear polarisation (DNP) system developed by Golman et al.[13] and since commercialised by OIMBL[29] has been shown to lead to dramatic ^{13}C polarisations with enhancements on the order of tens-of-thousand fold. Certain samples polarise very well, however numerous substances and mixtures do not polarise efficiently. A common feature in spectra of samples where polarisation is reduced has been negative signals for methyl carbons of compounds used as glassing agents, such as dimethyl sulphoxide (DMSO), and other proton bearing carbons. This effect originates from a methyl dependent effect and must be considered for optimal DNP enhancement[10,11]. The polarising effect originates on methyl protons as a consequence of symmetry conversion of the tunnelling states of hindered quantum rotors such as methyl groups. At the operating temperature of the HyperSense™ instrument, <1.5K, proton T_1's are sufficiently long to allow nuclear Zeeman polarisation to accumulate. Spin diffusion within the proton network and dipolar cross relaxation then lead to a spread of polarisation to nearby protons and heteronuclei bringing about an observable impact in the spectra we acquire. For many of the substances that exhibit this behaviour cooling without irradiation induced DNP leads to a moderately strong negative enhancement of proton attached carbons in the substance on dissolution with hot pressurised methanol and transfer to a secondary high field NMR magnet. The buildup of this 'negative' polarisation follows a modified version of the model described by Haupt[5]. This mechanism has proven to be fairly universal where hindered rotor containing substances are cooled to very low temperatures. As a mechanism this provides a new stand-alone route to achieve sample polarisation.

2.4.2   Theory

2.4.2.1   Rotational tunnelling

Where rotating molecular groups are present in a sample at low temperature it is important to consider the impact that rotational tunnelling effects can have. Classical physics describes molecular

motions by the Arrhenius equation[83]:

$$k = e^{\frac{-E_a}{RT}} \tag{2.46}$$

where k represents the probability of a given transition occurring based on the activation energy, E_a, which is characteristic of the transition in question, the gas constant, R, and the temperature in Kelvin, T. Where a particle is of low mass and the barrier between potential energy wells is narrow, i.e. the potential energy minima are close together, tunnelling type behaviour can replace the classical behaviour where the energy of a transition determines it's probability as described in the Arrhenius equation. Indeed, at low temperatures tunnelling behaviour can dominate. This tunnelling behaviour can take many forms but the rotation of molecular groups such as -NH_2, -NH_3 and -CH_3, is the subject of interest here. A wealth of work has been carried out on molecular rotors[84,85,86] with the methyl group being the most studied[87,88]. If the methyl rotor is considered to be a rigid, symmetrical equilateral triangle a 120º rotation around the axial bond superimposes the molecule in an identical state. It can therefore be described by group theory as having C_3 symmetry.[4,89,90]. Complex systems can be described in a number of ways. The simplest of these are called the irreducible representations; they cannot be reduced to a simpler form. The irreducible representations of a C_3 symmetrical system such as a methyl group are named, A, E_a and E_b where E_a and E_b are degenerate. In the ground state the A state has lowest energy but in the first excited state this is reversed with the E levels having the lowest energy. The reversal of lowest energy level with each excited state continues through higher excitation states. The A level describes an invariance in C_3 rotation, analogous to an absence of classical rotation, whereas the degenerate $E_{a/b}$ levels describe rotation in steps of $\pm 120°$.

The Pauli exclusion principle states that no two identical fermions may occupy the same quantum state. In NMR, under ordinary circumstances, this principle is only applied to the spin states of atomic nuclei because, in what would be considered normal circumstances, there are sufficient spatial energy levels that there is no restriction on the total spin-spatial product. Where hindered molecular rotors exist at very low temperatures the principle must be extended to include spatial degrees of freedom because only certain spin-spatial products are permissible[91]. The total

wave function must be symmetrical, and thus in the A state, therefore the allowable spin-spatial

state products are $A.A$, $E_a.E_b$ and $E_b.E_a$. Given that the methyl group is a three spin system the A

level has $m_I = \frac{3}{2}$ and the two degenerate E levels have spin $m_I = \frac{1}{2}$. This is summarised in tables

2.2 and 2.3 (adapted with permission from a detailed review of quantum rotors by A Horsewill[4]).

Rotor Functions	
$\psi A^n =$	$(\psi 1n + \psi 2n + \psi 3n)/\sqrt{3}$
$\psi E_a^n =$	$(\psi 1n + \epsilon^* \psi 2n + \epsilon \psi 3n)/\sqrt{3}$
$\psi E_b^n =$	$(\psi 1n + \epsilon \psi 2n + \epsilon^* \psi 3n)/\sqrt{3}$

Table 2.2: Rotor Functions for a methyl group. Adapted from[4].

Spin Functions	
$\chi A_{+3/2} =$	$\|\alpha\alpha\alpha>$
$\chi A_{+1/2} =$	$(\|\alpha\alpha\beta> + \|\alpha\beta\alpha> + \|\beta\alpha\alpha>)/\sqrt{3}$
$\chi A_{-1/2} =$	$(\|\beta\beta\alpha> + \|\beta\alpha\beta> + \|\alpha\beta\beta>)/\sqrt{3}$
$\chi A_{-3/2} =$	$\|\beta\beta\beta>$
$\chi E_{a+1/2} =$	$(\|\alpha\alpha\beta> + \epsilon\|\alpha\beta\alpha> + \epsilon^*\|\beta\alpha\alpha>)/\sqrt{3}$
$\chi E_{a-1/2} =$	$(\|\beta\beta\alpha> + \epsilon\|\beta\alpha\beta> + \epsilon^*\|\alpha\beta\beta>)/\sqrt{3}$
$\chi E_{b+1/2} =$	$(\|\alpha\alpha\beta> + \epsilon^*\|\alpha\beta\alpha> + \epsilon\|\beta\alpha\alpha>)/\sqrt{3}$
$\chi E_{b-1/2} =$	$(\|\beta\beta\alpha> + \epsilon^*\|\beta\alpha\beta> + \epsilon\|\alpha\beta\beta>)/\sqrt{3}$
$\epsilon =$	$exp(i2\pi/3)$

Table 2.3: Spin functions for a methyl group. Adapted with permission from[4].

The Hamiltonian for a methyl rotor is often expressed as:

$$H = (-\hbar^2/2I)(\partial^2/\partial\varphi^2) + V(\varphi) \tag{2.47}$$

The first term describes a free rotor, where I is the moment of inertia, and the second part a

hindered potential of three fold symmetry. The second $V(\varphi)$ term can be expressed as a Fourier

series:

$$V(\phi) = \sum \frac{V_{3l}}{2}[1 - cos(3l(\phi + \chi_{3l}))] \tag{2.48}$$

where l is an integer and χ_{3l} describes the rotational phase.
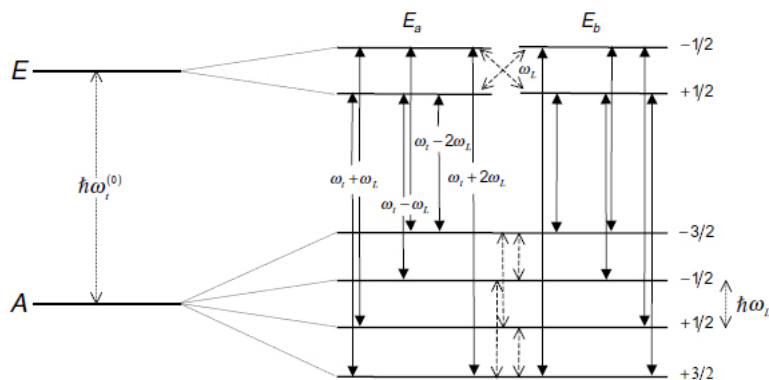
Figure 2.15: Energy levels for a methyl spin-spatial product. Adapted with permission from[4]

For a given methyl group the allowable spin spatial products give energy levels and transitions as shown in Figure 2.15. This shows the two possible levels of the degenerate spin $1/2$ E levels and the four levels of the spin $3/2$ A levels and all possible transitions and their energies.

2.4.2.2   The Haupt model

Haupt worked on a similar system to this, where he had observed a rotating molecular group at low temperature, during his doctoral studies[5]. He discovered that when a sample of γ-picoline (4-methyl pyridine) was rapidly shuttled between 8 and 30K a strong dipolar polarisation was seen on the methyl protons. The polarisation seen was reported to be on the order of a 10,000 fold but as the induced magnetisation was transverse only this value cannot be directly compared to the longitudinal DNP enhancement factors. At the higher temperature numerous excitation states are occupied whereas at the low temperature only the lowest state(s) are occupied. The transitions between different excited states is relatively fast as the spin state itself does not change, however the individual A-E transitions are very slow. Haupt took all the possible individual transitions between the first excited state and the ground state and determined the change in Zeeman order, phonon emission or absorption and the change in dipolar energy. He then summed these changes for the whole system and showed an imbalance in the dipolar order. Haupt's representation of this in an energy level diagram is shown in Figure 2.16.

Haupt described the system with a Hamiltonian:
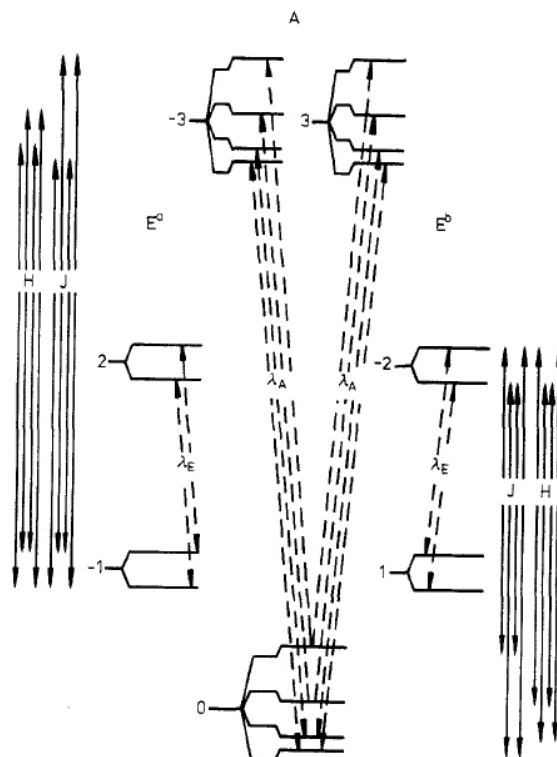
Figure 2.16: Energy level diagram showing the possible transitions in the spin-spatial system between the ground state and first excited rotational state. Dashed arrows represent transitions that are independent of spin and are subsequently fast. Solid arrows show transitions between A and E states and involve a change in spin and are slow. The net transitions are grouped and labelled H or J. H transitions have a decrease in dipolar energy whereas J transitions have an increase in dipolar energy. On a rapid change in temperature one or other group of transition is favoured depending on the direction of the temperature jump. The net dipolar shift gives the polarisation seen. Adapted with permission from[5]

$$\hat{H}_{total} = \hat{H}_R + \hat{H}_Z + \hat{H}_D \tag{2.49}$$

which combines the rotational, Zeeman and dipolar terms respectively. This figure shows the two groups of transitions that occur depending on the direction of the temperature jump; J for a downward jump and H for a upward jump. The J transitions lead to a decrease in dipolar energy where the H transitions cause an increase in dipolar energy and the combination of these energy shifts is the dipolar polarisation seen. The rate of buildup of the Haupt effect was described previously to follow the equation:

$$P_d(t) = C[e^{-t/a} - e^{-t/b}] \tag{2.50}$$

where P_d is the amplitude of the dipolar polarisation and a and b are the polarisation and depolarisation rates. The enhancement factor C is determined by the temperature change experienced by the sample. This empirical equation has been thoroughly evaluated by Beckman, Clough, Hennel and Hill[92] and shown to be robust. In this paper the assumption was made that those transitions that resulted in a +3 change in rotational quantum number occurred very rapidly. This is assumed to maintain thermal equilibrium within each of the three possible rotational states; A, E_a and E_b. In the analysis of this equation it was the $E_a \leftrightarrow E_b$ interconversion rate that largely accounted for the depolarisation time constant b of equation 2.50. Beckman et al.[92] showed that for a sum of all A and E levels respectively:

$$Z_A(T) = \sum_{m=0,\pm3,\pm6} \mu_m e^{-h\nu_t m^2/(kT)}$$

$$Z_E(T) = \sum_{m=\pm1,\pm2,\pm4} \mu_m e^{-h\nu_t m^2/(kT)}$$

This leads to:

$$Z(T) = Z_A(T)e^{\beta_0} + Z_E(T)e^{-\beta_0}$$

where the term β is a constant. It is the change in $(Z_A - Z_E)/(Z_A + Z_E)$ that represents the number of $A \leftrightarrow E$ transitions and therefore the size of the resulting polarisation. They further

showed that at low temperatures spin-symmetry conversion process depends on the modulation of dipolar matrix elements owing to rapid non spin-dependent transitions. In determining the polarisation rate, a, they showed that the fast spin-independent transition rate for A-state rotors, λ_A, is not much greater than its counterpart λ_E which implies that below 20K the dominant $A \leftrightarrow E$ interconversion route is via the $m = 0$ and $m = \pm 2$ levels. The depolarisation rate, b, does not show temperature dependence and is a result of $E_a \leftrightarrow E_b$ conversions. The $m = \pm 1$ state exchanges were shown to have a much greater impact on the rate b than the $m = \pm 2$ states.

Beckman's analysis of Haupt's experiments closed with an experiment to measure the energy released from the Haupt effect in the cooling process with 4-methylpyridine via a measurement of helium boil-off. The result showed twice the energy released as the theoretical prediction. This was remarked upon and on the basis of having identified an additional process that yields energy and will almost certainly be present in the experimental conditions cited, I speculate that it is those additional slow transitions between the A and E levels of the ground state that give rise to this additional energy release and subsequently observed helium boil-off. The Haupt mechanism depends on the fast transitions between excitation states that occur with a maximum effect seen around 5 minutes after cooling. The effect I have described occurs over many hours and depends on the slow A-E transitions. This much slower process will release $\hbar\nu_T R$ J/mole if all methyl groups make a rotational tunnelling level transition. When the sample cools the populations of the tunnelling states changes with the Boltzmann distribution. Taking this in to account $\approx 5J$ are released from the additional effect given the conditions described. Combined with the energy from the Haupt effect this gives $\approx 10J$, which is far closer to the $\approx 12J$ expected theoretically so it is reasonable to assume that this effect contributes significantly to the observations made by Beckman et. al[92].

2.4.2.3 Symmetry conversion leads to nuclear polarisation

At very low temperatures the motional spectrum for the rotational tunnelling system for a methyl group shows three clearly defined energy maxima corresponding to zero and $\pm\omega_t$. As temperatures increase a greater number of excitation states become populated allowing a greater number of barrier crossing pathways. These barrier pathways result in an incoherent character in the rotor's behaviour causing behaviour as a damped harmonic oscillator. As the temperature further

increases the motional spectrum is broadened such that it takes the form of classical Arhennius behaviour. At very low temperatures only the ground state is populated so a discontinuous energy surface results. It follows that if the spatial levels are limiting then the spin and spatial states of these systems being coupled, if a symmetry state conversion occurs this has a consequence on the allowable Zeeman states. Symmetry states are evident in the sidebands of some spectra[93] and have been widely studied[94]. The slow symmetry conversion process from the E state to the A state results in a loss of energy and a decrease in entropy as the system becomes polarised. This energy can be transferred to a proton spin leading to a proton spin flip. In the Provotorov spin temperature model the nuclear spin temperature is effectively raised by the rotational tunnelling system[95]. In terms of the thermal bath model the rotational tunnelling system is in contact with the Zeeman system. This process may be mediated by the phonon system and will now be described in more detail.

The natural symmetry conversion process leading to cooling of the methyl rotors in the absence of any level-crossing effect or suchlike is a slow one with[4]

$$\tau^{-1} = 2[3(sin^4\theta)r_0 + 2(1 - cos^2\theta)(r_1 + r_{-1}) + \frac{1}{2}(1 + 6cos^2\theta + cos^4\theta)(r_2 + r_{-2})] \qquad (2.51)$$

and

$$r_n = \frac{27}{128}(\frac{\mu_0}{4\pi})^2 \frac{\hbar^2\gamma_p^4}{r_{HH}^6}\delta^2 \frac{\tau_c}{1 + (\omega_t + n\omega_L)^2\tau_c^2} \qquad (2.52)$$

Where θ is the angle between the applied magnetic field and the rotational axis of the methyl group, r_{HH} is the inter-proton distance (usually 1.79Å) and δ is the spatial part of the intra-dipolar matrix element between the A and E state.

At high temperature the spin-lattice relaxation rate for methyl groups can be written as[96]:

$$\frac{1}{T_1} = \frac{9}{20}\frac{\gamma^4\hbar^2}{r^6}\left(\frac{\tau_c^H}{1 + (\omega_0\tau_c^H)^2} + \frac{4\tau_c^H}{1 + 4(\omega_0\tau_c^H)^2}\right) \qquad (2.53)$$

At low temperatures where only the ground state is occupied the correlation time of excitations to the first excited level can be described by[96]:

$$\tau_c^T = \tau_{c0}^T exp(E_{01}/RT) \tag{2.54}$$

Therefore where the temperature is low enough that only the ground rotational tunnelling state is occupied and the tunnelling frequency is greater than the Larmor frequency the relaxation rate can be expressed:

$$\frac{1}{T_{1AE}} = C_{AE} \sum_{m=-2}^{m=+2} \frac{m^2 \tau_c^T}{1+ <\omega_T>^2 (\tau_c^T)^2} \tag{2.55}$$

where $<\omega_T>$ is the tunnelling frequency at a given temperature, T_{1AE} is the A-E level relaxation time constant, C_{AE} and C_{EE} are the A-E and E-E relaxation strengths and τ_c^T is the tunnelling correlation time. As the order of lowest energy tunnelling levels alternates between A and E through excited states, the A and E levels are approximately equally populated at room temperature. As transitions between the rotational levels of different excitation states are fast, the A and E levels are also equally populated immediately after rapid cooling. Subsequently, both the Zeeman and rotational tunnelling levels seek a new Boltzmann equilibrium. For the rotational tunnelling system, cooling leads to an increased population for the A level. For systems where the energy difference between E and A rotational tunnelling levels, $\Delta E_{E,A}$, is larger than the energy difference between the Zeeman states $\Delta E_{\alpha,\beta}$, $E \rightarrow A$ transitions can drive proton Zeeman $\alpha \rightarrow \beta$ transitions. This causes larger polarisations for substances with larger rotational tunnelling energies, with acetic acid (GHz) > acetone (MHz) > DMSO (kHz)[87]. The buildup of magnetisation with the opposite sign to the Boltzmann magnetisation requires that the equilibration process leads to an increased population of β spin states. This would be consistent with $|-1/2, E_a> \leftrightarrow |+3/2, A>$ and $|+1/2, E_b> \leftrightarrow |-3/2, A>$ transitions[97]. Whether any other possible transitions occur is unclear although the net effect of increased Zeeman β population renders them rather unlikely. It is ultimately a balance between several slow and interdependent relaxation processes that drives the buildup of Zeeman polarisation.

For substances where rotational tunnelling levels are not present this effect cannot occur as there are no rotational energy levels to pass energy to the Zeeman system, so purely thermal signals are seen for substances such as formate[98] and acetonitrile. In any process of buildup and decay an

accumulation will only occur where the decay rate, longitudinal relaxation here, is less than the buildup rate. Above a few degrees Kelvin the proton polarisation is generally lost with T_1 faster than it arises and rotational polarisation will be lost with the b term of equation 2.50 due to $E_a \leftrightarrow E_b$ conversions. The Haupt effect is the exception to this but only occurs for a small number of substances with exceptionally high tunnelling frequencies.

At temperatures below 3K the nuclear T_1's for glycerol have been shown to increase as $R_1 \propto t^2$, where R_1 is equal to $\frac{1}{T_1}$ and t is the temperature, due to low frequency excitations (LFE's). In the case of glycerol the LFE's arise from the asymmetric double well potential of the hydrogen bonds in the glassy state. Other similar relaxation behaviour has been shown at low temperatures for other organic glasses and thus similar behaviour is likely to occur in these systems where glasses are present at 1-2K.[99] At operating temperatures of $\lessapprox 1.5K$ in a magnetic field of 3.35T the proton T_1's are long enough to allow the symmetry state conversion associated proton polarisation to accumulate. The b term from the quantum rotor system is not significantly temperature dependent. Also, the a term from the quantum rotor buildup is increased at low temperatures leading to a greater polarising effect. There is a simple balance between the rate of proton polarisation gain and loss so once the rate of gain exceeds the rate of loss we see an accumulation. After subsequent cross-relaxation to a hetero-nucleus this polarisation can also be transferred, and begin to accumulate, on the hetero-nucleus leading to the observed negative ^{13}C polarisation.

2.4.2.4   Spread of polarisation by spin symmetry diffusion, spin diffusion and dipolar cross relaxation

Polarisation arising from the methyl rotor system can spread throughout a glassy sample by a variety of mechanisms. Spin diffusion, particularly in the proton network, and dipolar cross relaxation play an important role in the spread of polarisation through a sample. There is a probability for two spins to flip simultaneously, either with opposing signs (a flip-flop or W_0 transition) or the same sign (a flip-flip or W_2 transition). So, when one spin makes a transition it is energetically favourable for a second spin to also flip. These paired transitions therefore allow the nuclear polarisation to be transferred. This process can act to transport polarisation around the sample. This process of spin diffusion relies on a series of Nuclear Overhauser effect exchanges. The

probability of these exchanges are given in equations 2.32,2.33 and 2.21 on page 16.

Dipolar cross relaxation then allows transfer of polarisation to nearby heteronuclei. The efficiency of this exchange is proportional to the ratio of the gyromagnetic ratios of the two spins so transfer from ^{1}H to ^{13}C is only $\frac{1}{4}$ as efficient as a ^{1}H to ^{1}H transfer. H$-$C dipolar couplings are also weaker than H$-$H couplings resulting in a yet weaker effect. If natural abundance carbon samples are used there is also only a 1% probability that any given carbon is the ^{13}C isotope, dramatically decreasing the likelihood of transfer further.

The system can be modelled assuming that both protons and ^{13}C nuclei are present but the magnetisation arises on ^{1}H as it is the methyl protons that are involved in the quantum rotor system and that therefore act as an energy source. The magnetisation is then distributed through the proton network by spin diffusion before transfer to ^{13}C where we observe the signal enhancements.

The rate of cross-relaxation between dipolar coupled spins C and H can be described by a set of coupled partial differential equations:

$$\frac{\partial \rho^C}{\partial t} = -R_{1C}(\rho^C - \rho_0^C) - \sigma(\rho^H - \rho_0^H)$$

$$\frac{\partial \rho^H}{\partial t} = -R_{1H}(\rho^H - \rho_0^H) - \sigma(\rho^C - \rho_0^C)$$

Assuming there is a huge ^{1}H polarisation and the rate of ^{13}C$\rightarrow^1$H is so low as to not effect the ^{1}H polarisation, the transfer of magnetisation can be assumed to only go ^{1}H$\rightarrow^{13}$C over the timescale of these experiments. Therefore the ^{1}H magnetisation can be treated as independent and the cross relaxation part of the proton equation can be ignored. This gives:

$$\frac{\partial \rho^C}{\partial t} = -R_{1C}(\rho^C - \rho_0^C) - \sigma\rho^H$$

$$\frac{\partial \rho^H}{\partial t} = -\rho^H$$

As a consequence of this the proton polarisation rate can be integrated separately. We assume that the change in proton polarisation can be described by the Haupt model as although it takes a different energy source to this mechanism, it follows the same kinetics. Therefore the proton polarisation can be described as[5]:

$$\rho^H = k(e^{-R_{1a}t} - e^{-R_{1b}t})$$

Then incorporating this description of the polarisation of protons into the partial differential equation for the carbon magnetisation we get[7]:

$$\frac{\partial \rho^C}{\partial t} = -R_{1C}(\rho^C - \rho_0^C) - \sigma k(e^{-R_{1a}t} - e^{-R_{1b}t}) \tag{2.56}$$

Or, in it's integrated form:

$$\rho_C = \rho_0^C(1 - e^{-R_{1C}t}) + \sigma k \frac{\Theta + \Gamma + \Xi}{\Lambda} \tag{2.57}$$

$$\Theta = (R_{1a} - R_{1b})e^{-R_{1C}t}$$

$$\Gamma = (R_{1b} - R_{1C})e^{-R_{1a}t}$$

$$\Xi = (R_{1C} - R_{1a})e^{-R_{1b}t}$$

$$\Lambda = (R_{1C} - R_{1a})(R_{1C} - R_{1b})$$

Where R_{1a} is the proton polarisation buildup rate, R_{1b} is the proton longitudinal relaxation rate, R_{1C} is the carbon nuclear longitudinal relaxation rate, ρ^C is the ^{13}C polarisation, σ is the heteronuclear dipolar cross relaxation efficiency factor and k is a constant[10]. This equation essentially shows the change in the ^{13}C polarisation level to be a balance of the rate of buildup on protons and the rate of polarisation loss from carbon nuclei. This is expressed in three rates; the first is the rate of decay of ^{13}C polarisation, R_{1C}. The second is the rate of proton polarisation build up, R_{1a} and the third is the rate of proton depolarisation, R_{1b}. The second and third terms follow the mathematical model of Haupt, as does k[5], because although the mechanism is different the process is equivalent. This proton-related part of the equation is mediated by cross relaxation rate, σ that reflects the low efficiency of heteronuclear polarisation transfer.

In principle there are two possible routes that polarisation can take to be transferred from the methyl protons to non-methyl carbon nuclei; either directly via a dipolar coupling or indirectly via the proton network. It is both rational, owing to the very small proton-carbon couplings, and evident from experiments that it is the proton mediated route that is taken.

Polarisation in the rotational tunnelling levels can also be transferred by a mechanism analogous to spin diffusion. Spin-symmetry diffusion (SSD) was first demonstrated using level-crossing phenomena[100] that can arise when e.g. the rotor frequency equals an electronic Larmor frequency and leads to a flow of energy between the two systems of equal frequency. SSD exhibits the same conservation of energy due to paired spin flips as the NOE spin flips of spin diffusion[101,102,103]. In the case of SSD it is the A and E states that are exchanged. As with spin diffusion the efficiency of transfer depends on distance but as r^{-5} rather that as r^{-6}. The efficiency also depends on the difference in tunnelling frequencies. It is difficult to distinguish between proton spin diffusion and spin-symmetry diffusion experimentally and likely both are important processes. From our experiments it is proton-proton spin diffusion that mediates the distribution of polarisation throughout a sample and the efficiency of heteronuclear dipolar cross relaxation that appears limiting.

2.4.3 Existing applications

2.4.3.1 Level-crossing phenomena

Clough, Horsewill and Palley described a process whereby a tunnelling methyl group is put in thermal contact with a resonant electron spin allowing rapid cooling of the methyl group. Ordinarily the cooling of a tunnelling methyl is too slow a process to yield any polarisation of the protons. However, by irradiating an ammonium acetate sample with γ-rays a radical of the form CH_2COOH is induced. The magnetic field can then be swept across a range of field strengths. When the electronic Larmor frequency ω_e matches the methyl rotational tunnelling frequency, ν_t, a level-crossing effect occurs. This level-crossing effect allows energy to be transferred between the levels of equal energy. This in turn allows rapid cooling of the methyl rotor as energy flows in to the electronic Zeeman system from the methyl group.

For each methyl rotor that cools from the E^0 state to the A^0 state, energy is lost from the rotational tunnelling system to the nuclear Zeeman system and hence a proton is converted from the α state to the β state. The resulting magnetisation is large enough to be measurable[101] but decays relatively rapidly once the rotational tunnelling system is cooled.

This effect is phenomenologically very similar to the process that discovered in this work. In

essence it appears that the two polarisation effects stem from the same mechanism. In the case of the Clough, Horsewill & Palley experiment the temperature is not sufficiently low to yield a proton T_1 long enough to maintain polarisation without the aid of a level-crossing phenomenon to the electron.

2.4.3.2 Haupt-CP induction of longitudinal polarisation

Tomasselli, Degen and Meier[6] performed an experiment using the Haupt effect with the aim of using the dipolar polarisation resulting from a temperature jump to a Zeeman polarisation on a hetero-nucleus. A sample of 4-methylpyridine was cycled between $4K$ and $55K$ to bring about the dipolar Haupt polarisation. A cross-polarisation scheme was then employed using an adiabatic Hartmann-Hahn (APHH) sequence. Where the sample was warmed the polarisation seen was positive, whereas when the sample was cooled a negative polarisation was observed. By employing the APHH scheme a longitudinal signal enhancement of ≈ 25 times was seen as shown in figure 2.17. This demonstrated that energy from the dipolar system can be transferred to the Zeeman system actively and one would assume that this effect also occurs passively to some extent, although probably at too low a rate to be measurable with a $\approx 50K$ temperature change.
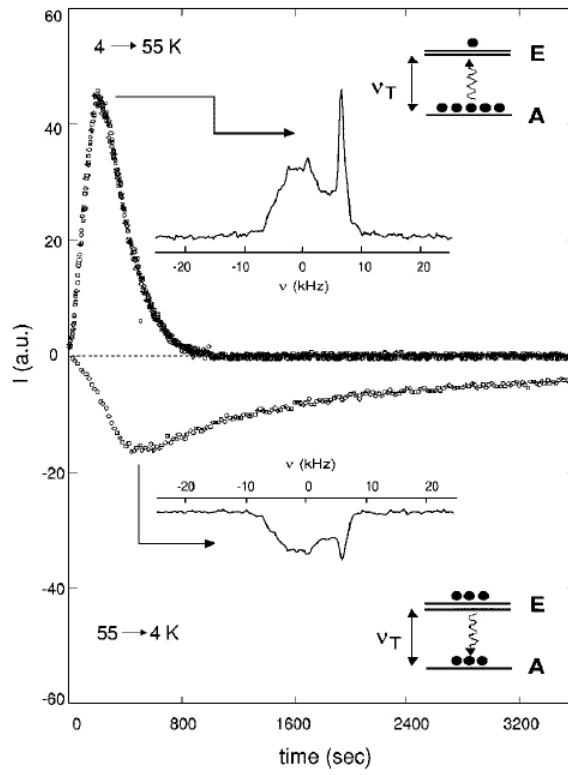
Figure 2.17: The transient polarisation arising from the Haupt-CP experiment of Tomasselli, Degen and Meier. Adapted with permission from [6].

Part II

Experimental

Chapter 3

Materials and methods

3.1 Sample preparation

3.1.1 Samples for polarisation

All samples for polarisation were prepared by dissolving in a glassing solvent matrix unless they self-glassed. The glassing matrices used were 50% dimethyl sulphoxide (DMSO) in water, 50% DMSO in methanol, 33% DMSO and 33% acetone in water. For DNP a glass is required for effective polarisation by preventing segregation of the constituents of the sample mixture. For all DNP experiments a trityl doping agent - either OX63 or Finland - was added to the sample to give a final concentration of 15mM. Non-DNP samples had no radical added.

3.1.2 Serum sample preparation

Serum samples were prepared for polarisation experiments by deproteinisation in 0.5ml spin-filtration tubes with a molecular weight cutoff of 3-5kDa to isolate the small molecules and ensure that no acetylated protein by-products are formed. These filters were pre-washed with distilled water eight times to remove all traces of glycerol preservative. The serum samples were spun at 13,000rpm in 20 minute runs until the sample had completely passed through the filter. The filtrate was then pooled and lyophilised to give the concentrated residue.
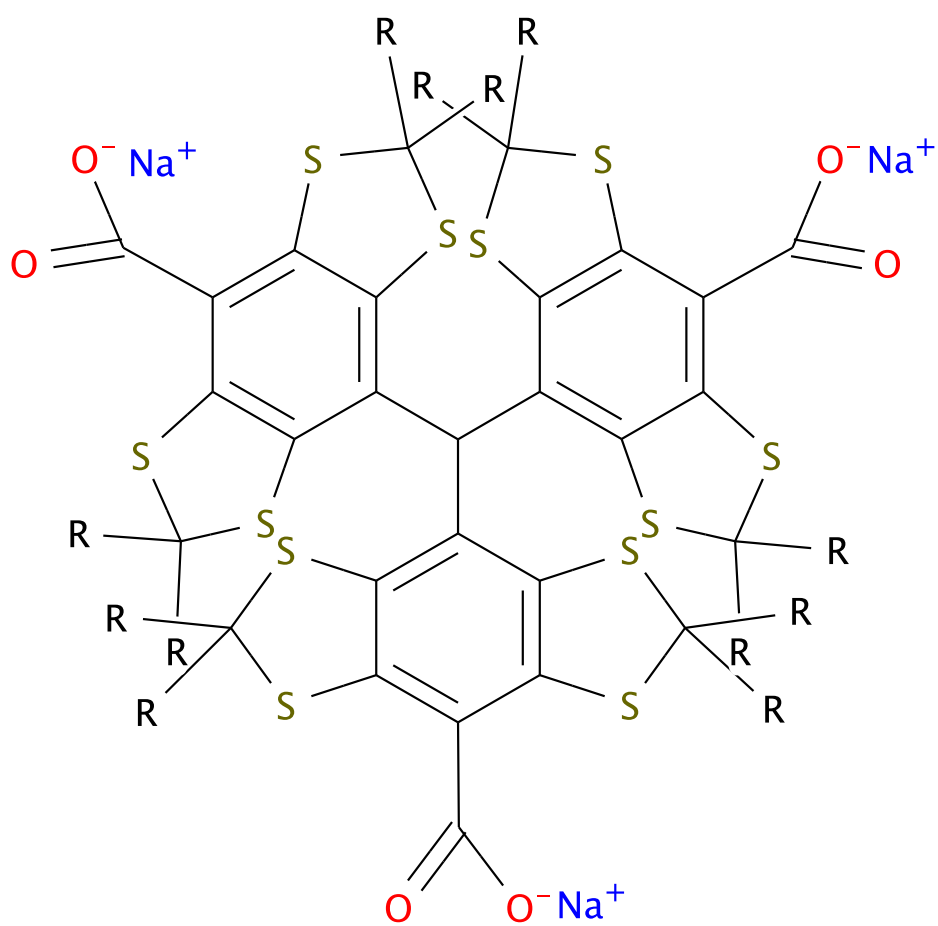
OX63   R = H

Finland   R = CH$_2$COOH

Figure 3.1: Structure of trityl radicals OX63 and Finland

3.1.3 Acetylation of bovine serum or an amino acid solution with acetic anhydride

The substance to be acetylated (fetal bovine serum or an amino acid solution) was dissolved in 20mM phosphate buffer pH 8.0 to ~13mM before 1.1 equivalents of acetic anhydride was added. The reaction was allowed to proceed overnight before the reaction mixture was placed on a freeze-drier to evaporate any remaining reactants, acetic acid by-product and to lyophilise the acetylated product.

3.1.4 Acetylation of 4-methoxyphenol with methylene chloride

The carboxyl bearing substance to be acetylated, 4-methoxyphenol, was dissolved to 1M in methylene chloride and 1.1 equivalents of diisopropylethylamine (DIPEA) was added. This mixture was cooled in a dry ice / acetone bath with magnetic stirring. Acetyl chloride, 1.1 equivalents, was added drop-wise. After 2 hours the mixture was allowed to warm to room temperature and the reaction continued for a further 2 hours. The reaction mixture was then rotary evaporated to remove the solvents and then freeze-dried to yield the purified acetate.

3.2 Polarisations

3.2.1 The HyperSense™ polariser

The HyperSense™ instrument is based on work by Golman et al.[13]. The apparatus essentially consists of a 3.35T supercooled, superconducting magnet with a cryostat insert and a sample delivery mechanism to deliver the sample to a high field liquid state NMR spectrometer. A sample is prepared in a solvent matrix that will form a glass at low temperatures. Examples of samples and solvent mixtures that form a glass include water:DMSO 1:1, water:glycerol 1:1, methanol:DMSO 1:1, water:acetone:DMSO 1:1:1, pure acetone and pure pyruvic acid. This sample is placed into a sample cup manufactured from PFE up to a volume of 200μl although for my experiments a volume of 100μl was used unless otherwise stated. The sample cup is inserted into the cryostat by use of a specific insertion tool that is a vented stick of approximately one meter and a release mechanism to eject the cup from the insertion tool to remain in the cryostat. The cryostat draws helium from the dewar and allows a high vacuum to be formed which allows the sample temperature to be driven

down by the Joule Thomson effect[104] to around 1.1K. The time between insertion of a sample and complete cooling is 3-5 minutes. The instrument also facilitates irradiation with microwaves at around 93GHz, the electronic Larmor frequency at 3.35T to induce DNP polarisation. The optimal microwave frequency is determined by a calibration process described below. After typically 60-90 minutes polarisation is complete and the sample can be transferred to a second, high field liquid state spectrometer with a field strength of 11.7T. The polarised sample is delivered through a 1mm lumen high density polyethylene (HDPE) line by a stream of heated, pressurised solvent. The time taken to heat the dissolution solvent is approximately 2 minutes at which time a pressure of 10bar is attained in the pressure vessel (the "bomb"). The transfer solvent used in my experiments was either water with 0.01% EDTA or pure methanol. During the transfer the sample does not pass through zero field at any point although it does pass through low field en-route. Figure 3.2 shows the magnetic field strength through the path that the sample is delivered. The delivery process itself takes 3-5 seconds and delivers the leading 0.5-1ml of dissolved sample in solvent. There are a number of alternate solvent delivery apparatus as described below that ensure that the sample is delivered into the 5mm NMR tube at the desired volume and with no air bubbles. The overall operation of the polariser instrumentation is summarised in Figure 3.3.

3.2.2 DNP microwave frequency calibration

In order to calibrate the ^{13}C DNP enhancement maxima a sample of ^{13}C pyruvic acid was placed in the instrument cryostat and the temperature was allowed to equilibrate. The sample was irradiated with a microwave frequency for a short time, typically 2-5 minutes and a small angle pulse from a radio-frequency coil was employed to measure the extent of polarisation. Any remaining polarisation was subsequently destroyed with train of small pulses and the microwave frequency was incremented. After a sweep of the microwave frequency two polarisation maxima should be seen. By default the lower frequency maximum is chosen although both have been used in this work. The choice of frequency defaults to the low frequency maximum as the summation with Boltzmann polarisation theoretically produces a greater DNP enhancement. Through the course of this work I have identified an additional mechanism that acts in the opposite direction to this making both frequencies important. The frequency itself will depend on the DNP mechanism active. The
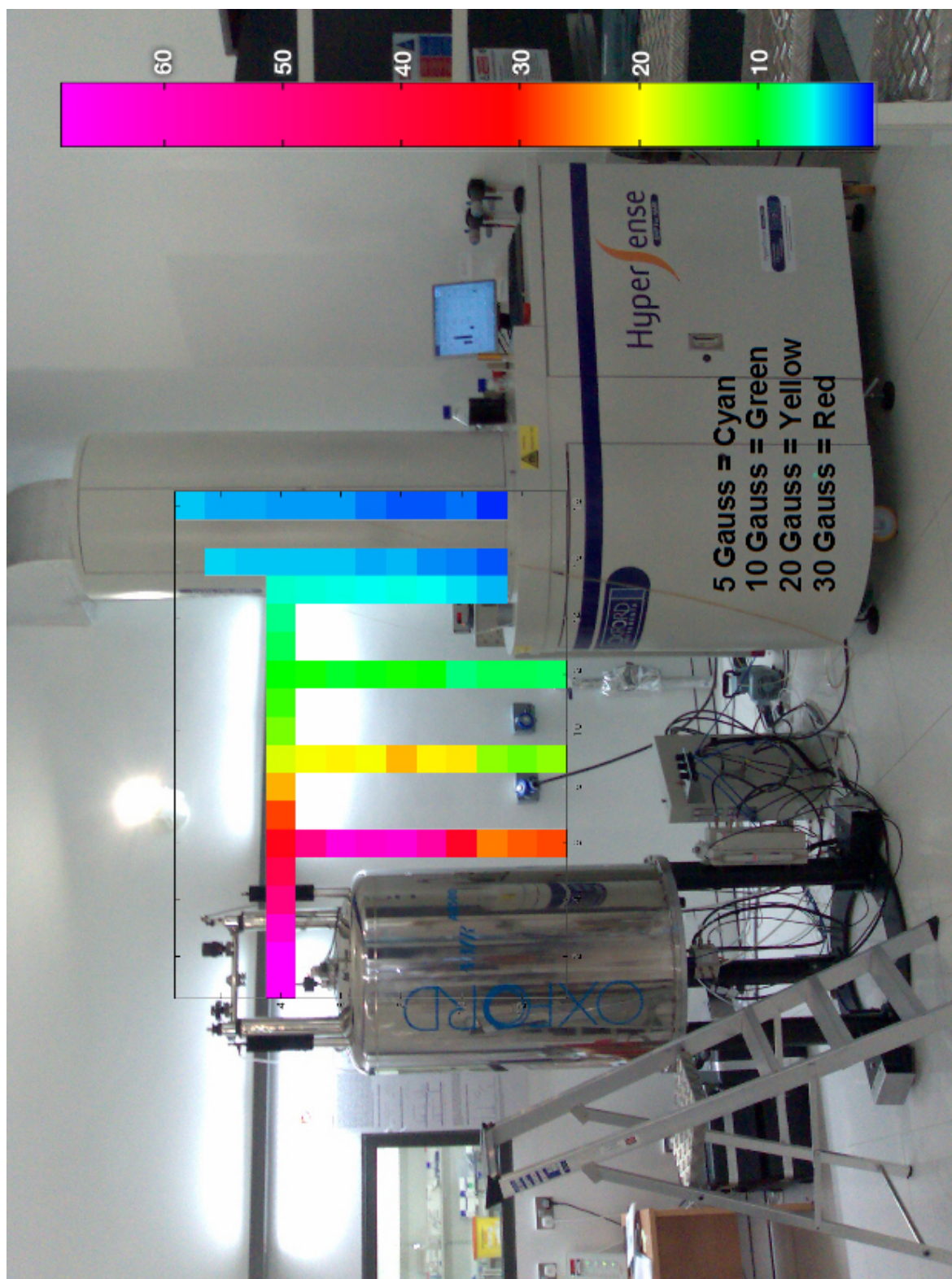
Figure 3.2: Mapping of the magnetic field strength around the HyperSense™ instrument and 500MHz NMR magnet installed at HWB-NMR. Adapted from[7] supplementary material.
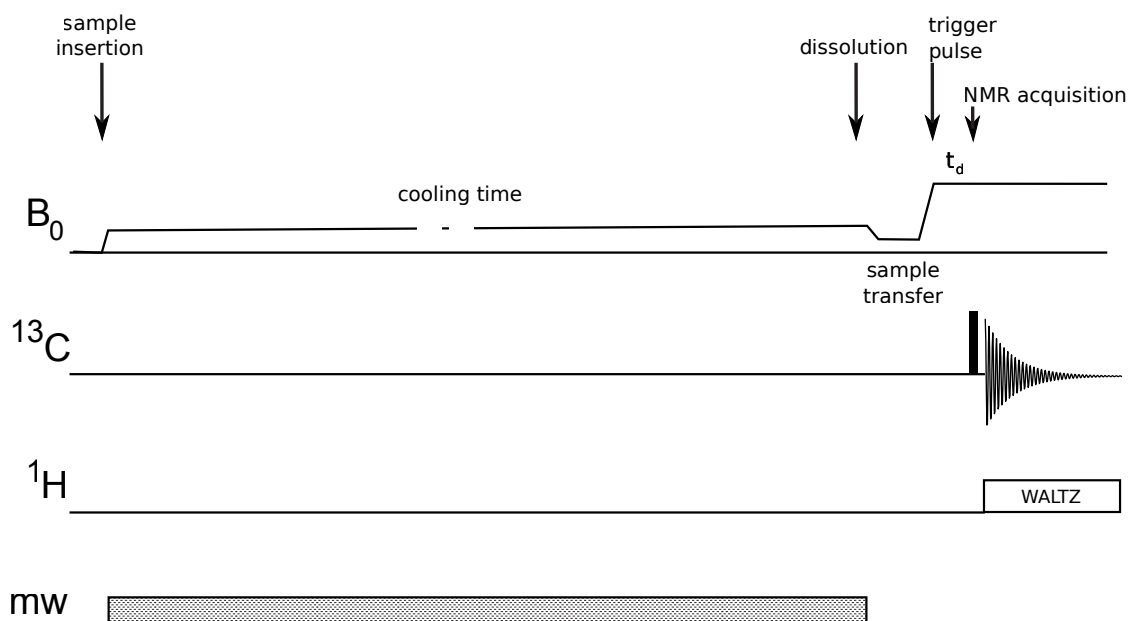
Figure 3.3: Time sequence for DNP / quantum rotor experiments showing the experienced field strength, B_0, the ^{13}C channel, the ^{1}H channel and the microwave irradiation which is only used in DNP experiments, (mw). On sample insertion the experienced field increases as the sample enters the 3.35T magnet. The sample is then cooled and optionally irradiated with microwaves. The sample is then dissolved with a hot transfer solvent, passes through low field and is then delivered to a higher field magnet where acquisition of a ^{1}H WALTZ decoupled ^{13}C NMR spectrum is performed. Adapted from [7]

frequencies of effect are listed in table 2.1 on page 35.

3.2.3 Sample delivery apparatus

A series of sample delivery apparatus are used to ensure that a consistent volume of liquid, polarised sample is delivered rapidly but without trapped air bubbles or excessive turbulence. The most simplistic delivery apparatus is used only for methanol delivery as the low surface tension of methanol results in only a small degree of bubble formation. On delivery a HDPE funnel forms a narrow jet of solvent that runs down the inside edge of the 5mm NMR tube. A vacuum pump is applied to the device to prevent back-pressure on delivery and for methanol this device works reliably. For aqueous samples however the surface tension of the liquid sample leads to air bubble formation that render this simplistic delivery device unusable.

A secondary delivery device was provided by Oxford Instruments that was designed to be more effective in the delivery of aqueous samples but this proved to be unreliable with an approximately 20-50% failure rate due to trapped air bubbles. This device followed the same principle as the methanol device but was far more accurate in its construction. In order to gain reliability in the delivery of aqueous samples and also to allow mixing of the polarised sample with a substrate pre-added to the NMR tube I created a device from laboratory spares that delivered the polarised sample down a glass pipette to the base of the NMR tube rather than injecting via a jet from the top. My initial sketch is shown in Figure 3.4a and a cartoon of the device is shown in figure 3.4b. I communicated my design to Oxford Instruments and in due course a third solvent delivery device was later created by Oxford Instruments that functioned exactly as my device did. Figure 3.4c shows a photograph of my device and Figure 3.4d shows a photograph of the Oxford Instruments device.

3.3 NMR

3.3.1 NMR acquisition

High resolution NMR spectra were acquired on a Varian Unity 500 liquid state NMR instrument with a direct X channel broadband probe tuned to ^{13}C . A schematic representation of the pulse sequence employed in hyperpolarisation experiments is shown in Figure 3.3.

Figure 3.4: Aqueous sample delivery device. a) initial sketch, b) cartoon of device, c) photograph of my device, d) photograph of Oxford Instruments device.
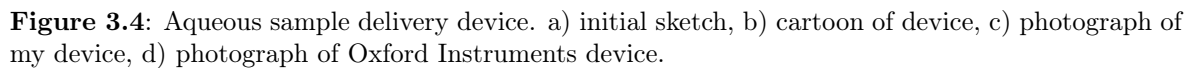
3.3.1.1 Fast 2D spectral acquisition

A fast HMQC method was employed following the pulse sequence shown in Figure 3.5. In this pulse sequence a small flip angle, α, and a selection gradient scheme converts a small proportion of the total magnetisation into a transverse ^{13}CH coherence that enables chemical shift evolution to occur for the secondary nucleus, protons in this case. However, the pulse sequence preserves the majority of the magnetisation in the sample as longitudinal allowing successive increments of the chemical shift evolution period, t_1, thus enabling two-dimensional NMR data to be acquired.

The pulse sequence commences with a selective ^{13}C π pulse followed by a small flip angle pulse of angle α which places a small amount of ^{13}C magnetisation in the transverse plane giving at position 1 of Figure 3.5:

$$I_z \cos(\alpha) - I_y \sin(\alpha)$$

The first gradient then acts to de-phase the transverse ^{13}C magnetisation which at 2 gives:

$$-I_z \cos(\alpha) - I_y \sin(\alpha).\cos(\gamma_1 z G_{z1} g t_1) - I_x \sin(\alpha).cos(\gamma_1 z G_{z1} g t_1)$$

After spatial integration this reduces to:

$$-I_z cos(\alpha) - I_y sin(\alpha).sinc(\gamma_1 z G_{z1} g t_1 \frac{r_{max}}{2})$$

The de-phasing at 2 is proportional to the gradient strength G_{z1}, the gradient time and the gyromagnetic ratio of the transverse nucleus γ_1. The delay δ allows anti-phase magnetisation to develop, so that at 3 the coherent terms (excluding the effects of the gradients) are:

$$-I_z \cos(\alpha) - 2I_x S_z.\sin(\alpha)$$

The following $\frac{\pi}{2}$ ^{1}H pulse then creates multi-quantum magnetisation at 3:

$$-I_z \cos(\alpha) + 2I_x S_y \sin(\alpha)$$

The second gradient then de-phases the multi-quantum coherence proportional to the gradient strength G_{z2}, the gradient time and due to the presence of double quantum magnetisation the sum of both gyromagnetic ratios$\gamma_1 + \gamma_S$. The broadband π ^{13}C pulse at 4 refocuses the ^{13}C chemical shift evolution in the double quantum coherence over time t_1 to 5 and flips the I_z term back to the
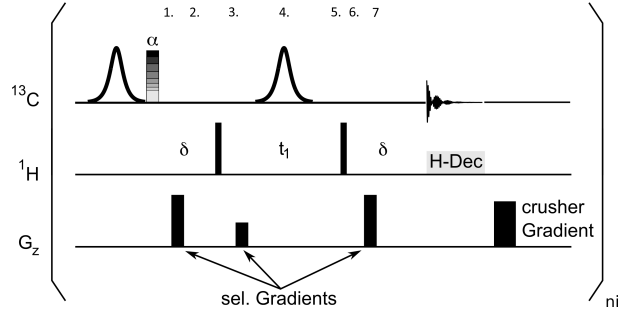
Figure 3.5: The fast 2D-HMQC pulse sequence where adiabatic π pulses were used on the carbon channel to avoid losses arising from B_1 inhomogeneity. The first ^{13}C flip angle, α, was increased (from 10° to 30°) in successive experiments to compensate for the decrease of available magnetisation for higher increments due to relaxation. Adapted from[8].

$+$ z axis. The $\frac{\pi}{2}$ ^1H pulse then takes the multi-quantum coherence back to single quantum magnetisation at 6:

$$I_z \cos(\alpha) - I_y \sin(\alpha).cos(\omega_H t_1)$$

The third gradient allows the de-phased transverse magnetisation proportional to the gradient strength $-G_{z3}$ (due to the π pulse on ^{13}C), the gradient time and the carbon gyromagnetic ratio γ_1. The total de-phasing of the double quantum magnetisation is proportional to:

$$\gamma_1 G_{z1} gt_1 + (\gamma_I + \gamma_S) G_{z2} gt1 - \gamma_I G_{z3} gt_1$$

To de-phase and refocus the double quantum magnetisation to 7 the gradient strengths fulfil the following equation (no overall de-phasing of magnetisation):

$$\gamma_1 G_{z1} gt_1 + (\gamma_I + \gamma_S) G_{z2} gt1 - \gamma_I G_{z3} gt_1 = 0$$

assuming $G_{z1} = -G_{z3}$ and $4\gamma_1 = \gamma_S$ it follows:

$$G_{z2} = -{}^2\!/_5 G_{z1}$$

The purpose of this gradient scheme is to isolate the multi-quantum term such that other coherences are destroyed in a single scan Any remaining transverse magnetisation after acquisition is destroyed by the crusher gradient and the sequence is repeated with an incremented t_1 delay.

3.3.2   NMR processing

All NMR processing was performed using NMRLab[105] within the Matlab programming environment. To remove DC offset artifacts which lead to a spike in the middle of the Fourier

transformed spectrum the last 256 data points of the FID were averaged and the average then subtracted from the entire FID. Prior to Fourier Transform the FID was apodized using an exponential window function with line broadening of typically 10Hz for DNP samples. No line broadening was used for quantum rotor experiments. This difference was a result of the differing line-widths for the two types of experiments. Spectral widths were 50kHz and 8192 points were acquired.

3.4   Data analysis

3.4.1 T_1 calculations

Longitudinal relaxation rates were determined using an inversion recovery scheme. In this scheme a π pulse is applied to the sample followed by a delay, τ, and then a $\pi/2$ pulse and FID acquisition. The intensity of the signals in the resulting spectra start at $-I$ and increase to a plateau at $+I$. The curve of signal intensity against time for each spin follows the equation,

$$I(t) = I_0(1 - 2e^{-t/T_1}) \tag{3.1}$$

where T_1 is the longitudinal relaxation time constant and I_0 the equilibrium polarisation for that spin. The T_1 value is then determined using a least squares regression method. The experimental protocol used 64scans with a spectral width of 50kHz and 8192 points. Delays of 0.05, 0.1, 0.2, 0.5, 1, 2, 3, 4, 5, 7.5, 10, 15, 20, 30 & 50 seconds were used.

3.4.2   Signal enhancement calculation

The enhancement for polarised samples is determined by the acquisition of a reference NMR spectrum after a suitable relaxation period for the previously polarised sample. The samples delivered to the high field spectrometer were allowed to equilibrate for at least 30 minutes at 298K. A simple NMR experiment was then performed where a $\pi/2$ pulse was applied before acquisition. Multiple scans were performed, with an inter-scan relaxation delay of 90s in order to gain a sufficiently high signal-to-noise ratio. The resulting peak integral divided by the number of scans

then gives an equivalent single scan intensity for that standard. The enhancement value is thus expressed as the fold enhancement in signal intensity in comparison to this standard.

As there is a change in both the applied magnetic field and the temperature for the dissolution and transfer process, the respective Boltzmann populations predicted indicate the enhancement in the polariser. For the system used in these experiments there is an increase in field from 3.35T to 11.7T and an increase in temperature from 1.1-1.5K to 298K. In conjunction these equate to an ≈65 fold enhancement in the polariser over that seen for the signals.

Chapter 4

Using a Nuclear Overhauser Effect to polarise secondary nuclei within a molecule after DNP and transfer

4.1 Introduction

Once a hyperpolarised sample is removed from the polarisation apparatus the polarisation level will begin to decay immediately. The decay of polarisation follows the longitudinal relaxation time constants, T_1 values, of the polarised nuclei. Many substances that are of great relevance to biomedical applications have ^{13}C nuclei with relatively short T_1's of less than a few seconds. As a result of the fast longitudinal relaxation for these nuclei the signal intensities are greatly reduced after the 3-5 seconds transfer and settling time required to transport the sample into the liquid state spectrometer. Any experiment with a duration that is significant on the timescale of the nuclear T_1's is therefore likely give erroneous results due to the decaying signal strengths despite the size of the initial polarisation. Conventional multi-dimensional experiments require multiple scans which become incomparable so these experiments are impossible with hyperpolarised samples.

A common experiment in NMR is the Nuclear Overhauser Effect Spectroscopy (NOESY)

experiment. This uses the through-space dipolar couplings between nuclei to transfer magnetisation from one to another. A dipolar coupling is a through-space coupling. Dipolar couplings do not depend directly on chemical bonds; the nuclei just have to be in close proximity of one another. This mode of polarisation transfer was originally proposed by Albert Overhauser and is the mechanism on which the DNP experiment relies. Between nuclei this effect is known as the Nuclear Overhauser Effect (NOE). As described in equation 2.32, 2.33 & 2.21 the strength of the NOE decreases with the internuclear distance, r^{-6} due to the b_{IS}^2 term. There will however be a uniform spread of polarisation through space to other nearby nuclei with the greatest and fastest enhancements occurring with those nuclei nearest to the donor nucleus. An NOE is driven by population differences which are vary large for hyperpolarised samples.

Some ^{13}C nuclei, such as quaternary and carbonyl carbons, consistently have long T_1's of up to 50 seconds. As a result of the long relaxation time constants these nuclei will yield polarisation levels that are relatively unaffected by the relaxation during the transfer and acquisition period of a DNP experiment. The high levels of retained polarisation for these nuclei can be transferred to other ^{13}C nuclei within a sample by numerous means. This can result in enhancements for nuclei that relax more rapidly. Effectively these long lived nuclear species can act as a hyperpolarisation reservoir that can be redistributed to enable observation of other fast-relaxing nuclei in *ex-situ* DNP experiments. In order to transfer magnetisation from the long lived species to other nuclei there are two types of couplings that can be exploited, these are the scalar and dipolar couplings. To achieve polarisation transfers through scalar couplings requires a pulse sequence that exploits one particular transfer route; i.e. a bond, and a specific J-coupling value. One such NMR experiment is a Total Correlation Spectroscopy (TOCSY) experiment where polarisation is spread across a network of coupled nuclear spins. In our case, observing ^{13}C, a natural abundance of $\approx 1\%$ renders it very inefficient. Additionally, the molecular topology (acetylated compounds) of the substances used leads to extremely low scalar coupling values owing to the distance between spins. However, the use of dipolar couplings provides a more efficient route to distribute polarisation throughout the molecule in question.

In the common heteronuclear NOE experiment a ^{1}H resonance is saturated, bringing about W_0 and W_2 relaxation with a nearby ^{13}C resonance. With the hyperpolarised samples here, we have

primarily a ^{13}C-^{13}C NOE where the imbalance in populations exists as a result of differential ^{13}C longitudinal relaxation rates. Two alternate pulse sequences can be used to develop NOE's in this way. In the first sequence (shown in Figure 4.2a) a selective π pulse with a sinc shape, tuned to the isotopically enriched carbonyl signal frequency and a mixing delay, τ_m, are followed by a $\pi/2$ broadband pulse on ^{13}C and subsequent acquisition of the NMR spectrum. Where there is a large ^{13}CO polarisation the initial π pulse can be omitted. This is especially the case where the other ^{13}C nuclei have almost completely relaxed after the dissolution and transfer process. By employing these pulse sequences to hyperpolarised samples a further increase in signal intensity was observed owing to polarisation transfer from the long lived hyperpolarised CO's to more rapidly relaxing CH's via a nuclear Overhauser effect. In this experiment it is only possible for the NOE to occur in the liquid sample as the effect requires motion in order to allow the polarisation transfer to occur. In the instrument cryostat spin diffusion can occur via spin flips but this is not an NOE. In principle the NOE can start as soon as the sample becomes liquid but the intercept of the buildup curves suggests that the effect is minimal during transfer.

4.2 Polarisation increases with an NOE mixing time post transfer in DNP experiments where slowly relaxing nuclei are present

The transfer of magnetisation from a long-lived polarised nucleus to a faster relaxing nucleus was examined by initially acetylating a test molecule, 4-methoxyphenol, with ^{13}C-acetyl chloride to yield 4-methoxyphenyl ^{13}C-1-acetate (see Figure 4.1). This reaction protocol was chosen as it is known to give a product of high purity and yield. The isotopic enrichment ensures that each molecule of the product will possess a ^{13}C nucleus with a sufficiently long T_1 to retain polarisation through the sample transfer process. Once transferred to the high field NMR spectrometer, the magnetisation is distributed across the molecule by a ^{13}C NOE.

A 1M sample of the derivatised, isotopically enriched 4-methoxyphenol ^{13}C-1-acetate molecule in a 50% mixture of methanol and DMSO with Finland radical (15mM) doping agent was polarised in the DNP polariser at 1.5K for 90 minutes. The polarised sample was then dissolved in 4ml
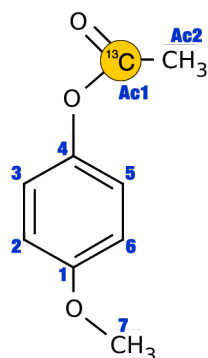
Figure 4.1: 4-Methoxyphenyl ^{13}C-1-acetate structure.

Carbon	Chemical Shift [ppm]	T1[s]
1	134.75	12.4
2/6	104.5	4.5
3/5	112.5	4.4
4	147.75	14.9
7	45.4	4.8
Ac1	161.25	10.9
Ac2	10.25	7.1

Table 4.1: Chemical shift and T1 values for 4-methoxyphenyl ^{13}C-1-acetate (figure 4.1). Adapted from[11].

methanol dissolution solvent, heated until a pressure of 9.0 bar was reached at ~150ºC, and transferred to a high field liquid state NMR spectrometer with a 500MHz proton frequency.

The spectra of DNP enhanced 4-methoxyphenyl ^{13}C-1-acetate in Figure 4.3 show two singlets at ~144ppm and ~158ppm that correspond to C1 and C4 and two doublets centred at ~114ppm & ~122ppm that correspond to C2/6 and C3/5. In Figure 4.3a the pulse sequence in Figure 4.2b was used with $\tau_m = 0$. The spectrum in Figure 4.3b was recorded with the pulse sequence in Figure 4.2b with $\tau_m = 10secs$. Comparing the two spectra, it is clear that where the mixing time was implemented, as in Figure 4.3b, an enhancement is seen for ^{13}C nuclei near to the long-lived isotopically enriched nucleus. The quaternary carbon signals, C1/4, show an approximately 3.5 fold increase in signal intensity compared to those in the spectrum where no NOE mixing time was used.
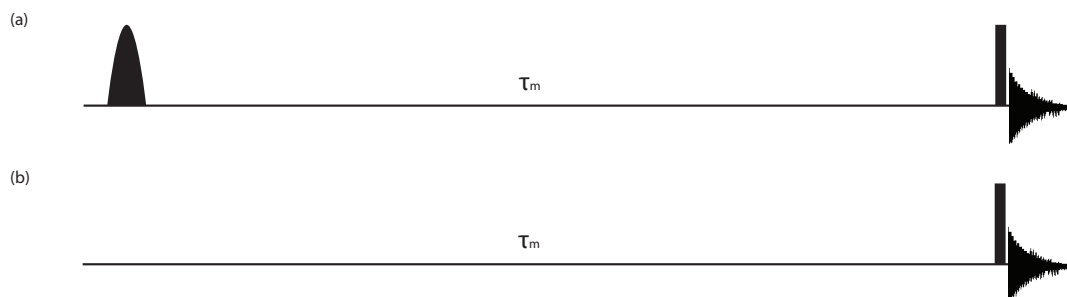
Figure 4.2: The NOE pulse sequences used in this work (a) a selective π sinc pulse tuned to the frequency of the isotopically enriched ^{13}C carbonyl followed by a mixing time τ_m, a $\frac{\pi}{2}$ broadband pulse and acquisition, and (b) a mixing time τ_m, followed by a $\frac{\pi}{2}$ broadband pulse and acquisition. Adapted from[9].
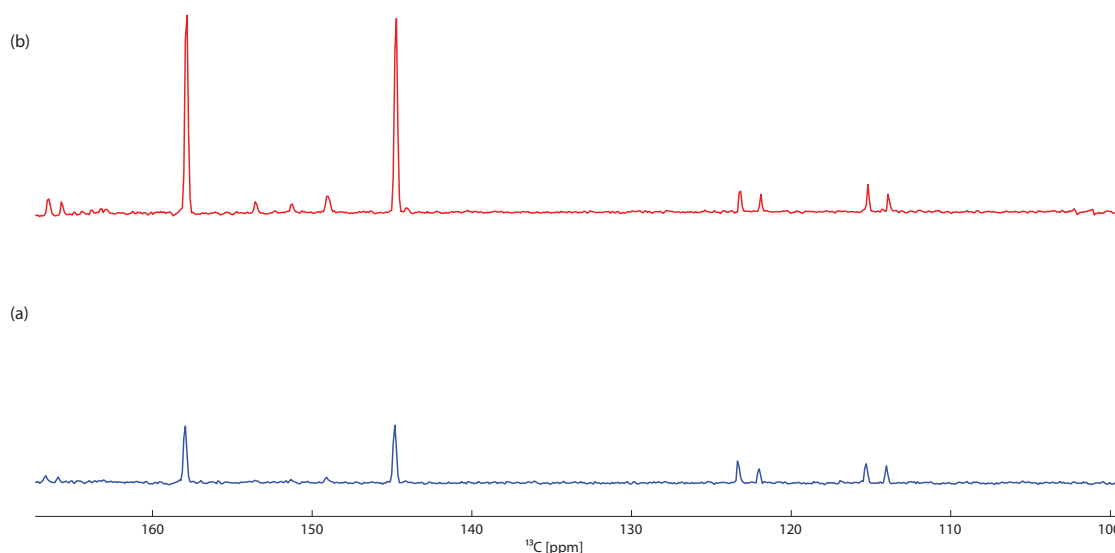
Figure 4.3: DNP spectra of 4-methoxyphenol ^{13}C-1-acetate polarised for 90 minutes in 50% methanol / DMSO with 0.15mM Finland radical before dissolution and transfer to a high field NMR spectrometer with a 500MHz proton frequency and acquisition of the NMR spectrum using the pulse sequence in Figure 4.2b, (a) with mixing time $\tau_m = 0s$ or (b) with mixing time $\tau_m = 10s$.

Carbon	Chemical Shift [ppm]	Enhancement (τ_m=0s)	Enhancement (τ_m=10s)
1	144	14.5	50.7
2/6	114	6.1	6.2
3/5	122	6.4	6.3
4	158	15	52.5

Table 4.2: Table of nuclear signal enhancement with τ_m=0 or 10 seconds. The enhancement value is expressed in terms of the fold enhancement from a non-DNP standard averaged over 32 scans.

4.3 As the NOE mixing time is varied for methoxyphenol ^{13}C-1-acetate a polarisation maximum exists for other fast-relaxing carbons at 5-10s

With the knowledge that polarisation can be transferred via a nuclear Overhauser effect it remains to ascertain the time dependence of the resulting signal intensities. As shown in Figures 4.4 and 4.5, after 90 minutes of polarisation, 4-methoxyphenyl ^{13}C-1-acetate in methanol/DMSO is dissolved with methanol and transferred to the high field NMR spectrometer for spectral acquisition. Using the pulse sequence described in Figure 4.2a the mixing time, τ_m, was varied with values of 0s, 1s, 5, 10s, 30s, 60s, 90s and 120s to determine the time dependence of the contribution to polarisation from the NOE. It is hard to give an absolute control for this experiment because there may be an NOE active during the transfer. However, the trend seen suggests that this effect does not cause a strong impact on the baseline. The quaternary carbons C1 and C4 show a signal strength maximum at ~10s whereas the tertiary carbons C2/6 and C3/5 show a maximum at ~5s. There is little difference in signal intensity between the two quaternary carbon signals or between the two tertiary carbon signals. It remains enigmatic why the pairs of signals have such similar intensities although it may be a result of the molecule's ring structure. Table 4.1 shows the T_1 values for the carbon nuclei in 4-methoxyphenyl ^{13}C-1-acetate. The quaternary carbons have T_1's of 13.0s and 9.8s whereas both tertiary carbons have T_1 values of 3.0s. During the NOE mixing time there is a balance of the rate of buildup due to the NOE from the isotopically enriched carbonyl carbon nucleus and loss of polarisation to the matrix via longitudinal relaxation with T_1. It is likely that it is the increased rate of relaxation for the tertiary carbon nuclei that leads to a maximum signal enhancement with a shorter mixing time using this NOE pulse sequence method.

4.4 Varying mixing time with natural abundance 4-methoxyphenyl acetate

Using natural abundance 4-methoxyphenyl acetate as the polarisation substrate in the NOE experiment gives a different result to that with the isotopically enriched molecule. Figure 4.6 shows
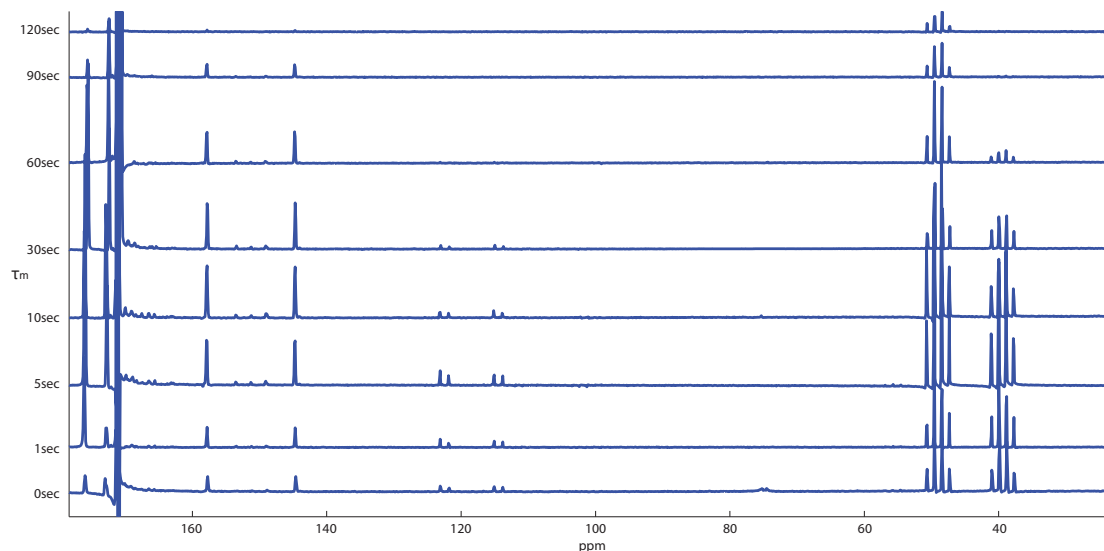
Figure 4.4: Mixing-time dependence on signal intensity for 4-methoxyphenyl ^{13}C-1-acetate polarised for 90 minutes with 0.15mM Finland radical at 1.5K before dissolution in hot, pressurised methanol and transfer to a high field liquid state spectrometer and acquisition with an NOE pulse sequence (see Figure 4.2a).
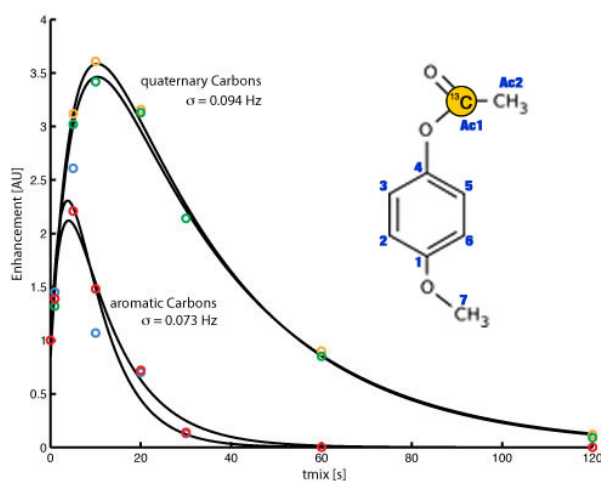
Figure 4.5: Relative intensity of signals from DNP-NOE experiments with 4-methoxyphenol over a range of mixing times. Lines are a fit by a least squares regression method with a numerically integrated Solomon equation (Equation 2.57) . Adapted from [9].
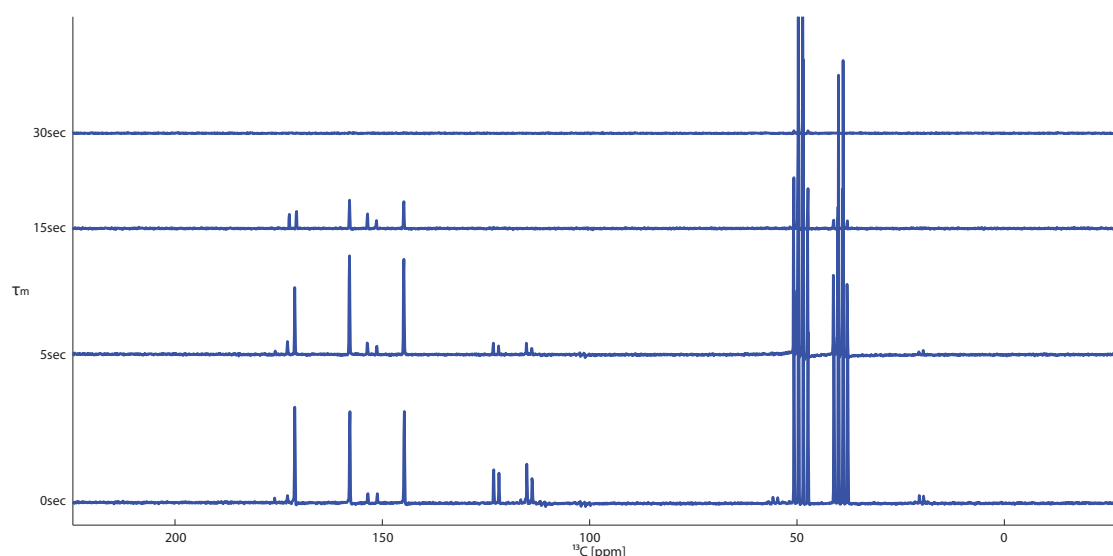
Figure 4.6: Mixing-time dependence on signal intensity for 4-methoxyphenyl acetate polarised for 90 minutes with 0.15mM Finland radical at 1.5K before dissolution in hot, pressurised methanol and transfer to a high field liquid state spectrometer and acquisition with an NOE pulse sequence (see Figure 4.2a).

Position	Chemical Shift	Enhancement at $\tau_m=$ 0s	Enhancement at $\tau_m=$ 5s	Enhancement at $\tau_m=$ 15s
1	144	49	52	16
2/6	114	19	7	-
3/5	122	17	7	-
4	158	49	53	16

Table 4.3: Signal enhancement by mixing time for polarised natural abundance 4-methoxyphenyl acetate expressed as a fold increased compared to a liquid state reference spectrum for this sample.

spectra for the non-enriched molecule with mixing times of 0s, 5s, 15s and 30s. There is a slight polarisation enhancement to 5s but the signal intensity rapidly drops from this point. The decrease in efficiency of the NOE polarisation enhancement is likely to be a consequence of the 100 fold decreased probability of a given ^{13}C nucleus having a polarised ^{13}C nucleus nearby from the acetyl tag carbonyl signal.

4.5   Using a selective pulse to invert the long lived nuclear population increases the NOE enhancement in some situations

For a NOE mediated polarisation transfer to occur there must be an imbalance in the populations of proximal spins. The hyperpolarised nuclear spins of DNP experiments automatically satisfy this criterion so the polarisation enhancement should occur without the selective pulse from the pulse sequence in Figure 4.2a giving a pulse sequence as Figure 4.2b.

Both natural abundance and isotopically enriched 4-methoxyphenyl acetate were separately polarised for 60 minutes with OX63 radical in a DNP experiment. Each then had both pulse sequences shown in figure 4.2 applied with the mixing time τ_m being varied over a series of time-points. The signal intensities observed for the C1/4 signal are shown in figure 4.7. For the isotopically enriched molecule there is little difference between the two pulse sequences. However, for the natural abundance molecule there is a significant difference in the mixing-time dependence of the polarisation enhancement. For the natural abundance sample the pulse sequence is as shown in Figure 4.2a, where a selective π pulse is employed prior to a variable mixing time, results in an enhancement to 15s that drops much more rapidly than with the isotopically enriched molecule. For the natural abundance sample using the pulse sequence in Figure 4.2b there is no visible enhancement due to an NOE. This suggests that the selective π pulse acts to increase the difference in populations sufficiently in the natural abundance case to allow the NOE dependent polarisation buildup rate to temporarily dominate the longitudinal relaxation rate.

One interesting trend seen in Figure 4.7 is that the natural abundance molecule shows a much higher initial polarisation level than the isotopically enriched sample. This can be explained by the abundance of ^{13}C in that each site only has a 1% chance of being the NMR active isotope in each individual molecule. With a natural abundance tag each site is equally likely to receive polarisation on irradiation via DNP. However, with the isotopically enriched tag the tag is 100 times more likely to NMR active than any resonance in the original molecule and while the DNP polarisation has not achieved a maximal level the tag is therefore more likely to be polarised than the ring carbons in this molecule before any NOE related enhancement.
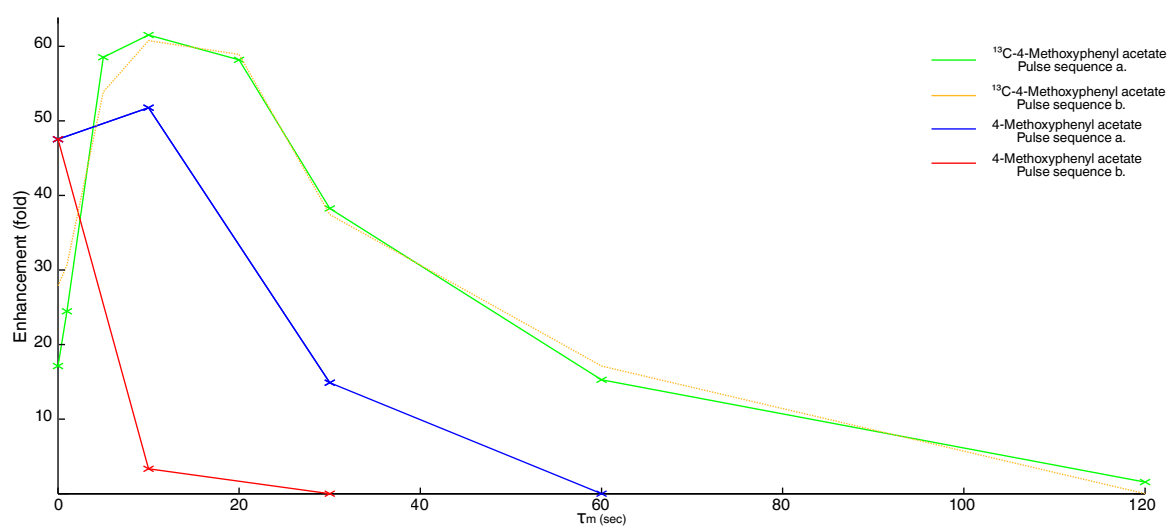
Figure 4.7: A comparison of the mixing-time dependence of the NOE derived polarisation enhancement on C1/4 for natural abundance and isotopically enriched 4-methoxyphenyl acetate with both pulse sequences described in Figure 4.2.

Chapter 5

Co-polarisation agents increase the polarisation efficiency in DNP experiments

5.1 Introduction

For a nucleus to become polarised during the DNP experiment it must be within close proximity of a radical. However, if the nucleus is too close to the radical then the paramagnetic effect originating from the electron increases the longitudinal relaxation rate such that the polarisation decays faster than it accumulates. As a result of these two factors only a small number of nuclei are potentially able to receive initial polarisation from the radical in the DNP experiment. The majority of polarisation arising in a DNP polarised sample occurs as a result of spin diffusion transporting polarisation from the primarily polarised nuclei throughout the bulk of the sample. The efficiency of this process depends on the internuclear distance with r^{-6} so the average distance between nuclei has a large impact on the efficiency of this process. The efficiency of spin diffusion also depends on the dipolar coupling and ratio of the nuclear gyromagnetic ratios making homo-nuclear polarisation more efficient than heteronuclear transfers.

For carbon nuclei only ~1% are the NMR active isotope ^{13}C with the remaining ~99% the inactive ^{12}C. This low natural abundance for the NMR active isotope has the effect of dramatically increasing the average internuclear distance in the glass. In comparison to a fully ^{13}C enriched sample, a natural abundance sample has an average internuclear distance that is ten times greater, consequently polarisation is much less likely to be transferred by spin diffusion in a natural abundance sample. In a DNP experiment the majority of spins receive polarisation indirectly via spin diffusion so a reduction in the efficiency of spin diffusion in turn causes DNP enhancements to be reduced. Nuclear longitudinal relaxation has the effect of depolarising spin populations and the nuclear longitudinal relaxation rate therefore has the effect of limiting the buildup of bulk polarisation for a sample in the DNP experiment. If relaxation rates are unaltered the nuclei are less likely to be polarised as the rate of buildup is decreased as a result of less efficient spin diffusion.

The effective average internuclear distance can be actively decreased by the addition of an isotopically enriched component to the glass. Examples of such components are a derivatisation tag or a ^{13}C enriched glassing solvent. By making this alteration to the experimental conditions the likelihood of each spin having a near neighbour to which polarisation can be passed is greatly increased thus increasing the overall spin diffusion efficiency through the sample. This enables polarisation to spread more easily through the sample resulting in a greater enhancement factor, ϵ as well as a greater number of polarised spins providing a stronger signal. If the isotopically enriched nucleus has an extended longitudinal relaxation rate this will additionally increase the DNP enhancement efficiency.

5.2 Isotopic enrichment in 4-methoxyphenyl acetate yields a greater DNP polarisation

In the previous section a model molecule, 4-methoxyphenol, was derivatised with an isotopically enriched acetyl tag to yield 4-methoxyphenyl ^{13}C-1-acetate. Spectra of the derivatised and non-derivatised molecule are given in Figure 5.1. From the T_1 values of the nuclei in methoxyphenyl ^{13}C-1-acetate, given in table 4.1, it is apparent that the ^{13}CO nucleus chosen for enrichment in the acetyl has a much longer T_1 value than many of the other nuclei in the molecule of interest. The act

of isotopic enrichment therefore has the action of significantly increasing the average longitudinal relaxation time constant for all ^{13}C spins in the sample. Consequently, the polarisation that is generated in the DNP experiment is retained for a greater time leading to a higher overall accumulation of polarisation. In addition to affecting the relaxation properties of the sample the increase in the total number of spins of the carbon isotope active in NMR, ^{13}C, is dramatically increased reducing the average distance between ^{13}C nuclei. This in turn increases the likelihood that polarisation is passed through the sample by carbon-carbon spin diffusion leading to an increased bulk polarisation.

Ex-situ DNP spectra for the derivatised molecule show a three-fold greater increase in signal enhancement from the non-derivatised sample spectrum for the isotopically enriched derivatised sample versus the natural abundance derivatised sample. This is a consequence of a combination of the raised average longitudinal relaxation time constant[106], the increased density of potential spin diffusion participants and the altered molecular configuration. Where the enriched tag has a ^{13}C spin with a much longer than average T_1 polarisation can be retained for longer although at low temperatures the T_1 values of most ^{13}C nuclei become so long that this is likely to be low impact. The majority of nuclei polarised via DNP gain their polarisation from transmission via spin diffusion rather than as the primarily polarised nucleus. This transmission is achieved by spin diffusion which depends on distance to the inverse power of six. Therefore as the concentration of NMR active nuclei increases and the average internuclear distance decreases the capacity for spin diffusion increases sharply. Additionally a much simpler mechanism that is supported in part by the data shown in figure 4.7 is simply that the altered chemical structure allows closer molecular packing also decreasing the average internuclear distance to facilitate spin diffusion. It should be noted that in figure 4.7 the non-isotopically enriched tag leads to an initial polarisation enhancement that is nearly three times greater than that with the isotopically enriched sample so the enhancement seen in figure 5.1 can be seen as all the more significant.
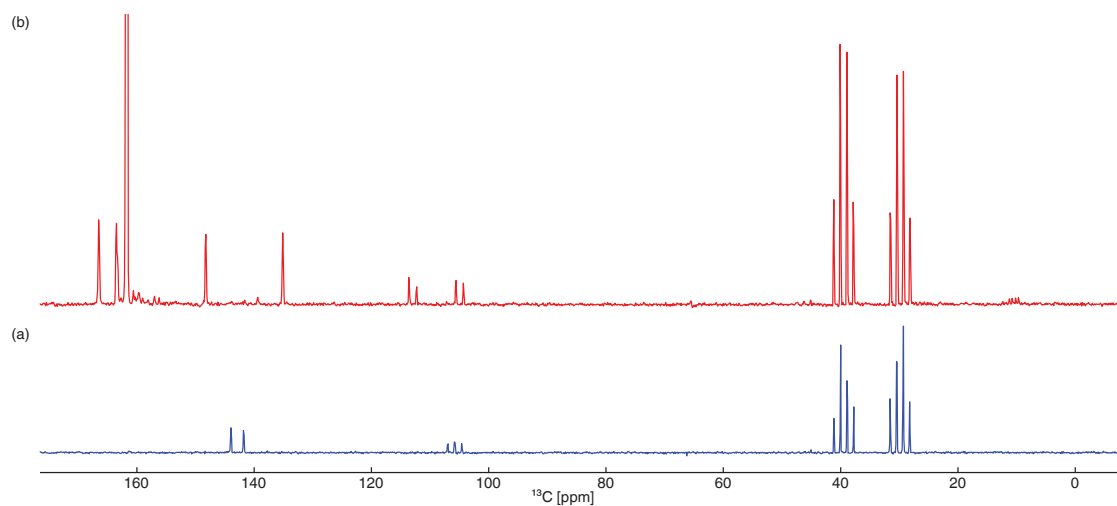
Figure 5.1: DNP spectra for (a) 4-methoxy phenol and (b) 4-methoxyphenyl ^{13}C-acetate

	4-Methoxyphenol Enhancement	4-Methoxyphenol ^{13}C-acetate Enhancement
1	8.9	26.3
2/6	3.8	11.7
3/5	3.8	11.6
4	8.5	26.3

Table 5.1: Nuclear enhancement factor per nucleus for 4-methoxyphenol with or without ^{13}C-acetate expressed in signal intensity fold change compared to a reference spectrum of this sample.

5.3 Citrate shows an 80 fold additional enhancement with a ^{13}C-2-acetone co-polarisation agent

The mode through which an isotopically enriched molecular tag, used to chemically derivatise a target molecule - for example an acetyl group, acts to increase the level of polarisation for a sample in a DNP experiment is dependent on the number of spins and their relaxation properties. There is no dependence on molecular bonds for this effect to occur so a similar effect should be seen in a mixture with a substance, as opposed to a chemical derivation, that has the desirable characteristics as outlined. A 1M sample of citric acid was dissolved in $100\mu l$ of 1:1:1 water/acetone/DMSO with 15mM OX63 trityl radical doping agent. The mixture was cooled to 1.5K and irradiated with resonant microwaves for 90 minutes before dissolution in water containing 0.01% EDTA as an ion pairing agent. On delivery to a high field NMR spectrometer the spectrum was acquired with a simple $\pi/2$ pulse followed by the acquisition of the NMR signal. This experiment was performed twice, once with natural abundance acetone and once with ^{13}C-2-acetone. Figure 5.2 shows the two spectra recorded. The spectrum with enriched acetone (red) shows very large enhancements for the citrate signals. In particular the citrate quaternary signal is enhanced by ~80 fold. Here the ^{13}C-2-acetone is providing a high concentration, slowly relaxing spin polarisation pool. This pool aids polarisation accumulation and spread through the sample via carbon-carbon spin diffusion ultimately leading to a dramatic increase in the polarisation enhancement achieved.
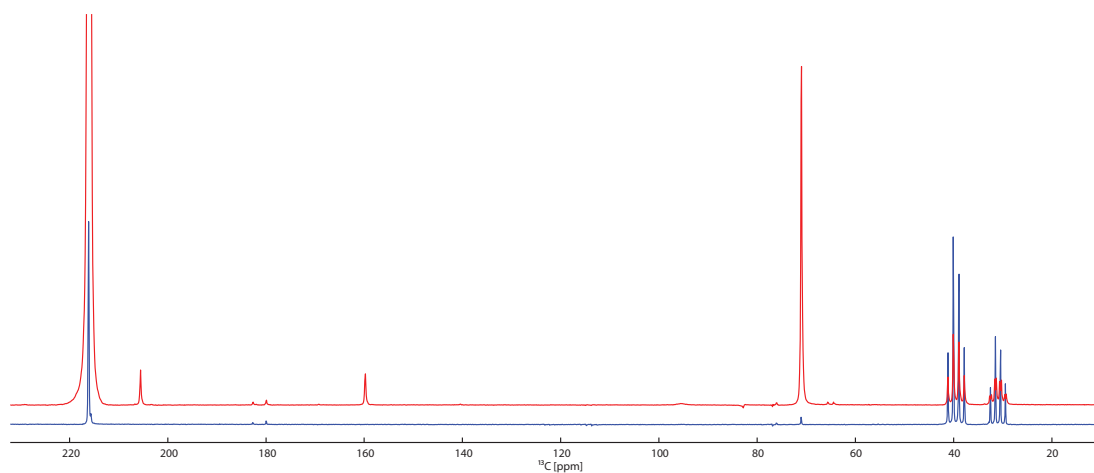
Figure 5.2: Citrate (1M) polarised for 90 minutes at 1.5K in 1:1:1 water/acetone/DMSO where the acetone is natural abundance (blue) or ^{13}C enriched at C1 (red). The quaternary citrate signal at ~71ppm shows an ~80 fold enhancement with enriched acetone when compared to the spectrum with natural abundance acetone.

Chapter 6

Quantum rotor mediated Zeeman polarisation enhancement

6.1 Introduction

DNP has the potential to provide enormous enhancements of five orders of magnitude or more but the number of substances with which this has proven possible is very limited. The vast majority of substances that would be attractive to polarise, under the standard DNP experimental conditions, do not yield more than a relatively small signal enhancement. In the DNP spectra of many such samples, I have observed negative signals for the methyl carbon nuclei of the glassing solvents and substrate as well as other protonated carbon nuclei on some occasions. Owing to the regularity of the correlation between these negative signals and poor DNP enhancement the question arises as to whether the cause of the negative signals could also be the reason that the DNP effect is not as efficient as with some other substances.

At the operating temperature of the polariser instrument the rotation of methyl groups displays the underlying rotational tunnelling behaviour. As the most consistent feature in the spectra of poorly polarising substances is negative methyl signals for certain glassing solvents, the initial postulate was that somehow energy was leaking from the rotational tunnelling system of the methyl groups to the nuclear Zeeman system. An initial experiment to confirm this possibility was to cool

$100\mu l$ of pure acetone to the DNP operating temperature of 1.5K for an hour, as with DNP experiments, but with no radical or microwave irradiation, before dissolution in unpolarised methanol. The ^{13}C NMR spectrum from this experiment showed a negative signal of significant intensity for the acetone methyl indicating that there was indeed an additional, assumed to be methyl related, process occurring in the environment of the *ex-situ* DNP experiment that leads to a negative polarisation component. As there are two competing polarisation processes in this system, where they are similar in intensity with opposite sign they can act to negate one another leading to poor DNP polarisation. In the absence of DNP the quantum rotor effect alone provides a significant polarisation enhancements that can prove an additional avenue to increase the signal strengths in NMR experimentation. As the DNP effect can increase the population of either nuclear Zeeman level, depending on the choice of microwave frequency used, the DNP enhancement can interfere either constructively or destructively with the quantum rotor effect. If the two effects are made to interfere constructively, by using the high DNP microwave frequency, then an increased final polarisation is seen. Alternatively, the rotating group can be manipulated by - for example deuteration to increase the rotors moment of inertia such that the rotor effect is abrogated[107,108], leading to a pure DNP derived enhancement. Combinations of these approaches allow experimental design to optimise polarisation for a wide range of substances.

6.2 Acetone, ethanol, isopropanol, DMSO and DMF cooled alone give negative methyl signals

In order to demonstrate the quantum rotor effect in a simple system, pure samples of acetone, acetic acid, isopropanol, DMF and ethanol ($100\mu l$ each) were cooled to 1.5K and the temperature maintained for 60 minutes before dissolution in hot pressurised methanol dissolution solvent. The samples did not contain any radical doping agent and there is no microwave irradiation as would be the case for a DNP experiment. Therefore any polarisation present in the sample can only have occurred as a result of a temperature dependent effect while the sample is in the instrument cryostat. The unpolarised methanol dissolution solvent signal used to transfer the sample to the liquid state NMR spectrometer provides a convenient standard phase reference. All of the listed
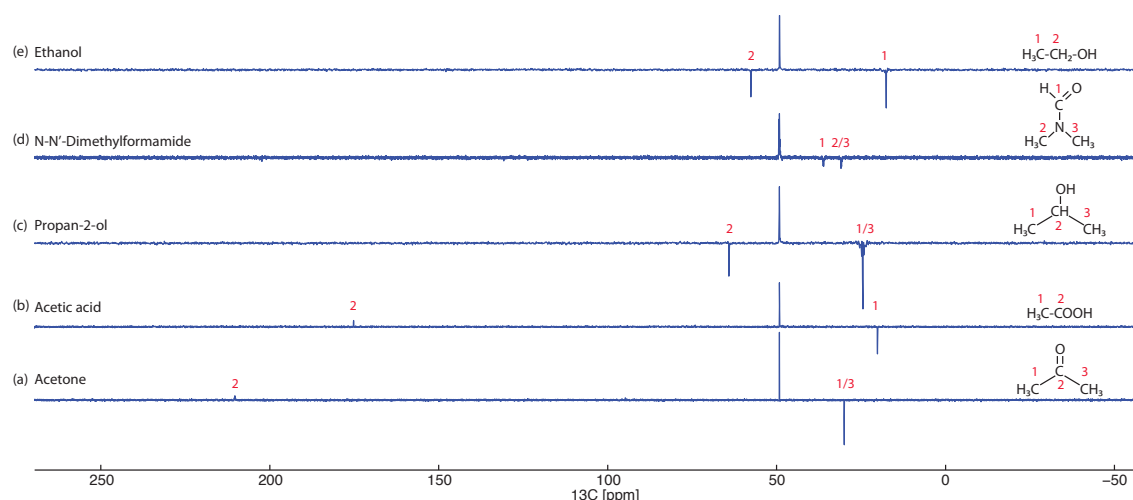
Figure 6.1: ^{13}C NMR spectrum for $100\mu l$ (a) acetone, (b) acetic acid, (c) propan-2-ol, (d) N,N'-dimethyl formamide & (e) ethanol after cooling to 1.5K for 60minutes before dissolution with hot, pressurised methanol and transfer to a high field NMR spectrometer for acquisition of the NMR spectrum with a simple $\pi/2$ pulse followed by acquisition of the NMR spectrum.

samples give spectra showing strongly enhanced negative signals for the methyl groups in the molecules as well as for any other proton attached carbon nuclei (see Figure 6.1). These results are consistently seen where the sample molecule contains hindered quantum rotors with a sufficiently high rotational tunnelling frequency. The negative enhancements arise as a result of a coupling between the rotational tunnelling and nuclear Zeeman systems. This coupling allows energy to slowly flow from the rotational tunnelling system into the nuclear Zeeman system when the sample is cooled to very low temperatures. Where nuclear T1's are sufficiently long this energy can accumulate as a Zeeman β level population enhancement.

6.3 Glycerol does not possess C3 symmetry but still shows negative polarisation on cooling

The quantum rotor mechanism relies entirely on the rotational symmetry of the molecular group in question. The CH$_2$OH groups of glycerol are not symmetrical but are free to rotate around the glycerol C2. Figure 6.2 shows a spectrum for a fully labelled sample of ^{13}C-glycerol treated similarly to the samples described in the previous section. This shows small negative signals for the

Acetone		
Carbon	Chemical Shift [ppm]	Enhancement
1	30.0	-2.90
2	210.3	0.89
3	30.0	-2.90
Acetic acid		
Carbon	Chemical Shift [ppm]	Enhancement
1	20.0	-3.40
2	179.0	0.97
Propan-2-ol		
Carbon	Chemical Shift (ppm)	Enhancement
1	24.5	-4.19
2	64.1	-4.10
3	24.5	-4.19
N-N'-Dimethylformamide		
Carbon	Chemical Shift [ppm]	Enhancement
1	163.2	-
2	34.9	-1.05
3	29.8	-1.14
Ethanol		
Carbon	Chemical Shift [ppm]	Enhancement
1	57.0	-3.40
2	17.31	-4.67

Table 6.1: Chemical shift and enhancement for carbon resonances in acetone, acetic acid, propan-2-ol, N,N'-dimethylformamide and ethanol $100\mu l$ cooled to 1.4K for 60 minutes prior to dissolution in methanol in all cases. Enhancements are expressed as a fold-change in peak height compared to a reference spectrum taken with a standard liquid state NMR spectrometer. Note that the enhancements could be considered to have an additional 1-fold enhancement to overcome the Boltzmann polarisation in addition to the values in this table.
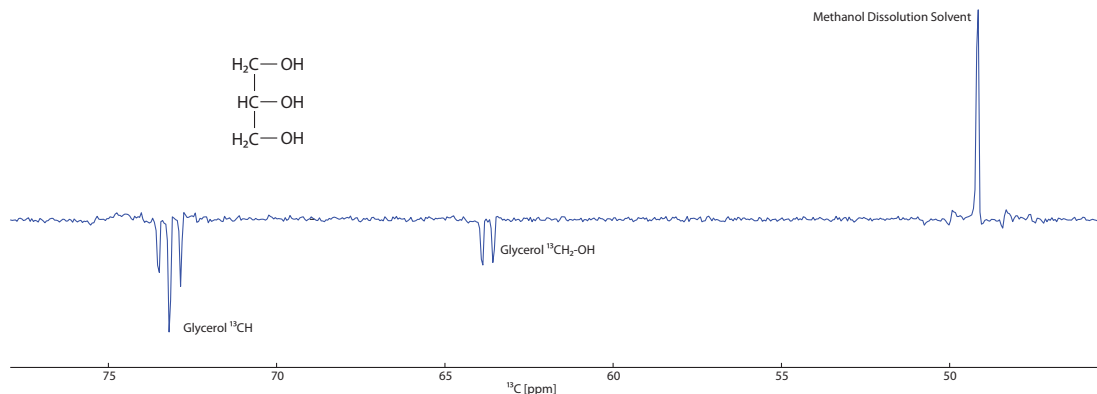
Figure 6.2: ^{13}C NMR spectrum for $100\mu l$ 50% ^{13}C-glycerol after cooling to 1.5K for 60minutes before dissolution with hot, pressurised methanol and transfer to a high field NMR spectrometer for acquisition of the NMR spectrum with a simple $\pi/2$ pulse followed by acquisition of the NMR spectrum.

	Chemical Shift [ppm]	Enhancement
CH	73.2	-1.88
CH$_2$OH	63.7	-0.37

Table 6.2: Table of enhancement for ^{13}C glycerol taken as the fold enhancement of the peak integrals compared to the same sample after 1 hour relaxation time.

CH$_2$OH and CH ^{13}C signals. Considering the 100% isotopic enrichment and the amplitude of results seen, for true symmetrical rotors these signals would be very small. However, these signals are of significant amplitude and are have a negative sign compared to the methanol reference.

The results seen here could stem from either the low probability of the CH$_2$OH group adopting a pseudo-symmetrical C3-like state or another spin-spatial coupling allowing this polarisation process to occur at a very low rate. Once proton polarisation is achieved the normal nuclear relaxation processes transfer polarisation as in other cases.

6.4 Time dependence of the quantum rotor effect for DMSO, acetone and acetate

Having identified a quantum rotor dependent effect that leads to a polarisation enhancement there is now a requirement to understand and characterise the phenomenological properties of the

	DMSO	Acetone	Acetate
ρ_0^C	-1.78×10^8	-9.0636×10^7	9.901×10^4
$R_{1a}[Hz]$	8.37×10^{-3}	1.06×10^{-2}	2.63×10^{-3}
$R_{1b}[Hz]$	8.37×10^{-3}	1.06×10^{-2}	1.01×10^{-1}
$R_{1C}[Hz]$	3.33×10^{-3}	3.33×10^{-3}	3.33×10^{-3}
$k\sigma[Hz]$	9.417×10^{-5}	3×10^{-4}	0.27

Table 6.3: Fitting data for least squared regression of equation 2.57

effect so that *ex-situ* experiments can be most effectively designed. Samples of $100\mu l$ DMSO, acetone and acetic acid were cooled to 1.5K and the temperature maintained for a number of different durations with no microwave irradiation before dissolution with methanol and transfer to a high field spectrometer for acquisition of a liquid state NMR spectrum. Crosses in Figure 6.3 show the methyl ^{13}C signal intensity post-dissolution. Tunnelling frequencies of kHz for DMSO, MHz for acetone and GHz for acetate[87] have been reported and there is a clear trend where a higher tunnelling frequency leads to an earlier and stronger absolute signal maximum. The buildup profiles are well described by equation 2.57 (shown in Figure 6.3, red, green & blue lines from a fit to the data by a least squares regression method according to equation 2.57). The fitted parameters are listed in table 6.3. There is also a near linear path between the absolute maxima of these substances although with only three substances this trend cannot be considered statistically reliable. The ^{13}C signal for the carbonyl of the acetate sample shows a signal intensity buildup that is consistent with the equilibration to a new Boltzmann polarisation for the low temperature that would be expected in the absence of the rotor effect.

6.5 Determination of the true quantum rotor effect enhancement factor

In a simple quantum rotor polarisation time-course experiment, signal intensities are seen to vary with time. With acetone, the non-proton attached carbonyl carbon shows a buildup as would be expected from the change in the Boltzmann distribution due to sample cooling in the absence of a quantum rotor effect, as has consistently been observed. The proton-attached methyl groups however show a buildup of polarisation with the opposite sign to the thermal signals and an
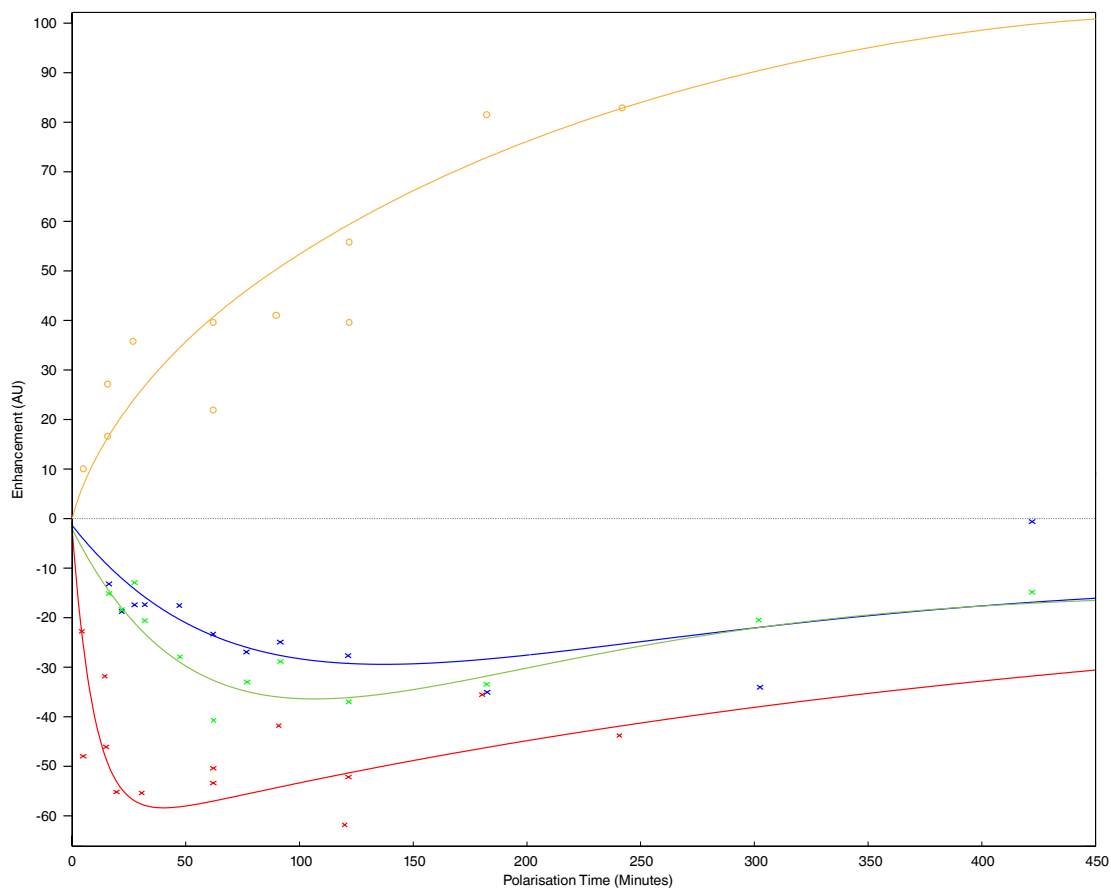
Figure 6.3: The time-dependence of the quantum rotor effect for the methyl signals for DMSO (blue), acetone (green) and acetate (red) samples and the acetate carbonyl signal (yellow) cooled to 1.5K for a number of durations before transfer by methanol to a high field NMR spectrometer for NMR spectral acquisition. The enhancement value is relative to the equilibrium polarisation of the acetate carbonyl resonance.

intensity that builds up to a maximum before falling back towards the thermal polarisation value.

For acetone the equation 2.57 shows a very close fit to the experimental data shown in Figure 6.4. Once all the constants of Equation 2.57 have been determined it is possible to predict a maximum enhancement. The buildup of polarisation on the carbonyl carbon of acetone follows equilibration towards the Boltzmann polarisation. This can therefore be used to determine the rate of buildup in the absence of a quantum rotor effect. The calculated constants now allow the simulation of the components of the quantum rotor enhancement to be performed. The maximum enhancement is determined as being the ratio of the maximum absolute quantum rotor enhancement and the Boltzmann polarisation in the absence of a quantum rotor effect.

The simulated maximum polarisation describes the quantum rotor enhancement separate from relaxation and in the low field, low temperature environment of the polariser instrument. For acetone an enhancement factor of $\approx$20 is obtained, the quantum rotor effect buildup rate is 1.5×10^{-4} Hz with a buildup time of 1.77 hours. The carbon relaxation rate is 2.24×10^{-6}Hz (T_{1C} = 124 hours). The fitted rates for several substances are displayed in Table 6.4 Interestingly the buildup rate for acetone increases considerably when mixed with other substances such as DMSO.

6.6 Temperature dependence of the quantum rotor effect for acetate

In addition to the duration the sample spends at the low temperature the resulting polarisation is also dependent on the actual temperature itself. The temperature that an acetate sample is cooled to was varied where the duration at the low temperature is maintained at 60mins. A trend emerges where a lower temperature generates a greater polarisation enhancement as shown in Figure 6.5. The resulting total polarisation is a balance between several different relaxation rates and it is known that below 3K proton nuclear Zeeman relaxation has a quadratic dependence (with general form $ax^2 + bx + c$) on temperature due to intrinsic low frequency excitations in amorphous glasses[99]. Whether a simple link to this effect exists remains enigmatic but the trends are similar.

Two important facts about the temperature dependence of this system emerge from these results. Firstly, a lower operating temperature results in a significantly larger polarisation so, in

Compound	Nucleus	$R_{1C}[10^{-5}Hz]$	$R_{1A}[10^{-5}Hz]$	$R_{1B}[10^{-5}Hz]$	$\sigma k[10^{-5}Hz]$	ρ_0^C	Enhancement
Acetone	Me	0.224±0.137	15.67±14.85	4.83±1.34	-127.50±71.41	1.00±0.037	18.6
	CO	10.00±1.31				1.00±0.037	
6-Chloro-2-hexanone	CO	12.83±0.49				1.00±0.0109	
	C1	20.47±2.53	376.76±47.26	185.92±11.37	-86.56±10.89	0.1116±0.0084	2.11(0.24)
	C2	21.34±2.17	376.76±47.26	185.92±11.37	-102.89±12.49	0.1434±0.0085	1.95(0.28)
	C3	22.52±2.30	376.76±47.26	185.92±11.37	-109.42±13.18	0.1492±0.0085	1.99(0.29)
	Me	27.08±4.68	376.76±47.26	185.92±11.37	-170.89±21.01	-0.2334±0.0082	-1.99(0.47)
	C4	23.39±2.65	376.76±47.26	185.92±11.37	-98.25±12.47	0.1292±0.0084	2.07(0.27)
Pentanol	C1	4.016±0.243	2603±82	2375±72	-15515±15500	0.9230±0.0377	0.62
	C2	4.310±0.281	2603±82	2375±72	-14675±14485	0.8308±0.0372	0.65
	C3	3.669±0.234	2603±82	2375±72	-14582±14485	1.0607±0.0439	0.51
	C4	3.073±0.203	2603±82	2375±72	-15432±15161	1.3073±0.0574	0.43
	Me	4.708±0.335	2603±82	2375±72	-21487±21098	0.4227±0.0343	1.87
Acetic acid	CO	3.5243±0.83				1.00±0.0531	
	Me	0.5316±0.194	14.626±16.57	5.511±1.55	-121.65±84.7	1.00±0.0531	13.76
Acetic acid/Water	Co	3.157±0.65				1.00±0.0712	
	Me	0.0860±0.033	262±316	88±15	-72.6±17.6	1.00±0.0712	0.55

Table 6.4: Simulation data according to equation 2.57 for the buildup of quantum rotor polarisation on acetone, 6-chloro-2-hexanone, pentanol, acetic acid and acetic acid / water. Adapted from[7]. For each substance a least squared regression method was then used to fit a curve to the data with the fitting parameters shown. These parameters allow the prediction of the total isolated polarisation due to this effect and this is given in the last column. Errors of fitted constants were determined using a Monte Carlo simulation.
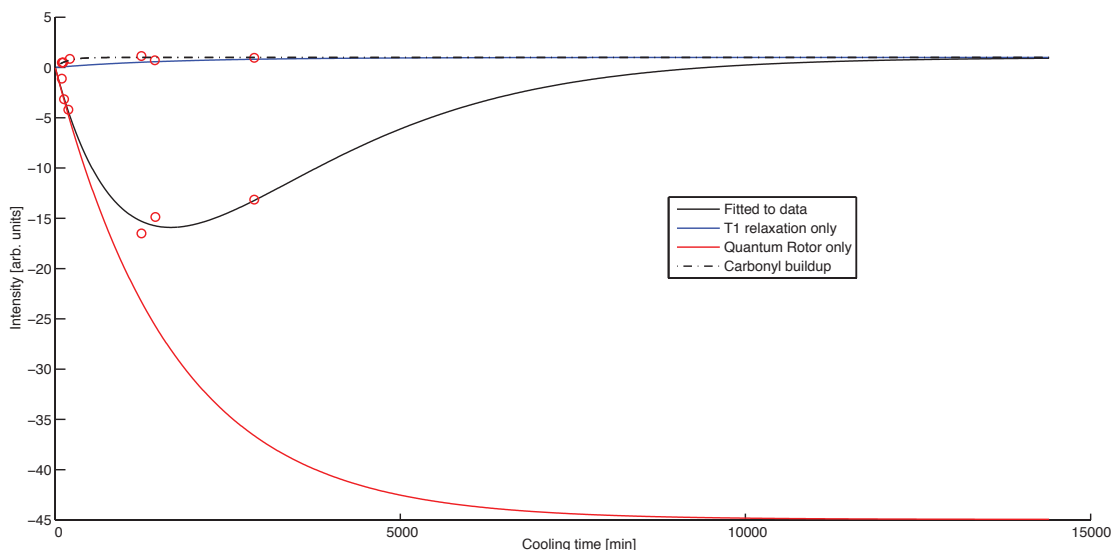
Figure 6.4: Experimental and fitted buildup of polarisation of QR polarisation for pure acetone. Red circles: Experimental signal intensities for the methyl group. Black circles: signal intensities for CO. Black lines: fitted data according to equation 2.57 for the methyl carbon and to a saturation recovery curve for CO. Red line: Simulated QR buildup curve using values obtained form the experimental data. Blue curve: Simulated Boltzmann buildup for the methyl ^{13}C neglecting the quantum rotor contribution.. Adapted from [7].

experiments where a large rotor effect is desired the lowest temperature possible should be used. Secondly, there is still a distinguishable signal at 3.4K; the upper limit for our instrument. At temperatures such as these, slow sample spinning starts to become possible which may enable future MAS solid state analysis of these samples.

6.7   Pre-cooled acetone shows decreased polarisation

The energy that drives the quantum rotor polarisation enhancement effect is derived from the change in temperature that the sample experiences. Therefore the magnitude of the polarisation enhancement effect will depend upon the difference between the initial quantum rotor spin temperature and the cooled lattice temperature. A larger temperature gradient will result in a greater polarisation. If an acetone sample is pre-cooled in liquid nitrogen at 100K for 18 hours prior to cooling to 1.5K, on dissolution and transfer, the spectrum shown in Figure 6.6 is seen where no visible methyl signal is observed. This is consistent with the expected decrease in energy available to
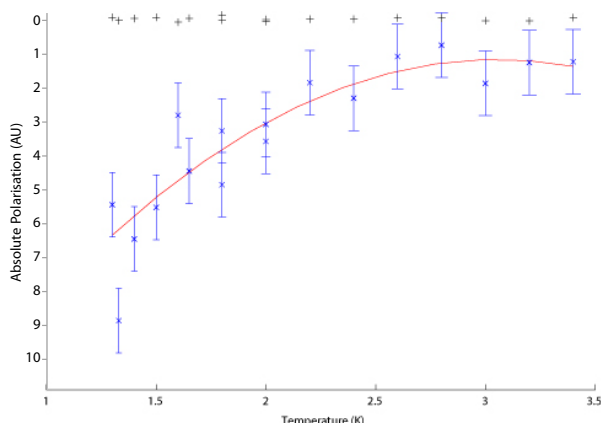
Figure 6.5: The temperature dependence of the ^{13}C signal for the methyl group of acetate cooled to several temperatures for 60 minutes before dissolution in methanol and transfer to a high field NMR spectrometer for acquisition of an NMR spectrum. Here 'x' shows data, '+' shows the baseline noise, the red line is the quadratic fit determined by a least squares regression method and the error bars are the RMSD for the quadratic fit with general form $ax^2 + bx + c$.

drive this effect as a result of the decreased temperature gradient experienced by this sample. This result provides validation of the concept that energy is transfered in cooling from the rotor system to the nuclear Zeeman system which is central to this section of my thesis.

6.8   Deuteration of methyl groups in hindered rotors results in a loss of the polarisation effect

The rotational tunnelling frequency of a molecular group depends on the moments of inertia of its substituents. In the case of a deutero-methyl group the moment of inertia of the deuteron is sufficiently large when compared to a protonated methyl group to greatly decrease the rotational tunnelling frequency. Consequently, in our system deuteration of methyl groups has the effect of abrogating the polarisation enhancement effect. Additionally, as the deuteron is a quadrupolar nucleus, the deuteron polarisation relaxes much more quickly than in the case of protons.

Where it is desirable to abolish the quantum rotor effect in an experiment, for example where a DNP effect alone is desired, for example where the rotor effect confuses the experimental results (see glucose below), the use of per-deuterated solvents and sample molecules will result in no observable quantum rotor enhancement effect. This has been verified by the cooling of per-deuterated acetone
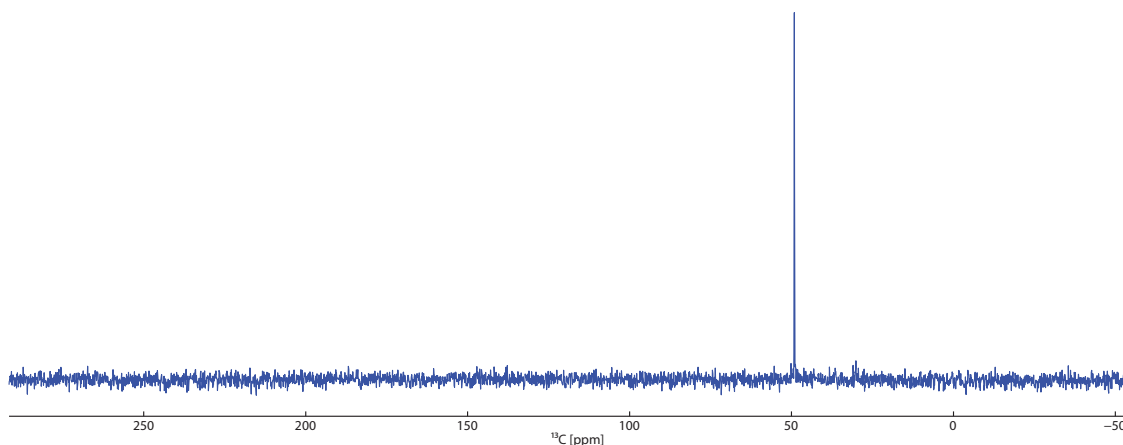
Figure 6.6: ^{13}C spectrum of an acetone pre-cooled in liquid nitrogen for 18 hours before cooling to 1.5K for 60 minutes.

and per-deuterated DMSO in the same manner as other quantum rotor polarisation experiments. In all cases there is no sign of the negative quantum rotor polarisation.

6.9 The effect of the concentration of protonated methyl groups in a sample of acetone and DMSO

With DNP experiments the resulting enhancement depends to a great extent on the transmission of polarisation from one spin to others by spin diffusion and thus throughout a sample. If there is too low a concentration of active nuclei this effect is limiting. To demonstrate the dependence on the proton-bearing methyl group density figure 6.7 shows four spectra for a 10% mixture of ^{13}C-1-acetone in DMSO with varying percentages of DMSO methyl per-deuteration. This was achieved by mixing per-deuterated DMSO with protonated DMSO. With 100% DMSO methyl per-deuteration the polarisation enhancement effect for the acetone methyl signal is reduced to around a tenth of the full enhancement. With 33-100% DMSO methyl protonation the maximal acetone polarisation enhancement is achieved. This suggests that there is a minimum proton concentration required for efficient spin diffusion through the proton network. Once this threshold is reached there seems to be little additional effect on the acetone methyl signal. For the DMSO methyl signal there is a steady increase with the proportion of protonated methyl groups that suggests that
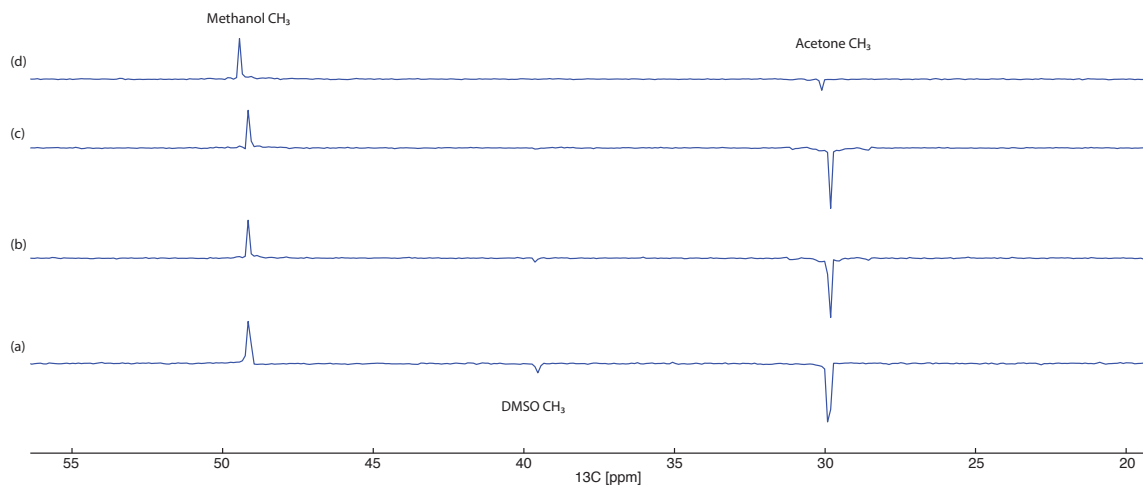
Figure 6.7: Concentration effects for $10\mu l$ ^{13}C-1-acetone in $90\mu l$ DMSO with (a) 100% DMSO protonation, (b) 67% DMSO protonation, 33% DMSO per-deuteration, (c) 33% DMSO protonation, 67% DMSO per-deuteration and (d) 100% DMSO per-deuteration.

DMSO protonation [%]	DMSO Methyl signal [AU]	Acetone Methyl Signal [AU]
0	1.00	0.28
33	1.03	1.56
67	0.94	1.53
100	1.09	1.50

Table 6.5: Table of relative intensities for ^{13}C-1-acetone and DMSO methyl signals over a range of DMSO protonation percentages. Two replicates of $10\mu l$ ^{13}C-1-acetone in $90\mu l$ DMSO at four different degrees of deuteration were cooled for 60 minutes at 1.5K before dissolution with hot pressurised methanol and transfer to an external liquid state NMR spectrometer for acquisition.

the route of transfer to the DMSO methyl ^{13}C nucleus is via the DMSO methyl protons.

6.10   Intramolecular polarisation transfer in acetone and isopropanol

The concentration dependence described in the previous section supports that the preferred route of polarisation transfer within a cryogenically cooled methyl containing sample is via the proton network. For natural abundance samples this is in part because of the low probability of two adjacent carbon nuclei being the ^{13}C isotope. However, the dipolar couplings between protons are generally much higher than between carbons or for proton-carbon couplings.
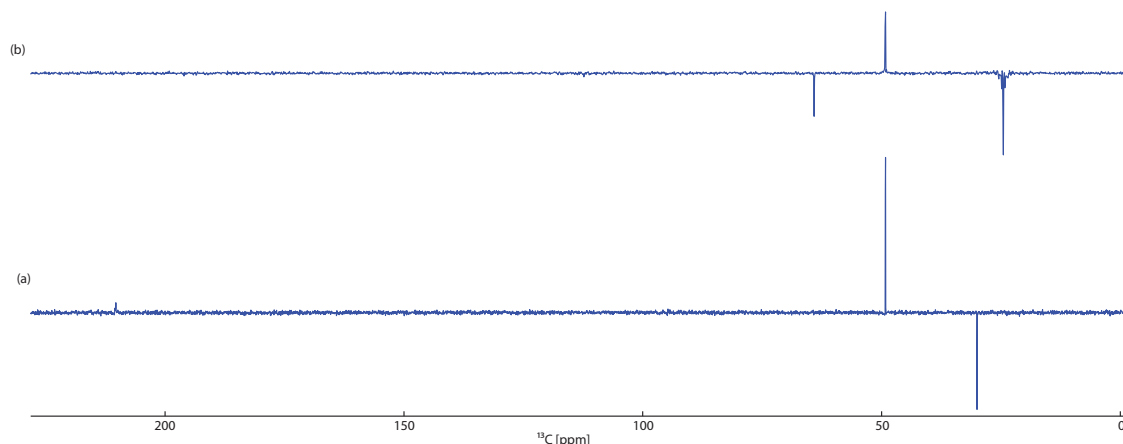
Figure 6.8: Spectra for (a) $100\mu l$ acetone (b) $100\mu l$ isopropanol, after cooling to 1.5K for 60minutes before dissolution with hot, pressurised methanol and transfer to a high field NMR spectrometer for acquisition of the NMR spectrum with a simple $\pi/2$ pulse followed by acquisition of the NMR spectrum. Enhancement values are as per table 6.1.

As a direct comparison of proton-network dependent spin diffusion and carbon-carbon spin diffusion in this system ^{13}C dissolution spectra for acetone and isopropanol are compared in Figure 6.8. The acetone spectrum shows a small positive signal for the carbonyl C2 signal with an intensity slightly lower than expected from the temperature and magnetic field jumps in the dissolution and transfer process (0.89 fold) but this is likely do to incomplete equilibration. The acetone methyl signal shows a strong negative signal with an -2.9 fold enhancement. For isopropanol both the CH C2 signal and the methyl signal show strong enhancements. Adjusting for two methyl carbon nuclei per C2 carbon both signals have approximately equal intensity with an enhancement of -4.19. The contrast of a 0.89 fold enhancement for the acetone C2, without an attached proton, and 4.10 fold for the isopropanol C2, with an attached proton, strongly indicates that by far the most efficient route of polarisation transfer in methyl rotor containing samples under cryogenic conditions is via spin diffusion in the proton network before transfer from a proton to a ^{13}C nucleus.

In ex-situ DNP experiments the time delay required by the sample transfer process is too great for significant proton polarisation to survive, due to their short T_1 values. The process described here has the potential to be exploited in *ex-situ* DNP experiments in that the proton network could be actively polarised with e.g. TEMPO radical at low temperature but ^{13}C observed after transfer to the high field magnet.

6.11   Intramolecular polarisation transfer in pentanol and 6-chloro-2-hexanone

Similar to the cases with acetone and isopropanol, pentanol and 6-chloro-2-hexanone show polarisation for all proton-attached carbons when cooled in the quantum rotor experiment. These molecules are interesting in that their multi-carbon chain nature will allow the underlying mode of intramolecular polarisation transfer to be elucidated. One possibility is that the polarisation; arising on the methyl protons, is transferred throughout the proton network and then to carbon nuclei from a directly attached proton. The other possibility is that the polarisation travels from carbon to carbon along the linear chain. The experimental data shown in Figures 6.9 and table 6.4 show that there is no significant difference in the rates of polarisation buildup on the chain carbons in these molecules. This indicates that the preferred route takes polarisation rapidly throughout the proton network and then more slowly to the carbon nuclei[7].

6.12   Intermolecular polarisation transfer between acetate and acetonitrile

For any polarisation enhancement methodology to become widely applicable it must satisfy the criterion that polarisation can be transferred easily to a target molecule as desired. If one takes the knowledge that quantum rotor derived Zeeman polarisation is transferred favourably within the proton system in a sample then the desirable ability of being able to transfer polarisation to an included target molecule simply requires that the target molecule is protonated. To demonstrate this Figure 6.10 shows acetonitrile alone and when mixed with acetic acid as a polarisation donor. In a similar way any desired target molecule, in a sufficient concentration of a quantum rotor effect polarisation donor molecule, will become polarised thus increasing the signal available for NMR spectral acquisition. Table 6.6 shows the fold enhancement for each resonance in each case here. In the case where acetonitrile is cooled alone the two signals are as expected. The introduction of acetate cases the acetonitrile methyl signal to become more intense and negative, suggesting a transfer of polarisation derived from the quantum rotor effect and curiously the acetonitrile CN

a) Pentanol
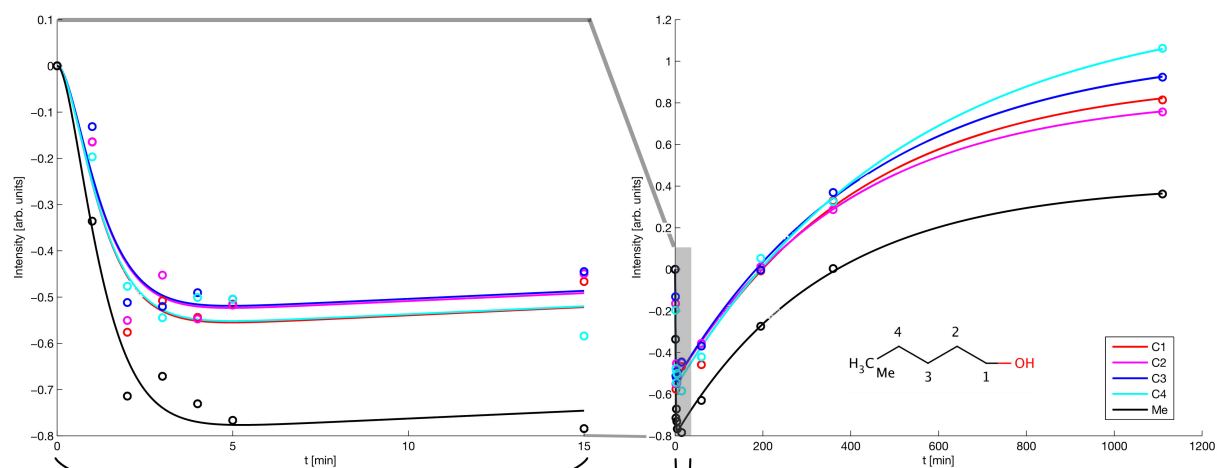
b) 6-Chloro-2-hexanone
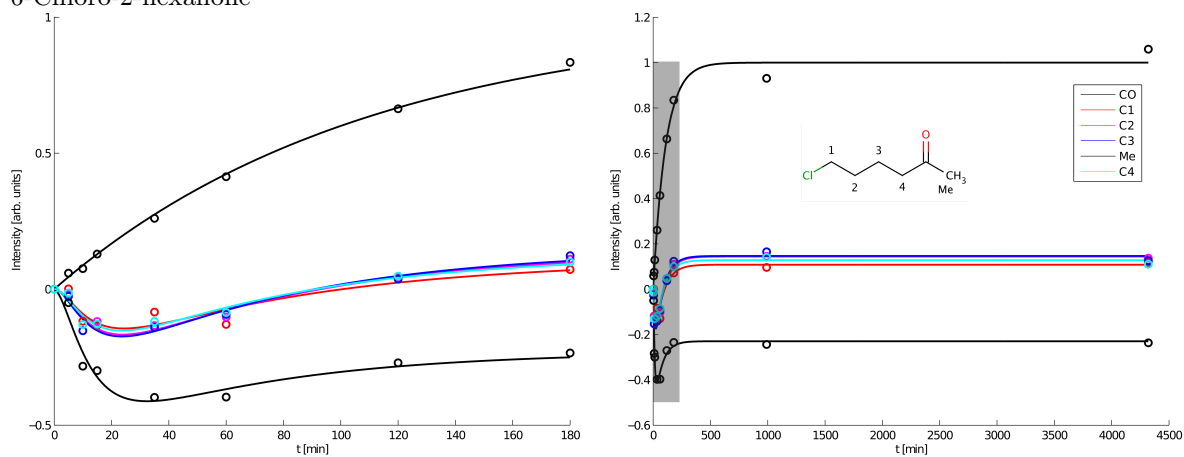
Figure 6.9: Charts of quantum rotor polarisation for each carbon in pentanol (top) and 6-chloro-2-hexanone (bottom) with time. The non-methyl signals have a grouped buildup that supports polarisation transfer through the proton network initially before subsequent transfer to heteronuclei at a much lower rate.Adapted from[7].
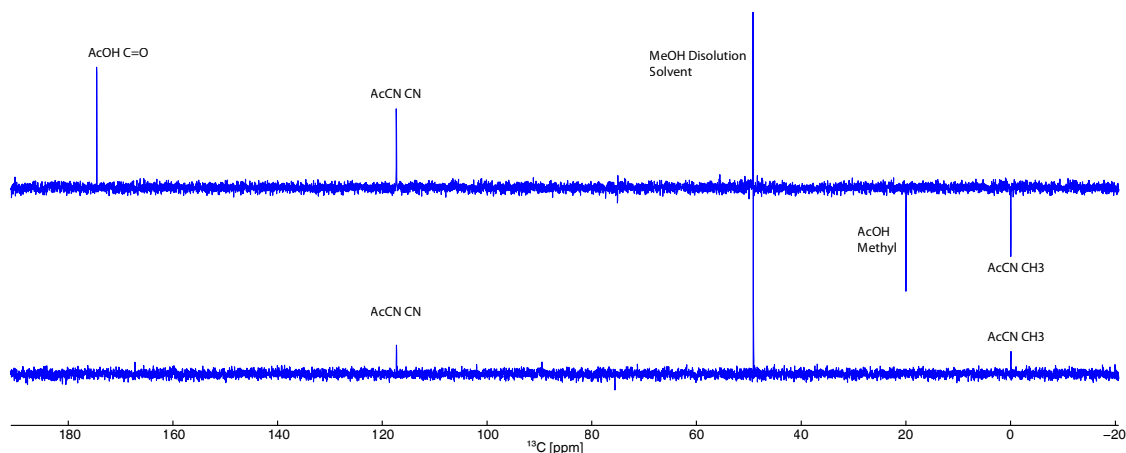
Figure 6.10: Spectra for (a) $100\mu l$ 50% acetonitrile 50% water (b) $100\mu l$ 50% acetonitrile 50% acetic acid, after cooling to 1.5K for 60minutes before dissolution with hot, pressurised methanol and transfer to a high field NMR spectrometer for acquisition of the NMR spectrum with a simple $\pi/2$ pulse followed by acquisition of the NMR spectrum.

	Chemical shift	Acetonitrile	Acetonitrile and acetic acid
Acetonitrile CH$_3$	1.39	0.9	-2.35
Acetonitrile CN	118.7	1.0	2.7
Acetic acid CH$_3$	20.0	-	-4.1
Acetic acid COOH	179.0	-	4.0

Table 6.6: Table of the chemical shift and enhancement factors for $100\mu l$ acetonitrile or $100\mu l$ acetonitrile plus $100\mu l$ acetic acid cooled to 1.4K for 60 minutes prior to dissolution with methanol solvent. Enhancement factors are expressed as a fold enhancement compared to a reference spectrum of these samples.

signal increases in intensity by 2.7 fold perhaps due to an unexpected cross relaxation pathway.

Acetonitrile does not show quantum rotor polarisation alone as it is a linear molecule. When acetonitrile is mixed with acetic acid and then cooled similarly a negative signal is seen for the acetonitrile resonances. However, the introduction of acetic acid may break the symmetry of the acetonitrile leading to a directly occurring quantum rotor effect in acetonitrile rather than a clear-cut intermolecular transfer. This effect has been previously reported by Häberlen et. al.[109]. Although polarisation transfer has to occur when other experiments such as NOE distance measurements in proteins are considered, the design of a clear cut test is very difficult with factors such as these. So, while there is a compelling logical argument that intermolecular polarisation transfer occurs in this system it is very difficult to prove.

Chapter 7

Applications

7.1 Oxaloacetate polarised by DNP in a number of experimental conditions

The goal of any hyperpolarisation experiment is to attain the greatest amount of polarisation possible to give a maximal signal for the ensuing NMR experiment. While there are several available routes to hyperpolarisation, it is possible to utilise more than one method in an individual experiment to give a combined, constructive interference effect. Examples of this approach yielding large improvements over a simple DNP experiment are shown in Figure 7.1[10]. Here the DNP experiment was performed with oxaloacetate at both possible DNP microwave frequency maxima and with a mixture of solvents used as a matrix that form a glass at low temperatures and that are either protonated or deuterated. A polarisation time of 90 minutes, or 18 hours was used. In the "Standard" DNP conditions, Figure 7.1b, the low frequency microwave DNP maximum at $\approx \omega_e - \omega_N$ is used in conjunction with a protonated glassing solvent matrix. This yields a spectrum with very low intensity signals. The simple act of changing the microwave frequency to the high frequency DNP maximum at $\approx \omega_e + \omega_N$ results in a spectrum with relatively intense signals with the opposite sign. At a microwave frequency of $\approx \omega_e + \omega_N$ the DNP and quantum rotor effects interfere constructively giving a polarisation that is effectively the sum of the two effects.

The initial pair of experiments are repeated with a deuterated glassing solvent matrix in Figure
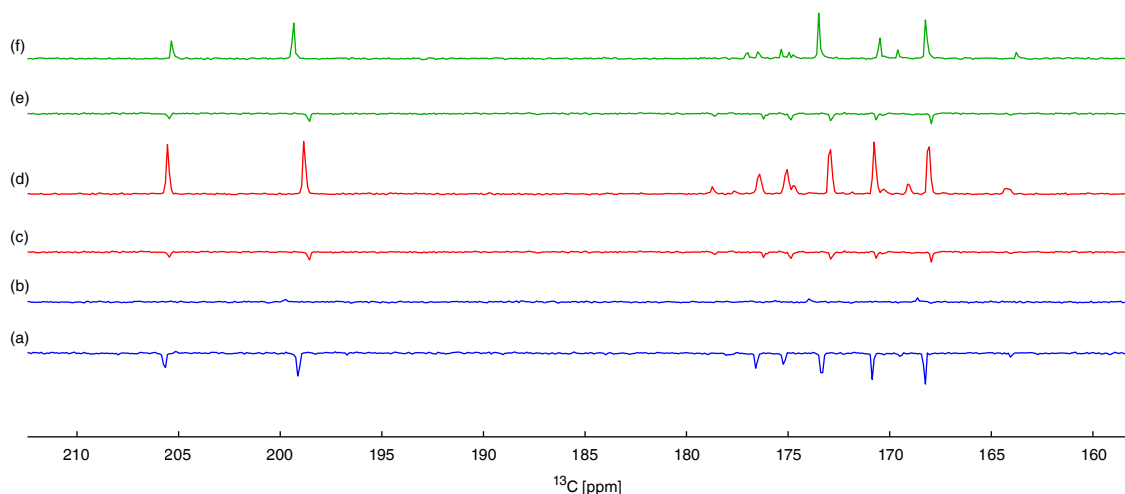
Figure 7.1: Oxaloacetate (1M) in (blue) 1:1:1 water/acetone-H6/DMSO-H6 polarised for 90 minutes with a microwave frequency approximately equal to (a) $\omega_e + \omega_N$ and (b) $\omega_e - \omega_N$, (red)1:1:1 water/acetone-D6/DMSO-D6 polarised for 90 minutes with a microwave frequency approximately equal to (c) $\omega_e + \omega_N$ and (d) $\omega_e - \omega_N$, and (green) 1:1:1 water/acetone-H6/DMSO-H6 polarised for 18 hours with a microwave frequency approximately equal to (e) $\omega_e + \omega_N$ and (f) $\omega_e - \omega_N$.[10]

7.1(red). Here, the deuteration of solvent methyl groups results in the abrogation of the quantum rotor effect and consequently,where the low frequency is used, a greater enhancement than that with the high frequency is seen. This is as would be expected from the Boltzmann polarisation at 1.5K. Returning to a protonated glassing solvent matrix in Figure 7.1(green) but with an extended polarisation time of 18 hours the low frequency again gives the greatest polarisation as the energy in the rotational tunnelling system becomes depleted. These observations give three potential avenues to improve DNP enhancements. Firstly, by using the microwave frequency corresponding to the high DNP enhancement maximum, secondly by using deuterated solvents in the gassing matrix and lastly by using extended polarisation times.

7.2 Glucose polarisation efficiency varies in different conditions

As a major metabolic precursor molecule that is easily transported into cells, glucose is very desirable for use as a metabolic probe in hyperpolarised *ex-vivo* metabolism experiments. However,

Frequency	Solvents?	Polarisation time [mins]	Average Enhancement
$\omega_e + \omega_N$	Protonated	90	-7.62
$\omega_e - \omega_N$	Protonated	90	0.11
$\omega_e + \omega_N$	Deuterated	90	-2.35
$\omega_e - \omega_N$	Deuterated	90	16.94
$\omega_e + \omega_N$	Protonated	1080	-2.65
$\omega_e - \omega_N$	Protonated	1080	11.72

Table 7.1: Table of enhancement factor for oxaloacetate in 1:1:1 water:acetone:DMSO using either protonated or deuterated solvents and a microwave frequency of either $\omega_e - \omega_N$ or $\omega_e + \omega_N$. Enhancement values are a fold enhancement compared to a liquid state NMR spectrum of the same sample.

Frequency	Solvent Deuteration	Polarisation time [mins]	Average Enhancement
$\omega_e - \omega_N$	Protonated	90	0
$\omega_e - \omega_N$	Deuterated	90	19.9
$\omega_e + \omega_N$	Protonated	90	4.6

Table 7.2: Table of enhancement values for glucose polarised using a solvent mixture of 1:1:1 water:acetone:DMSO where these solvents were either protonated or per-deuterated. The microwave frequency was also varied between $\omega_e - \omega_N$ and $\omega_e + \omega_N$. The enhancement value is expressed as a fold enhancement over a reference spectrum of the same sample.

despite having relatively long ^{13}C T_1 values, glucose has proven difficult to polarise effectively with DNP. Figure 7.2 shows three DNP spectra for glucose. Figure 7.2a represents the "normal" case where protonated glassing solvents and a microwave frequency of $\approx \omega_e - \omega_N$ are used. Here no visible signals exist in the dissolution DNP spectrum. In either the case where deuterated glassing solvents (Figure 7.2b) or the high DNP microwave frequency, $\approx \omega_e + \omega_N$ (Figure 7.2c) is used enhanced signals are seen. The greatest signal intensity is seen where deuterated glassing solvents are used, here giving an enhancement of 19.9 fold compared to a liquid state NMR spectrum of the same sample after the DNP polarisation had fully relaxed.

7.3 Serum polarised with co-polarisation agent and both microwave DNP maxima

The field of metabolomics has exploded in recent years with a very wide and varied range of applications, all exploiting chemical markers in bio-fluids. Metabolomics performed with NMR suffers greatly from the inherent low sensitivity of NMR so it is highly desirable to be able to
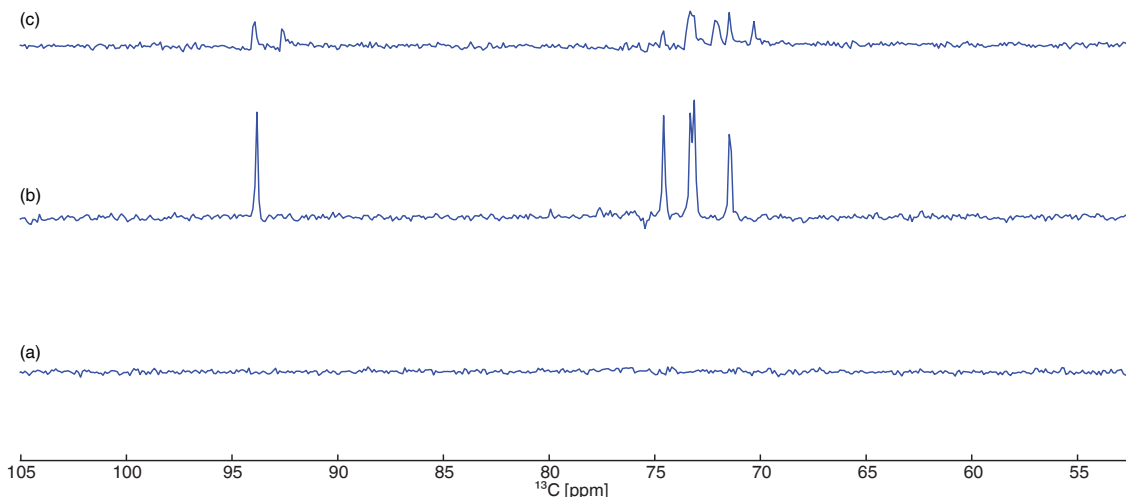
Figure 7.2: *Ex-situ* DNP spectra for glucose polarised in 1:1:1 water/acetone/DMSO for 90 minutes at 1.5K before dissolution and transfer to a high field NMR spectrometer. a) Using protonated solvents and a microwave frequency of $\approx \omega_e - \omega_N$, b) using deuterated solvents and a microwave frequency of $\approx \omega_e - \omega_N$ and c) using protonated solvents and a microwave frequency of $\approx \omega_e + \omega_N$.

Frequency	Solvents	τ_{pol} [mins]	Urea signal	Amino acid signals
$\omega_e - \omega_N$	Protonated	90	11.56	0
$\omega_e - \omega_N$	Deuterated	90	13.36	12
$\omega_e + \omega_N$	Protonated, ^{13}C-2-acetone	90	1.00	14+

Table 7.3: Table of signal enhancements for urea and the number of putative amino acid signals from a sample of processed bovine serum polarised using different conditions. The Urea signal is a relative intensity and the amino acid signals are putative.

enhance the signal intensity for biological liquids such as serum. A DNP spectrum of concentrated, deproteinised and lyophilised foetal bovine serum polarised in 1:1:1 water/acetone/DMSO with a microwave frequency of $\approx \omega_e - \omega_N$ is shown in Figure 7.3a where only a small signal, most likely corresponding to urea, is seen at $\approx$182ppm. The same experiment repeated with a microwave frequency of $\approx \omega_e + \omega_N$ gives a spectrum as shown in Figure 7.3b. Here the urea signal is enhanced but an additional $\approx$12 signals are seen. Returning to a frequency of $\approx \omega_e - \omega_N$ but his time using ^{13}C-2-acetone in the sample matrix as a co-polarisation agent (Figure 7.3c) results in at least an additional 2 sample peaks although there are many artifacts in this spectrum rendering it less useful.
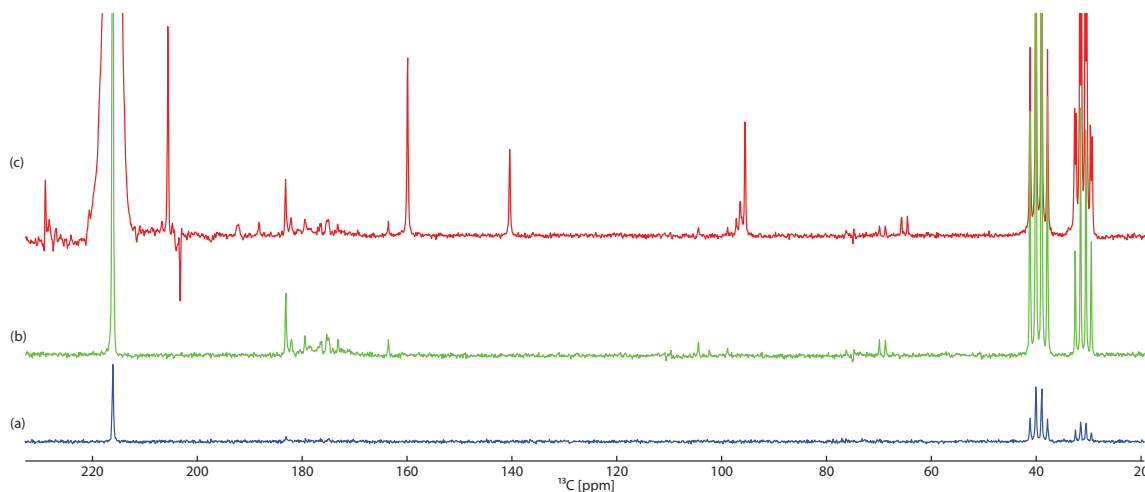
Figure 7.3: *Ex-situ* DNP spectra for concentrated, deproteinised and lyophilised foetal bovine serum (a) with a microwave frequency of $\approx \omega_e - \omega_N$ in 1:1:1 water/acetone-H6/DMSO-H6, (b) with a microwave frequency of $\approx \omega_e - \omega_N$ in 1:1:1 water/acetone-D6/DMSO-D6, and (c) with a microwave frequency of $\approx \omega_e - \omega_N$ in 1:1:1 water/^{13}C-2-acetone-H6/DMSO-H6.

7.4 Fast 2D naproxen spectrum enhancement with co-polarisation agent and using both DNP maxima.

Modern NMR experimentation boasts a huge array of multidimensional experiments that enable different spin components to be correlated. This allows structural relationships such as relative position or chemical bonding to be elucidated. An example of a simple two-dimensional experiment is the hetero-nuclear multi-quantum correlation (HMQC). To adapt this method to a rapidly relaxing sample a protocol was implemented where a small part of the available magnetisation is used to readout the correlation while maintaining the remainder for subsequent spectra. This scheme is summarised in Figure 3.5. A sample of naproxen, a small non steroidal anti-inflammatory drug (NSAID) molecule, was polarised prior to dissolution and transfer to a high field NMR spectrometer for acquisition of a fast 2D-HMQC spectrum. Figure 7.4 shows a 2D overlay of two spectra acquired with the fast 2D-HMQC method. The spectrum in blue was acquired after polarisation of naproxen with ^{13}C-2-acetone co-polarisation agent and a microwave frequency of $\approx \omega_e - \omega_N$. The spectrum in red also used the co-polarisation agent but used a microwave frequency $\approx \omega_e + \omega_N$. It is important to note that without the co-polarisation agent no useful signals were
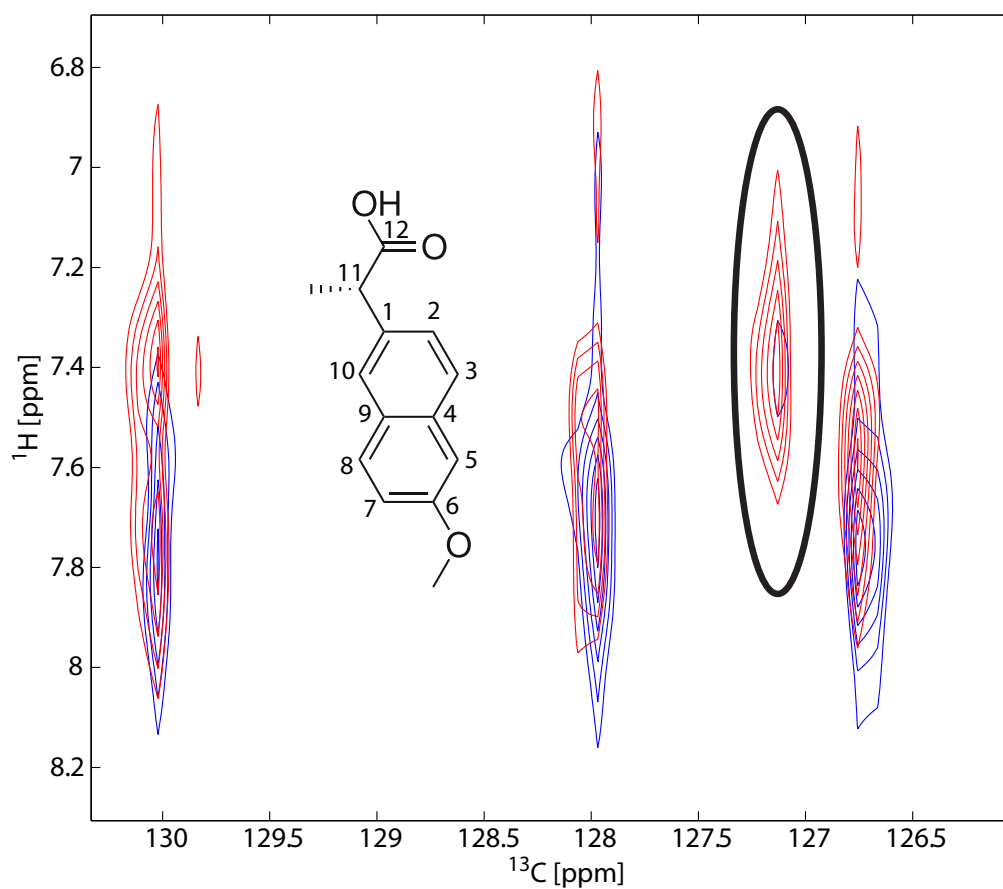
Figure 7.4: Fast 2D-HMQC spectra for naproxen overlaid where naproxen was polarised with ^{13}C-2-acetone co-polarisation agent at a microwave frequency of $\approx \omega_e - \omega_N$ (blue) or $\approx \omega_e + \omega_N$ (red). An extra signal (circled) is seen with the high microwave frequency. Reproduced with permission of Ildefonso Marin-Montesinos.

observed. With the high frequency an additional signal corresponding to C7 is seen. Even with the inclusion of the co-polarisation agent, neglecting the quantum rotor effect would have resulted in missing additional signals unnecessarily.[8]

Part III

Conclusions

Chapter 8

Discussion

The research work in this thesis falls into two broad areas but the findings in each section have an impact on any experiment in the conditions of the HyperSense™ polariser and this is demonstrated in the final applications section.

The derivatisation of samples with a molecular 'tag' can have the effect of improving the molecular packing structure in the glass state. This is likely to occur by removing charged groups from the molecular structure such as phenol hydroxyls or carboxylic acid groups. The derivatised molecules are able to come into closer proximity with each other and this makes spin diffusion more efficient so that when a spin is polarised via DNP the polarisation can be more easily transmitted throughout the sample. It is understood that the majority of spins gain polarisation in a DNP experiment secondarily through spin diffusion rather than due to primary polarisation directly from the paramagnetic group. This finding leads to the conclusion that in experiments with mixtures of components, such as a biological sample, the bulk derivatisation of charged groups with an e.g. acetyl group will increase the signal enhancements seen in a DNP experiment.

If a molecular tag is isotopically enriched with ^{13}C a decrease in DNP signal enhancement is seen for molecular signals compared to those with the natural abundance tag where short polarisation times are employed. This is likely to be because the enriched tag is 100 times more likely to be a ^{13}C than any other carbon resonance in the sample. Therefore, early in a DNP experiment, as only a finite number of polarisation events have occurred, the resonances not in the

tag acquire polarisation 100 times more slowly than they would with a natural abundance tag. Therefore where an isotopically enriched molecular tag is used, extended polarisation times should be used to ensure that maximal polarisation is achieved.

When the sample is dissolved in an *ex-situ* DNP experiment for transfer to the high field magnet, the polarisation will immediately begin to decrease with the resonances T_1's[11]. This can cause signals for resonances with short T_1's to not be seen in the resulting DNP-NMR spectrum. However, it is possible to use magnetisation stored in long lived ^{13}C nuclei to increase the intensity of these short lived spins' signals. This can be achieved by a transfer of magnetisation with either a scalar or dipolar coupling. The dipolar case is far more generally applicable and an NOE was utilised to achieve a signal enhancement of 5 times for the aromatic signals of 4-methoxyphenyl ^{13}C-acetate with a maximum enhancement at 10 seconds. This shows that where it is desirable to observe short lived spins in a DNP spectrum it is possible to use techniques such as an NOE based pulse sequence to transfer polarisation from a reservoir of long lived spins to the target resonances. This will clearly not be quantitative but in the context of some, e.g metabolomic, experiments the presence of a resonance is the critical information over the quantitative signal intensity.

Some substances polarise very poorly in the HyperSense™ polariser, often for no clear reason. A trend of increased signal enhancement with an isotopically enriched tag raises the question as to whether the additional ^{13}C nuclei in the sample are reducing the average inter-spin distance in addition to the packing effect seen with natural abundance tags. If this were the case then the ^{13}C enriched spins need not be chemically bound to the target molecule. This is preferable to having a bound tag as the chemical nature of the sample will be unchanged so it is more likely that results be representative of the original target molecule. Where a sample polarises particularly poorly or not at all, the addition of a copolarisation agent such as ^{13}C-2-acetone to the glassing matrix can dramatically enhance the signal intensities in the DNP spectrum. The most dramatic example seen was for citric acid where enriched or natural abundance acetone were used in the glassing matrix and the experiment with isotopically enriched acetone resulted in an 80 fold increase in signal intensity. This therefore demonstrates that in at least a subset of DNP experiments where little or no signal enhancement occurs it is likely to be the capacity for spin diffusion that is the limiting factor.

In DNP-NMR spectra that show poor polarisation levels it is common to see matrix solvent

methyl signals with an inverted intensity. These arise from an additional effect that has not been previously considered in the context of the *ex-situ* DNP experiment and HyperSense™ polariser. There is ultimately a leakage of energy from the rotational tunnelling system of methyl groups into the nuclear Zeeman system of the ^{13}C nuclei observed in such experiments. The test for this was an experiment with acetone in water dissolved and transfered to the high field magnet with methanol. The resulting spectrum showed a strong negative signal for the acetone methyl and not for the methanol indicating that the effect arose from the incubation at low temperature rather than mere transit through the apparatus itself. As there was no microwave irradiation in this experiment and no radical present the only energy available to bring about the polarisation seen is thermal, driven by the cooling process. As it is the methyl groups that show the enhancement the methyl system is implicated, in particular the rotational tunnelling system. A range of other methyl group containing substances treated in this same way show the same effect consistently so this effect is seen to be general to the presence of methyl groups[10].

A similar effect was reported by Haupt[5] but the effect seen here has a few differentiating features from the effect that Haupt reported. The primary difference from the Haupt effect is that we observe ^{13}C rather than protons. We also observe Zeeman polarisation rather than dipolar polarisation but it is entirely possible that there is an interconversion during the long incubation time at low temperature. The Haupt effect is only seen in a very small number of substances with very high tunnelling frequencies whereas the effect described here occurred in virtually every methyl containing substance that could be tested. The Haupt effect arises due to a flux between rotational tunnelling excitation states. This is a quick process and is complete within a few minutes but the maximum of the effect seen in this work is 1-2 hours. This is because it is the slow A-E tunnelling level conversions that leads to the polarisation observed in these experiments. If the buildup of polarisation is modelled on a pair of Solomon equations the relaxation component can be separated from the observed trend such that a prediction of the enhancement effect alone can be made that allows this effect to be quantitatively separated from relaxation in the system. This projection informs of a quantum rotor derived polarisation that is 45 fold greater than the Boltzmann polarisation at room temperature.

A remarkable observation is made with the quantum rotor polarisation enhancement

time-courses for pentanol and 6-chlorohexanone in that the ^{13}C spins do not noticeably to relax even after three days, the limit of the machine[7]. Once the sample is cooled fully the T_1 values for these spins must become so long as to render longitudinal relaxation virtually non-existent on this timescale. The implications of this are that, as spin diffusion depends on T_1, polarisation transfer will be hindered decreasing the polarisation buildup rate in DNP experiments. It has been shown that the addition of gadolinium to the DNP sample matrix increases the polarisation efficiency in ex-situ DNP experiments[110] and it may be the case that the paramagnetic gadolinium is simply allowing spin diffusion to proceed more effectively by increasing the relaxation rates of the ^{13}C nuclei.

The rotor effect seen arises from a change in temperature so an understanding of the thermal dependence of this effect is important. If the incubation temperature is varied a trend of decreasing signal strength approximately proportional to the inverse of the cryostat temperature is seen. Relaxation has been seen in other glassy substances that also follows this trend due to low frequency excitations and the implication here is that as the temperature is lowered the signal intensity will increase to a power of two. At the opposite end of the temperature range it is surprising to see significant polarisation surviving at 3.5K, the upper limit of this instrument, and if this trend continues it may become possible to introduce magic-angle spinning in an alternative instrument to study the glassy sample more directly in a solid-state NMR experiment. The sample temperature can also be varied prior to insertion into the polariser instrument. This can be achieved by pre-cooling a sample in liquid nitrogen to decrease the energy available in the quantum rotors to enter into this mechanism. As is predicted, pre-cooled acetone shows no signal enhancement using the quantum rotor experimental protocol confirming the enthalpic dependence of this process. A further experiment that could be carried out would be to pre-heat the sample and determine the extent to which this increases the signal enhancement seen.

The polarisation that results from the quantum rotor effect initially causes proton polarisation enhancement. In the *ex-situ* experiment the transfer time is too great to allow proton polarisation to be retained so it has not been possible to observe it directly. However, the resulting polarisation is observed on ^{13}C so there must be a transmission route from protons to ^{13}C. This route could either be through the proton network and then to carbon in a final step, or directly to carbon and through the carbon chain. The natural abundance of the ^{13}C isotope makes the second route unlikely with

our samples and as the dipolar coupling values for ^{1}H-^{1}H are much greater than for ^{13}C-^{13}C and ^{1}H-^{13}C the first route would be favoured anyway. This presumption is evidenced by the C2 signals for acetone vs isopropanol in a QR-NMR spectrum. The isopropanol C2, which bears a proton, shows a negative signal whereas the acetone carboxyl C2 does not demonstrating the dependence the ^{13}C has on the attached proton to receive polarisation derived from the quantum rotor effect. The polarisation time-courses for two long-chain molecules, pentanol and 6-chlorohexanone, show a virtually identical polarisation profile for all backbone carbons and this also provides evidence that the polarisation travels quickly through the proton network in a sample before transfer to the ^{13}C nucleus where it is observed. Given that polarisation from the quantum rotor mechanism is seen to travel through the proton network rapidly this could be used to aid in structural determination by identifying carbons spins that are proton bound.

It is expected that once the protons in a sample are polarised this polarisation will travel by spin diffusion to other molecules as would be expected in any context. To test this however requires a control experiment and as virtually every possible solvent shows this effect it is very hard to show the intermolecular polarisation transfer clearly. Even with acetonitrile it has been shown that addition of acetate to the solvent matrix causes a change in the molecular structure. This is likely to be such that it introduces enough asymmetry to the acetonitrile structure that the quantum rotor effect is allowed to occur. Rationally however intermolecular polarisation transfer must occur and to counter the low relaxation rates that would limit spin diffusion a future experiment might be to introduce gadolinium to perhaps a ring structure molecule with or without a rotor to maximise the polarisation effect.

From a practical perspective the findings of this thesis can be demonstrated in that DNP experiments can be optimised[8,9] and this is seen with the differential polarisations seen for oxaloacetate, glucose, serum and naproxen. With a greater awareness of the processes in the HyperSense™ polariser a more effective experiment can be designed that delivers a greater consistency and maximised signal allowing experiments such as metabolomics and metabolic flux analysis as well as spectroscopy of pharmaceutical molecules. There are also numerous potential future studies that extend from this work. The quantum rotor polarisations show that magnetisation can transverse the proton network before transfer to ^{13}C so a DNP experiment could be designed

that follows this route. If TEMPO or TOTAPOL radical were included in the polarisation sample and the microwave frequency set to the enhancement maximum of protons a DNP effect would raise the polarisation in the protons of the sample. This will then be transfered to ^{13}C to be observed after dissolution in the *ex-situ* style experiment. The potential addition of gadolinium may counter the very slow relaxation seen at the operating temperature of the HyperSense™ instrument. To study the rotor mechanism further a CF$_3$ rotor could be used in place of a CD$_3$ rotor to isolate the impact of the moment of inertia of the rotor from the quadrupole effect. Intermolecular polarisation transfer experiments could be performed using ringed substances or other molecules that bear CH's but not methyl groups, e.g. CF$_3$CH$_2$OH. Another set of experiments that could be performed are those that influence the quantum rotor mechanism through alternative means. Field cycling could be used to induce a rapid polarisation effect where a level-crossing phenomenon occurs. A multi-channel probe that can operate in the solid state of the HyperSense™ instrument would allow a cross-polarisation experiment to be performed to increase the efficiency with which magnetisation is transferred to ^{13}C from the protons with the quantum rotor effect. The sample could also be physically inverted after a period of time to investigate the differential polarisation build up rates for ^{1}H and ^{13}C.

Chapter 9

Concluding Comments

NMR is a hugely versatile and potent spectroscopic method that can provide information which is not easily accessible by any other methods. However, where many other techniques surpass NMR is sensitivity. Hyperpolarisation techniques extend the frontier of sensitivity in NMR. DNP has especially proven to be a very powerful technique with the capability to allow innumerate NMR experiments that would otherwise be impossible. However, there are a number of factors that limit the applicability of DNP. These limitations arise from either experimental constraints or from the behaviour of polarised species. Depending on the implementation of the DNP experiment, temperature, time or chemical factors may limit the experiments that are possible. Once polarised, the sample may exhibit unexpected properties by virtue of the now imbalanced populations.

In the case of *ex-situ* DNP there are certain restrictions such as that the sample must form a glass, must be soluble in an available dissolution solvent and must be able to withstand rapid cooling to and heating from 1.1K. Assuming that these criteria are met there is an inherent time delay between the end of the polarisation process and the beginning of the NMR experiment and during this time relaxation processes can occur. So, during this period events are lost and more rapidly relaxing nuclei will be more difficult to observe than slower relaxing ones. There are two strategies that can be adopted to overcome this. Without altering any parameters of the polarisation process itself it is possible to further improve on the enhancements in the NMR spectrum recorded after dissolution. By utilising a ^{13}C-NOE, polarisation can be passed from a slowly relaxing nucleus to

more rapidly relaxing signals. This technique allows signals to be observed that would ordinarily relax too quickly to be seen, even when hyperpolarised to a relatively large extent prior to dissolution and transfer to the NMR spectrometer.

Within certain bounds, sufficient polarisation will allow a signal to be observed, if only briefly. In early experiments to polarise biologically useful substances I have observed many inexplicably poor DNP enhancement results. Prime examples of this are citrate and oxaloacetate which would appear to have several slow-relaxing nuclei; such as carbonyl and quaternary carbons, and a structure similar to other substances that are known to polarise well. The results of the NOE experiments above revealed a trend where a greater signal enhancement was seen prior to the NMR mixing time on inclusion of an isotopically enriched derivatisation tag. As the primary mechanism for polarisation enhancement of most spins in a DNP sample is secondary spin diffusion rather than direct polarisation, the likely cause of this is the increase in density of more slowly relaxing ^{13}C spins from the ^{13}CO tag.

Another trend seen with samples that have a low polarisation efficiency was the presence of inverted signals for methyl groups of the glassing agent and often other protonated carbons in the sample. To this point all DNP experiments had been performed using the low frequency DNP maximum corresponding to approximately $\omega_e - \omega_n$ on the assumption that the enhancement of the nuclear Zeeman α population will reinforce the effect of the Boltzmann distribution for the low temperature. Knowing that the high frequency maximum polarises the β Zeeman population, giving an inverted signal, an experiment was performed at the $\omega_e + \omega_n$ microwave frequency to exclude the negative methyl signals as artifacts. The resulting spectrum of oxaloacetate showed a polarisation of a similar size to those of previous successful DNP experiments but with the opposite sign suggesting other factors present. The prevalence of methyl groups in the inverted signals suggested an initial postulate that energy was somehow leaking from the methyl group to the nuclear Zeeman system. Before elucidating the mechanism of this secondary effect it became clear that by considering its presence a more effective DNP experiment could be performed by either changing the microwave frequency used, polarising for a long time until such a time as the secondary effect had declined or by using deuterated methyl groups to abrogate the effect stemming from the methyls.

The impact of using perdeuterated methyl glassing agents gave a tentative confirmation that

the secondary effect was indeed originating from the methyl groups. As a control a sample of pure acetone was cooled without any radical or microwave irradiation before dissolution in the same manner as DNP experiments. This experiment was to either confirm or disprove that an independent mechanism was allowing energy from the rotation of the methyl groups to polarise the nuclear Zeeman system. The resulting NMR spectrum bore a clear inverted signal for the acetone methyl groups against the positive signal of the methanol arising from the Boltzmann polarisation. The cause of these inverted signals was an inefficient coupling between the rotational tunnelling system of the methyl groups and the nuclear Zeeman system that allowed energy lost in relaxation of the tunnelling methyl to accumulate in the nuclear Zeeman system. This had become possible because, at the very low temperatures experienced by the sample, the nuclear T_1's had become longer than the tunnelling relaxation rate.

As an isolated mechanism the polarisation derived from the rotational tunnelling dependent effect is sufficient to allow observation of proton attached ^{13}C nuclei in several highly concentrated mixtures of substances that bear methyls that possess a high tunnelling frequency. The polarisation originates from the methyl protons and by following the enhancement rates of signals in a linear molecule it is apparent that the polarisation seen on non-rotating proton-attached carbons is primarily transferred via the proton network and secondarily from proton to carbon.

As an applied methodology, quantum rotor induced polarisation provides a route to achieve polarisation enhancement for many substances. In the observation of ^{13}C signals enhanced via this method the greatest limiting factor is the inefficient transfer from ^1H to ^{13}C. This process is mediated by a coupling factor, σ. Given that σ is likely to be very small, but we still see relatively large ^{13}C enhancements, it is highly likely that the ^1H nuclei are very strongly polarised. It is unfortunate that equipment has not been available to directly measure this but if this is the case a solid-state NMR experiment that actively transfers magnetisation from ^1H nuclei to ^{13}C nuclei, such as a Hartmann-Hahn cross polarisation or a symmetry re-coupling pulse sequence would result in a much greater ^{13}C polarisation that could rival DNP.

In answer to my original aims I have revealed mechanisms that lead to decreases in the efficiency of DNP experiments and have derived experimental methods that allow greater DNP enhancements to be achieved as well as identifying an unexpected process that can also lead to

polarisation enhancements in the HyperSense™ instrument. These methods could facilitate many diverse experiments in bio-medicine, pharmaceuticals and in *in-vivo* imaging and will hopefully aid advancements of numerous varied areas of science.

Chapter 10

Appendices

Appendix A: Credit for experimental work

The experiments and analysis reported in section 3.3.1.1, 6.5 & 6.11 were performed by C. Ludwig and I. Marin-Montesinos.

Development of the mathematical model for quantum rotor polarisation buildup and analysis was performed by C. Ludwig.

The experiment reported in section 7.4 was performed by I. Marin-Montesinos.

Appendix B: Individual contribution to publications

Abdul-Hamid Emwas, Christian Ludwig, Ulrich L. Günther., Martin G. Saunders (2008). Determinants for optimal enhancement in *ex-situ* DNP experiments. *Applied Magnetic Resonance*, 34, 483-494.

For this paper I started with a data set and went on to repeat the chemical synthesis, data acquisition and data analysis. I also contributed to the writing of the paper.

Martin G. Saunders, Christian Ludwig, & Ulrich Günther. (2008). Optimizing the signal enhancement in cryogenic *ex-situ* DNP-NMR spectroscopy. J. Am. Chem. Soc., 130 (22), 6914-6915.

This was the first paper describing the quantum rotor derived effect that I found. I performed all experiments, created all the figures and performed the analysis. I also wrote the manuscript with assistance from my supervisors.

Christian Ludwig, Ildefonso Marin-Montesinos, Martin G. Saunders, Abdul-Hamid Emwas, Zoe Pikramenou, Stephen P. Hammond and Ulrich L. Günther (2010). Application of *ex-situ* dynamic nuclear polarization in studying small molecules. Phys. Chem. Chem. Phys., 12, 5868.

I prepared samples and performed experiments as shown in figure 2a and c. I also processed data in preparation for the experiments and prepared figure 2c.

Christian Ludwig, Ildefonso Marin-Montesinos, Martin G. Saunders, Ulrich L Günther (2010). Optimizing the Polarization Matrix for *ex-situ* Dynamic Nuclear Polarization. J.Am.Chem. Soc., 132(8),2508-2509

I performed the experiments for and prepared figure 1.

Christian Ludwig, Martin Saunders, Ildefonso Marin-Montesinos and Ulrich Günther (2010). Quantum Rotor Induced Hyperpolarization. Proc. Nat. Acad. Sci 107 (24) 10799-10803.

I discovered the effect reported and performed research. I performed experiments and prepared figure 1 parts A, B and C. I also worked on early drafts of the text.

Appendix C: Relationship of data presented to existing patents

In patent W/O 2008/149118 I originated the concept and independently performed all experiments for, and created, all figures shown.

References

[1] H C Dorn, R Gitti, K H Tsai, and T E Glass. The flow transfer of a bolus with proton dynamic nuclear polarization from low to high magnetic fields. *Chem. Phys. Lett*, 155:227–32, 1989.

[2] P. C. A. Vanderwel, K. N. Hu, J. Lewandowski, and R. G. Griffin. Dynamic Nuclear Polarization of Amyloidogenic Peptide Nanocrystals: GNNQQNY, a Core Segment of the Yeast Prion Protein Sup35p. *J. Am. Chem. Soc.*, 128:10840–10846, 2006.

[3] Joo. Chan-Gyu, Hu. Kan-Nian, Bryant. Jeffrey A, and Robert G. Griffin. In Situ Temperature Jump High-Frequency Dynamic Nuclear Polarization Experiments: Enhanced Sensitivity in Liquid-State NMR Spectroscopy. *Journal of the American Chemical Society*, 128: 9428–9432, 2006.

[4] A.J. Horsewill. Quantum tunnelling aspects of methyl group rotation studied by NMR. *Progress in Nuclear Magnetic Resonance Spectroscopy*, 35:359–389, 1999.

[5] J Haupt. A New Effect of Dynamic Polarization in a Solid Obtained by Rapid Change of Temperature. *Phys Lett*, 38A:389–90, 1972.

[6] C. Degen Tomaselli and B. H. Meier. Haupt magnetic double resonance. *J. Chem. Phys.*, 118: 8559, 2003.

[7] Christian Ludwig, Martin Saunders, Ildefonso Marin-Montesinos, and Ulrich Günther. Quantum Rotor Induced Hyperpolarization. *Proc. Nat. Acad. Sci*, 107:10799–10803, 2010.

[8] Christian Ludwig, Ildefonso Marin-Montesinos, Martin G. Saunders, and Ulrich L Günther. Optimizing the Polarization Matrix for ex-situ Dynamic Nuclear Polarization. *J.Am.Chem. Soc.*, 132:2508–2509, 2010.

[9] Christian Ludwig, Ildefonso Marin-Montesinos, Martin G. Saunders, Abdul-Hamid Emwas, Zoe Pikramenou, Stephen P. Hammond, and Ulrich L. Günther. Application of ex-situ dynamic nuclear polarization in studying small molecules. *Phys. Chem. Chem. Phys.*, 12: 5868–5871, 2010.

[10] Martin G. Saunders, Christian Ludwig, and Ulrich L. Günther. Optimizing the Signal Enhancement In Cryogenic ex situ DNP-NMR Spectroscopy. *Journal of the American Chemical Society*, 130:6914–6915, 2008.

[11] A.-H. Emwas, M. Saunders, C. Ludwig, and U. L. Günther. Determinants for Optimal Enhancement in Ex Situ DNP Experiments. *Applied Magnetic Resonance*, 34:483–494, 2008.

[12] O. Warburg, K. Posener, and E. Negelein. Ueber den Stoffwechsel der Tumoren. *Biochemische Zeitschrift*, 152:319–344, 1924.

[13] Jan H. Ardenkjaer-Larsen, Byrn Fridlund, Andreas Gram, Georg Hansson, Lennart Hansson, Mathilde H. Lerche, Rolf Servin, Mikkel Thaning, and Klaes Golman. Increase in signal-to-noise ratio of $> 10,000$ times in liquid-state NMR. *Proceedings of the National Academy of Sciences of the United States of America*, 100:10158–10163, 2003.

[14] M Levitt. *Spin Dynamics, Basics of Nuclear Magnetic Resonance, 2nd Edition*. Wiley, 2008.

[15] Konstantin Pervushin, Roland Riek, Gerhard Wider, and Kurt Wuthrich. Attenuated T2 relaxation by mutual cancellation of dipole-dipole coupling and chemical shift anisotropy indicates an avenue to NMR structures of very large biological macromolecules in solution. *Proceedings of the National Academy of Sciences of the United States of America*, 94: 12366–12371, 1997.

[16] Felix Bloch. Nuclear Induction. *Phys. Rev.*, 70:460–474, 1946.

[17] Richard R. Ernst. Nuclear magnetic resonance Fourier transform spectroscopy. *Bioscience Reports*, 12:143–187, 1992.

[18] H. Ruterjans. Self-consistent 3J coupling analysis for the joint calibration of Karplus coefficients and evaluation of torsion angles. *Journal of Biomolecular NMR*, 14:7081–93, May 1999.

[19] RR Ernst, G Bodenhausen, and A Wokaun. *Principles of Nuclear Magnetic Resonance in One and Two Dimensions*. Clarendon, Oxford, 1987.

[20] Ad Bax and Stephan Grzesiek. Methodological advances in protein NMR. *Accounts of Chemical Research*, 26:131–138, 1993.

[21] D Hoult and R Richards. Signal-to-noise ratio of nuclear magnetic resonance experiment. *J Magn Reson*, 24:71–85, 1976.

[22] P Styles, N Soffe, C Scott, D Cragg, F Row, D White, and P White. A High-Resolution NMR Probe in Which the Coil and Preamplifier are Cooled with Liquid Helium. *J Magn Reson*, 60:397–404, 1984.

[23] H Kovacs, D Moskau, and M Spraul. Cryogenically cooled probes - a leap in NMR technology. *Prog NMR Spectroscopy*, 46:131–155, 2005.

[24] A Abragam and M Goldman. *Nuclear Magnetism: Order and Disorder*. Oxford Univ. Press, Oxford, 1982.

[25] Albert W. Overhauser. Polarization of Nuclei in Metals. *Phys. Rev.*, 92:411–415, 1953.

[26] R. A. Wind, M. J. Duijvestijn, C. van der Lugt, A. Manenschijn, and J. Vriend. Applications of dynamic nuclear polarization in ^{13}C NMR in solids. *Progress in Nuclear Magnetic Resonance Spectroscopy*, 17:33–67, 1985.

[27] Evan R McCarney, Brandon D Armstrong, Ravinath Kausik, and Songi Han. Dynamic Nuclear Polarization Enhanced Nuclear Magnetic Resonance and Electron Spin Resonance Studies of Hydration and Local Water Dynamics in Micelle and Vesicle Assemblies. *Langmuir*, 24:10062–10072, 2008.

[28] Changsik Song, Kan-Nian Hu, Chan-Gyu Joo, Timothy M. Swager, and Robert G. Griffin. TOTAPOL: A Biradical Polarizing Agent for Dynamic Nuclear Polarization Experiments in Aqueous Media. *J. Am. Chem. Soc.*, 128:11385–11390, 2006.

[29] A Sowerby. Molecules in minute detail. *Chemistry and Industry*, pages 21–23, 2005.

[30] W Demtröder. *Laser Spectroscopy: Basic Concepts and Instrumentation*. Springer, 1998.

[31] MA Bouchiat, TR Carver, and CM Varnum. Nuclear Polarization in ^{3}He Gas Induced by Optical Pumping and Dipolar Exchange. *Phys. Rev. Lett*, 5:373–375, 1960.

[32] A Bifone, Y Q Song, R Seydoux, R E Taylor, B M Goodson, T Pietrass, T F Budinger, G Navon, and A Pines. NMR of laser-polarized xenon in human blood. *Proc Natl Acad Sci U S A*, 93:12932–6, 1996.

[33] G Navon, Y-Q Song, T Room, S Appelt, R E Taylor, and A Pines. Enhancement of Solution NMR and MRI with Laser-Polarized Xenon. *Science*, 29:1848–1851, 1996.

[34] F. D. Colegrove, L. D. Schearer, and G. K. Walters. Polarization of ^{3}He Gas by Optical Pumping. *Phys. Rev.*, 132:2561–2572, 1963.

[35] Yi-Qiao Song. Spin polarization-induced nuclear Overhauser effect: An application of spin-polarized xenon and helium. *Concepts in Magnetic Resonance*, 12:6–20, 2000.

[36] John P. Mugler III, Bastiaan Driehuys, James R. Brookeman, Gordon D. Cates, Stuart S. Berr, Robert G. Bryant, Thomas M. Daniel, Eduard E. De Lange, J. Hunter Downs, Christopher J. Erickson, William Happer, Denise P. Hinton, Neal F. Kassel, Brian T. Saam Therese Maier, C. Douglas Phillips, Karen L. Sauer, and Mark E. Wagshul. MR imaging and spectroscopy using hyperpolarized ^{1}29Xe gas: Preliminary human results. *Magnetic Resonance in Medicine*, 37:809–815, 1997.

[37] M. S. Albert, G. D. Cates, B. Driehuys, W. Happer, B. Saam, C. S. Springer, Jr, and A. Wishnia. Biological magnetic resonance imaging using laser-polarized ^{1}29Xe. *Nature*, 370:199–201, 1994.

[38] L.T. Muus, P.W. Atkins, K.A. McLauchlan, and J.B. Pedersen. Chemically Induced Magnetic Polarization. *Editors*, 1977.

[39] Levanon H. Blank A. Optimal magnetization in liquids, generated by triplet-doublet interaction. *Molecular Physics*, 100:1477–1488(12), 2002.

[40] Kazuyuki Takeda, K. Takegoshi, and Takehiko Terao. Dynamic Nuclear Polarization by Electron Spins in the Photoexcited Triplet State: I. Attainment of Proton Polarization of 0.7 at 105K in Naphthalene. *Journal of the Physical Society of Japan*, 73:2313–2318, 2004.

[41] Kazuyuki Takeda, K. Takegoshi, and Takehiko Terao. Dynamic Nuclear Polarization by Electron Spins in the Photoexcited Triplet State: II. High Polarization of the Residual Protons in Deuterated Naphthalene. *Journal of the Physical Society of Japan*, 73:

2319–2322, 2004.

[42] M. Iinuma, Y. Takahashi, I. Shak'e, M. Oda, A. Masaike, T. Yabuzaki, and H. M. Shimizu. High Proton Polarization by Microwave-Induced Optical Nuclear Polarization at 77 K. *Phys. Rev. Lett.*, 84:171–174, 2000.

[43] Rolf Boelens, Alexei Podoplelov, and Robert Kaptein. Separation of net polarization and multiplet effect in coupled spin systems by two-dimensional CIDNP. *Journal of Magnetic Resonance (1969)*, 69:116 – 123, 1986.

[44] CR Bowers and DP Weitekamp. Parahydrogen and synthesis allow dramatically enhanced nuclear alignment. *J Am Chem Soc*, 109:5541–5542, 1987.

[45] C. R. Bowers and D. P. Weitekamp. Transformation of symmetrization order to nuclear-spin magnetization by chemical reaction and nuclear magnetic resonance. *Phys Rev Lett*, 57: 2645–2648, 1986.

[46] C. R. Bowers and D. P. Weitekamp. Nuclear magnetic resonance by measuring reaction yield of spin symmetry species. *Solid State Nucl Magn Reson*, 11:123–8, 1998.

[47] Thomas C Eisenschmid, Rein U Kirss, Paul P Deutsch, Sven I Hommeltoft, Richard Eisenberg, Joachim Bargon, Ronald G Lawler, and Alan L Balch. Para Hydrogen Induced Polarization in Hydrogenation Reactions. *J. Am. Chem. Soc*, 109:8089–8091, 1987.

[48] P. J. Carson, C. R. Bowers, and D. P. Weitekamp. The PASADENA effect at a solid surface: high-sensitivity nuclear magnetic resonance of hydrogen chemisorption. *J Am Chem Soc*, 123:11821–2, 2001.

[49] Johannes Natterer and Joachim Bargon. Parahydrogen induced polarization. *Progr NMR Spectroscopy*, 31:293–315, 1997.

[50] Marina Carravetta and Malcolm H. Levitt. Theory of long-lived nuclear spin states in solution nuclear magnetic resonance. I. Singlet states in low magnetic field. *The Journal of Chemical Physics*, 122:214505, 2005.

[51] Meike Roth, Joachim Bargon, Hans Wolfgang Spiess, and Achim Koch. Parahydrogen induced polarization of barbituric acid derivatives: [1]H hyperpolarization studies. *Magnetic Resonance in Chemistry*, 46:713–717, 2008.

[52] F.H. Jardine, J.A. Osborn, G. Wilkinson, and G.F. Young. *Chem. Ind. (London)*, page 560, 1965.

[53] Michael G. Pravica and Daniel P. Weitekamp. Net NMR alignment by adiabatic transport of parahydrogen addition products to high magnetic field. *Chemical Physics Letters*, 145:255 – 258, 1988.

[54] Ralph W. Adams, Juan A. Aguilar, Kevin D. Atkinson, Michael J. Cowley, Paul I. P. Elliott, Simon B. Duckett, Gary G. R. Green, Iman G. Khazal, Joaquin Lopez-Serrano, and David C. Williamson. Reversible Interactions with para-Hydrogen Enhance NMR Sensitivity by Polarization Transfer. *Science*, 323:1708–1711, 2009.

[55] R D Bates Jr. and Walter S. Drozdoski. Use of nitroxide spin labels in studies of solvent-solute interactions. *The Journal of Chemical Physics*, 67:4038–4044, 1977.

[56] T. R. Carver and C. P. Slichter. Polarization of Nuclear Spins in Metals. *Phys. Rev.*, 92: 212–213, 1953.

[57] M Schoberl, H Kuiper, R Schmelzer, G Mertens, and W Tornow. A neutron-proton spin correlation experiment at 14 MeV. *Journal of Physics G: Nuclear Physics*, 10:L247–L250, 1984.

[58] G.J. Hill, J. Wu, and M.J.R. Hoch. Satellite structure of DNP enhanced ^{13}C NMR spectra in diamond. *Hyperfine Interactions*, 120-121:81–86, 1999.

[59] Sam E Day, Mikko I Kettunen, Ferdia A Gallagher, De-En Hu, Mathilde Lerche, Jan Wolber, Klaes Golman, Jan Henrik Ardenkjaer-Larsen, and Kevin M Brindle. Detecting tumor response to treatment using hyperpolarized ^{13}C magnetic resonance imaging and spectroscopy. *Nature Medicine*, 13:1382–1387, 2007.

[60] D. M. Bartels, R. G. Lawler, and A. D. Trifunac. Electron T measurements in short-lived free radicals by dynamic polarization recovery. *The Journal of Chemical Physics*, 83:2686–2707, 1985.

[61] K Hausser and D Stehlik. Dynamic nuclear polarization in liquids. *Adv. Magn. Reson*, 3, 1979.

[62] Brandon D. Armstrong and Songi Han. A new model for Overhauser enhanced nuclear magnetic resonance using nitroxide radicals. *The Journal of Chemical Physics*, 127:104508,

2007.

[63] W. T. Wenckebach. The Solid Effect. *Applied Magnetic Resonance*, 34:227–235, 2008.

[64] T. A. Galantowicz. Lineshape Measurement for Coupling to Waveguide Modes in the Prism—Film Coupler. *Appl. Opt.*, 13(11):2525–2528, Nov 1974.

[65] David S. Wollan. Dynamic nuclear polarization with an inhomogeneously broadened ESR line. I. Theory. *Phys. Rev. B*, 13:3671–3685, 1976.

[66] David S. Wollan. Dynamic nuclear polarization with an inhomogeneously broadened ESR line. II. Experiment. *Phys. Rev. B*, 13:3686–3696, 1976.

[67] M. Borghini. Spin-Temperature Model of Nuclear Dynamic Polarization Using Free Radicals. *Phys. Rev. Lett.*, 20:419–421, 1968.

[68] M. Goldman. *Spin Temperature and NMR in Solids.* Clarendon Press, Oxford, 1970.

[69] V S Bajaj, C T Farrar, M K Hornstein, I Mastovsky, J Vieregg, J Bryant, B Elèna, K E Kreischer, R J Temkin, and R G Griffin. Dynamic nuclear polarization at 9T using a novel 250GHz gyrotron microwave source. *J Magn Reson*, 160:85, 2003.

[70] Kan-Nian Hu, Hsiao hua Yu, Timothy M Swager, and Robert G Griffin. Dynamic nuclear polarization with biradicals. *J Am Chem Soc*, 126:10844–5, 2004.

[71] LR Becerra, GJ Gerfen, BF Bellew, JA Bryant, DA Hall, SJ Inati, RT Weber, S Un, T Prisner, AE Mc Dermott, KW Fishbein, KE Kreischner, RJ Temkin, DJ Singel, and RG Griffin. A Spectrometer for Dynamic Nuclear Polarization and Electron Paramagnetic Resonance at High Frequencies. *J. Magn. Reson., Ser. A*, 117:28–, 1995.

[72] DA Hall, DC Maus, GJ Gerfen, SJ Inati, LR Becerra, FW Dahlquist, and RG Griffin. Polarization-enhanced NMR spectroscopy of biomolecules in frozen solution. *Science*, 276: 930–932, 1997.

[73] Melanie Rosay, Volker Weis, Kenneth E Kreischer, Richard J Temkin, and Robert G. Griffin. Two-Dimensional ^{13}C-^{13}C Correlation Spectroscopy with Magic Angle Spinning and Dynamic Nuclear Polarization. *Journal of the American Chemical Society*, 124:3214–3215, 2002.

[74] V. Weis, M. Bennati, M. Rosay, J. A. Bryant, and R. G. Griffin. High-Field DNP and ENDOR with a Novel Multiple-Frequency Resonance Structure. *Journal of Magnetic Resonance*, 140:293 – 299, 1999.

[75] Colin D Joye, Robert G Griffin, Melissa K Hornstein, Kan-Nian Hu, Kenneth E Kreischer, Melanie Rosay, Michael A Shapiro, Jagadishwar R Sirigiri, Richard J Temkin, and Paul P Woskov. Operational Characteristics of a 14-W 140-GHz Gyrotron for Dynamic Nuclear Polarization. *IEEE Trans Plasma Sci IEEE Nucl Plasma Sci Soc*, 34:518–523, 2006.

[76] C. T. Farrar, D. A. Hall, G. J. Gerfen, M. Rosay, J. H. Ardenkjær-Larsen, and R. G. Griffin. High-Frequency Dynamic Nuclear Polarization in the Nuclear Rotating Frame. *Journal of Magnetic Resonance*, 144:134 – 141, 2000.

[77] W. A. Barker, Mohan Lal Narchal, Sushil Misra, Albert J. Bevolo, Francis X. Haas, Claire M. Birkbeck, Barbara M. Kuehne, and John C. Witte. Low-Temperature Dynamic Nuclear Polarization. *Rev. Mod. Phys.*, 36:872–879, 1964.

[78] Zandt-Rene Golman, Klaes and Mikkel Thaning. Real-time metabolic imaging. *Proceedings of the National Academy of Sciences*, 103:11270–11275, 2006.

[79] Gerold U Bublitz and Steven G. Boxer. Effective Polarity of Frozen Solvent Glasses in the Vicinity of Dipolar Solutes. *Journal of the American Chemical Society*, 120:3988–3992, 1998.

[80] M K. Kevan L Bowman. Electron spin-lattice relaxation mechanisms of radiation produced trapped electrons and hydrogen atoms in aqueous and organic glassy matrices: modulation of electron nuclear dipolar interaction by tunnelling modes in a glassy matrix. *Faraday discussions of the Chemical Society*, 63:7–17, 1977.

[81] Lucio Frydman, Adonis Lupulescu, and Tali Scherf. Principles and Features of Single-Scan Two-Dimensional NMR Spectroscopy. *Journal of the American Chemical Society*, 125: 9204–9217, 2003.

[82] L Frydman and D Blazina. Ultrafast two-dimensional nuclear magnetic resonance spectroscopy of hyperpolarized solutions. *Nature Physics*, 3:415–419, 2007.

[83] DeLos F. DeTar. Least squares treatment of the Arrhenius equation by a programmable

calculator. *Computers & Chemistry*, 2(3-4):143–148, 1978.

[84] Bèatrice Nicolaï, Alain Cousson, and François Fillaux. Interplay of quantum methyl rotation and crystal structure in the lithium acetate dihydrate: neutron diffraction, inelastic neutron scattering and theory. *Chemical Physics*, 290:101 – 120, 2003.

[85] Qiang Xu, Taro Eguchi, Hirokazu Nakayama, and Nobuo Nakamura. Proton magnetic resonance of C_nH_{2n+2} - n=1-4 adsorbed in mordenite. Dynamic behaviour and host-guest interaction. *Journal of the Chemical Society, Faraday Transactions*, 92:1039 – 1042, 1996.

[86] T. Ratajczyk and S. Szymanski. Theory of damped quantum rotation in NMR spectra. I. Fundamental aspects. *The Journal of Chemical Physics*, 123:204509, 2005.

[87] M Prager and A. Heidemann. Rotational Tunneling and Neutron Spectroscopy: A Compilation. *Chemical Reviews*, 97:2933–2966, 1997.

[88] K W H Stevens. The theory of planar methyl rotation. *Journal of Physics C: Solid State Physics*, 16:5765–5772, 1983.

[89] W. Demtröder. *Molecular Physics: Theoretical Principles and Experimental Methods*. Springer, 2005.

[90] G McHale and K W H Stevens. A group theoretical study of planar methyl rotation. *Journal of Physics: Condensed Matter*, 2:7257–7264, 1990.

[91] R. A. Wind and S. Emid. Influence of Sample Rotation on the NMR Spin-Lattice Relaxation of CH3 Groups in Solids. *Phys. Rev. Lett.*, 33:1422–1424, 1974.

[92] P Beckmann, S Clough, J W Hennel, and J R Hill. The Haupt effect: coupled rotational and dipolar relaxation of methyl groups. *J. Phys. C: Solid State Phys*, 10:729–742, 1977.

[93] A J Horsewill and A Aibout. The CH3 tunnelling sidebands of Δm=0 studied by dipole-dipole driven low-field NMR in the frequency domain. *Journal of Physics: Condensed Matter*, 1: 10533–10547, 1989.

[94] U Haeberlen. ^{13}C NMR of tunnelling methyl groups. *Molecular Physics*, 96:927–940(14), 1999.

[95] S.T. Goertz. The Dynamic nuclear polarization process. *Nucl. Instrum. Methods Phys. Res.*, 526:28–42, 2004.

[96] F Koksal, E Rossler, and H Sillescu. Spin-lattice relaxation by tunnelling motions of methyl groups in four acetates. *Journal of Physics C: Solid State Physics*, 15:5821–5827, 1982.

[97] S. Emid, R. A. Wind, and S. Clough. Rotational Polarization of Molecular Groups in Solids. *Phys. Rev. Lett.*, 33:769–771, 1974.

[98] Matthew E. Merritt, Crystal Harrison, William Mander, Craig R. Malloy, and A. Dean Sherry. Dipolar cross-relaxation modulates signal amplitudes in the 1H NMR spectrum of hyperpolarized ^{13}C-formate. *Journal of Magnetic Resonance*, 189:280 – 285, 2007.

[99] Yoshiro Akagi and Nobuo Nakamura. Tunnelling molecular motion in glassy glycerol at very low temperatures as studied by 1H SQUID nuclear magnetic resonance. *J. Phys.: Condens. Matter*, 12:5155–5168, 2000.

[100] S. Clough, AJ Horsewill, and PJ McDonald. Methyl tunnelling spectroscopy and level crossing phenomena in solid acetone. *J. Phys. C: Solid State Phys.*, 17:1115, 1984.

[101] S Clough, AJ Horsewill, and MNJ Paley. Diffusion of Methyl Group Tunnelling Energy. *Phys. Rev. Lett.*, 46:71, 1981.

[102] S Clough and J R Hill. Flip-flop motion and spin symmetry conversion of methyl groups. *Journal of Physics C: Solid State Physics*, 9:L645–L652, 1976.

[103] S Clough, A J Horsewill, and M N J Paley. Dynamic nuclear polarisation by the cooling of tunnelling methyl groups. *Journal of Physics C: Solid State Physics*, 15:3803–3808, 1982.

[104] J R Roebuck. The Joule-Thomson Effect in Air. *Proc Natl Acad Sci U S A*, 12(1):55–8, Jan 1926.

[105] Ulrich L. Günther, Christian Ludwig, and H. Rüterjans. NMRLAB-Advanced NMR Data Processing in Matlab. *Journal of Magnetic Resonance*, 145:201 – 208, 2000.

[106] David M. Wilson, Ralph E. Hurd, Kayvan Keshari, Mark Van Criekinge, Albert P. Chen, Sarah J. Nelson, Daniel B. Vigneron, and John Kurhanewicz. Generation of hyperpolarized substrates by secondary labeling with 1,1-^{13}C-acetic anhydride. *Proceedings of the National Academy of Sciences*, 106:5503–5507, 2009.

[107] S Clough, T Hobson, and S M Nugent. The change of frequency of methyl group tunnelling rotation following deuteration. *Journal of Physics C: Solid State Physics*, 8:L95–L97, 1975.

[108] S Clough and S M Nugent. The change of frequency of methyl group tunnelling rotation following deuteration. II. *Journal of Physics C: Solid State Physics*, 9:L561–L563, 1976.

[109] A. Detken, P. Schiebel, MR. Johnson, H. Zimmermann, and U. Haberlen. Rotational tunneling of methyl groups in the hydroquinone/acetonitrile clathrate: A combined deuteron NMR, INS, and computational study. *Chem Phys*, 238:301–314, 1998.

[110] Haukur Jûhannesson, Sven Macholl, and Jan Henrik Ardenkjaer-Larsen. Dynamic Nuclear Polarization of [1-13C]pyruvic acid at 4.6 tesla. *Journal of Magnetic Resonance*, 197:167 – 175, 2009.

[111] W. Pauli. The Connection Between Spin and Statistics. *Phys. Rev.*, 58:716–722, 1940.

[112] M. Gell-Mann. A schematic model of baryons and mesons. *Physics Letters*, 8:214 – 215, 1964.

[113] James Clerk Maxwell. A dynamical theory of the electromagnetic field. *Philosophical Transactions of the Royal Society of London*, 155:459–512, 1864.

[114] M Bazrafshan, G Fickenscher, M v Schickfus, A Fleischmann, and C Enss. Impact of nuclear dipoles on polarization echoes in glasses. *Journal of Physics: Conference Series*, 92:012135 (4pp), 2007.